Microseismicity in the vicinity of the Japan Trench and the Kuril Trench as derived from ocean bottom seismographic observations

by

Naoshi Hirata

Laboratory for Earthquake Chemistry
Faculty of Science, The University of Tokyo
Tokyo, 113, Japan

Dissertation
Presented to the Univesity of Tokyo
for the degree of
Doctor of Science

January 1985

Abstract

A series of experiments was carried out by four ocean bottom seismograph (OBS) arrays to investigate microseismicity near the Japan Trench and the Kuril Trench in 1980, 1981, 1982 and 1983. Each OBS array consisted of 10 OBSs which recorded ground signals continuously for 10-30 days; the total period of recording amounted to 15,000 hours.

To process the large amount of OBS records, a paly-back system was developed. The system enables us to obtain digital waveform data from which earthquakes are chosen and arrival time data for locating earthquakes are produced. A new method of the arrival time inversion for locating the earthquakes was developed on the basis of the generalized inversion theory.

From analyses of the OBS data, the following results about seismicity in the Japan Trench area and the Kuril Trench area were obtained:

(1) About 50 microearthquakes per day were recorded by each OBS. Out of these events 5-10 earthquakes per day were located in and around the OBS array.

(2) A highly active region of microseismicity beneath the seaward trench wall was found. The seaward seismicity is concentrated within 100 km of the trench axis and low beneath the Northwest Pacific basin; no detectable event with magnitude greater than 2 was observed.

(3) A seismicity gap was found beneath the landward trench wall, while the seismicity is high beneath the continental slope.

(4) Microearthquakes beneath the seaward trench wall were

distributed 0-30 km in depth and just beneath the trench axis they were 0-50 km; microearthquake activity is concentrated within the upper part of the lithosphere.

The hypocenter distribution obtained in the present study is related to the the physical properties and the stress state of the subducting oceanic lithosphere in the vicinity of the trench.

Microseismicity in the vicinity of the Japan Trench and the Kuril Trench as derived from ocean bottom seismographic observations

海底地震計多点観測による日本海溝及び千島海溝付近の微小地震活動

東京大学　理学部附属地殻化学実験施設　平田直

要旨

1　目的

本研究の目的は，海底地震計による多点観測を海溝近傍で行ない，微小地震活動，特にその空間的分布の詳細を明らかにすることにある。

近年，微小地震観測網の発達により，深発地震の詳しい空間的分布が明らかにされ，リソスフェアーの力学的・運動学的構造に関する知識が蓄積されてきている。ところが，リソスフェアーの沈み込み開始点である海溝軸近傍の微小地震活動は重要であるにもかかわらず十分に調べられていない。これは，海溝軸が陸上の観測網から離れているために，震源決定精度が著しく悪くなっているからである。

特に震源の深さ分布に関して，陸上の観測結果からは，海溝軸直下から深さ100km つまりリソスフェアー全体で微小地震が発生している様に見えるが，その分布は疑問視されていた。海底地震計によって観測点を海溝近傍にまで広げる事が，この問題を解決する為に重要であった。

2　観測及びデータ

1980年から1983年にかけて，日本海溝及び千島海溝付近で，海底地震計多点観測を４回行った。

１回の観測で約１０台，合計で４４台の地震計を設置した。各観測点で10日～30日間の連続記録を行い，全体で約15,000時間の地動記録を得た。この記録には１観測点あたり平均して50個／日の多数の地震が記録された。このうち，震源を決めるに十分な振幅をもった近い地震は５～10個／日であった。

3　解析方法

観測された地動信号から，震源分布を求める為の新たな解析方法を確立した。

3－1　自動再生処理システム

連続記録された多量のアナログ記録から，地震波形データを能率よく，かつ精度よく抽出するための自動再生処理システムを新たに開発した。

自動処理を行なうための最大の問題点は，地動信号の記録を大量に処理しなければならない点にある。海底地震計１点のデータ量は約 760メガバイトのデジタルデータに相当する。また，再生のスピードが，記録時の数 100倍であることも再生処理を難しくしている。

本研究では，高速のA／D変換器と比較的大容量の磁気ディスクを持つミニコンピュータを用いて，更に，低速及び高速の2度にわけたA／D変換を行う方式を採用することによってこれらの問題点を解決した。この再生処理システムによって，精度の高い地震波到着時刻データが迅速に得られるようになった。

3－2　震源決定法

先験的情報を用いた準線形のインヴァース理論を発展させ，震源決定法に適用した。速度連続モデルを採用し安定で高精度の震源を求める方法を開発した。

新たに展開された理論によって，データに伴う誤差とデータの持つ分解能（resolution）を評価した新しい規範を最小二乗問題に導入した。これに基き，“一般化された最小二乗解”を定義した。

4　解析結果

日本海溝北部及び千島海溝南部付近での微小地震活動について，以下の事実が解った。

（Ⅰ）海溝海側斜面下には活発な微小地震活動が存在する。この活動域には東限が存在し，水深5500ｍの等水深線で特徴づけられる海溝周縁隆起帯の西縁より海側では，地震活動が低く，検知しうる微小地震（$M \gtrsim 2$）は存在しなかった。

（Ⅱ）海溝陸側斜面では地震活動が低い。この領域は，三陸沖日本海溝の場合，水深4000ｍと6000ｍの間に相当する。一方大陸斜面下には活発な微小地震活動が存在する。

（Ⅲ）震源の深さ分布は海溝海側斜面下では0から30km以浅，海溝軸直下ではやや深く0から50kmをわずかに越える深さまでの範囲に存在する。大陸斜面下の地震は，陸に近づくにつれてわずかに深さを増し，傾斜の角度は10°以下である。これは，三陸沖日本海溝では，二重深発面の上面に，十勝沖千島海溝では，下面につながっている。

従って，陸の観測結果からはあたかも存在するかのように見えていたリソスフェアー全体にわたる海溝軸近傍での微小地震活動の存在は海底地震計による観測によっては支持されない。

5　議論

日本海溝海側斜面の微小地震活動の存在は，これまでの海底地震計による研究結果と調和的である。海盆で微小地震活動が低いということは，千島，伊豆小笠原，マリアナなどの地域について報告されている。中央アリューシャンでは海溝海側斜面に高活動域，陸側斜面に低活動域が存在することが確認されている。また，琉球海溝北部，アリューシャン海溝東部，ニュー・ヘブリデス海溝などでは，陸側斜面で，地震活動が低いことが示唆されている。従って本研究で得られた微小地震の空間的分布の特徴は，海溝近傍での海洋リソスフェアーの一般的性質を反映していると思われる。

TABLE OF CONTENTS

1 Introduction

1-1 Necessity of observations by ocean bottom seismographs

The spatial distribution of earthquakes beneath an island-arc trench system provides useful information about the mechanical properties and the stress state of the subducting oceanic lithosphere. A number of local seismic networks have been operated in trench areas to observe these earthquakes. Since Wadati (1927) found deep earthquakes beneath Japan, there are many investigations on the deep seismic zone (eg., Wadati, 1928, 1929, 1931, 1935; Benioff, 1949, 1954, 1955; Wadati and Iwai, 1953, 1956; Katsumata, 1955, 1956, 1967; Miyamura, 1962; Yoshii, 1979; Suzuki and Motoya, 1981; Hasegawa et al., 1983; Susuki et al., 1983). The Tohoku District, north-eastern Honshu, is one of the most thoroughly investigated areas beneath which deep seismic zones are located. Detailed studies of the seismic activity associated with the subduction of the Pacific plate, for example, have ascertained the existence of the double-planed structure of the deep seismic zone beneath the Tohoku District, using the highly sensitive network operated by Tohoku University (Umino and Hasegawa, 1975; Hasegawa et al., 1979).

These studies shows that a double seismic zone exists in the depth range 50-150 km. However, the seismicity in the shallower part of the descending lithospher is poorly resolved because these activities occur outside the network. In particular, the focal depth distribution beneath the Japan Trench is considerably scattered because the trench is located about 200 km from the

coast, where the location of earthquakes is difficult from land network data (Ishii and Takagi, 1978).

Moreover, it has been pointed out that for events occurring in the vicinity of the Japan Trench off the east coast of Sanriku (north-eastern Honshu) focal depths determined by the Tohoku University land network and by the Japan Meteorological Agency (JMA) are usually deeper than those determined by the International Seismological Center (ISC) or the United States Geological Survey (USGS) (Utsu, 1967; Fujita et al., 1981). By means of computer simulations, Ichikawa (1978, 1979) attributed these discrepancies to the lateral heterogeneity of the uppermost mantle under the region which lies between the Japan Trench and north-eastern Honshu.

In order to obtain a clear view of the seismicity associated with plate subduction beneath the trench, on-site observations by ocean bottom seismometers (OBS) are obviously needed. The recent developement of OBS systems enables us to operate reliable and low-noise OBSs which have been particularly successful in long-range refraction experiments in deep ocean (eg.,Asada and Shimamura, 1979; Shimamura et al., 1983).

1-2 Subject of the present study

In this study, by using data obtained by OBS observations, we will clarify a fine structure of the spatial distribution of microearthquakes beneath the trench areas with better resolution than was previously possible from land observations. In particular, we give attention to the seismic activity largely

scattered from 0 km to more than 100 km in depth just beneath the trench axis; the accuracy of hypocenter determination in depth by land observations have been quastionable(Fig.1-1).

For this purpose, first, four observations have been carrried out in and around the Japan Trench and the Kuril Trench during 1980 - 1983. Second, new methods of analyzing OBS data have been established; one is that of compilation of waveform data of earthquakes from a large amount of continuous tape records and the other is that of inversion of arrival time data to locate hypocenters by means of a singular value decomposition technique. Third, applying these methods to OBS data, we determine the spatial distribution of microearthquakes beneath the trench areas. Finally, the seismic activity in and around the Japan Trench and the Kuril Trench is discussed in terms of the mechanical properties of the ocenic lithosphere.

Special care is given to softwares for processing of OBS data; the linear inverse theory is investigated in detail and a new solution to the least-squares problem is presented in a general and rigorous manner.

1-3 Summary of contents

First, the OBS experiments the author participated in are described in chapter 2 which includes observations in the trench area and those for aftershocks of some large earthquakes occurred in the sea area. Next, the methods of data processing for records obtained by OBS observations are discussed in chapters 3 and 4. Third, the actual data obtained in observations mentioned above

are presented in chapter 5, and hypocentral distributions are discussed in chapter 6. In chapter 7, the picture of oceanic lithosphere obtained by the present study is compared with results by previous OBS observations, those by land observation and other seismological studies in different trench areas. Finally, the summary of the study of seismicity by OBS observations are presented in chapter 8.

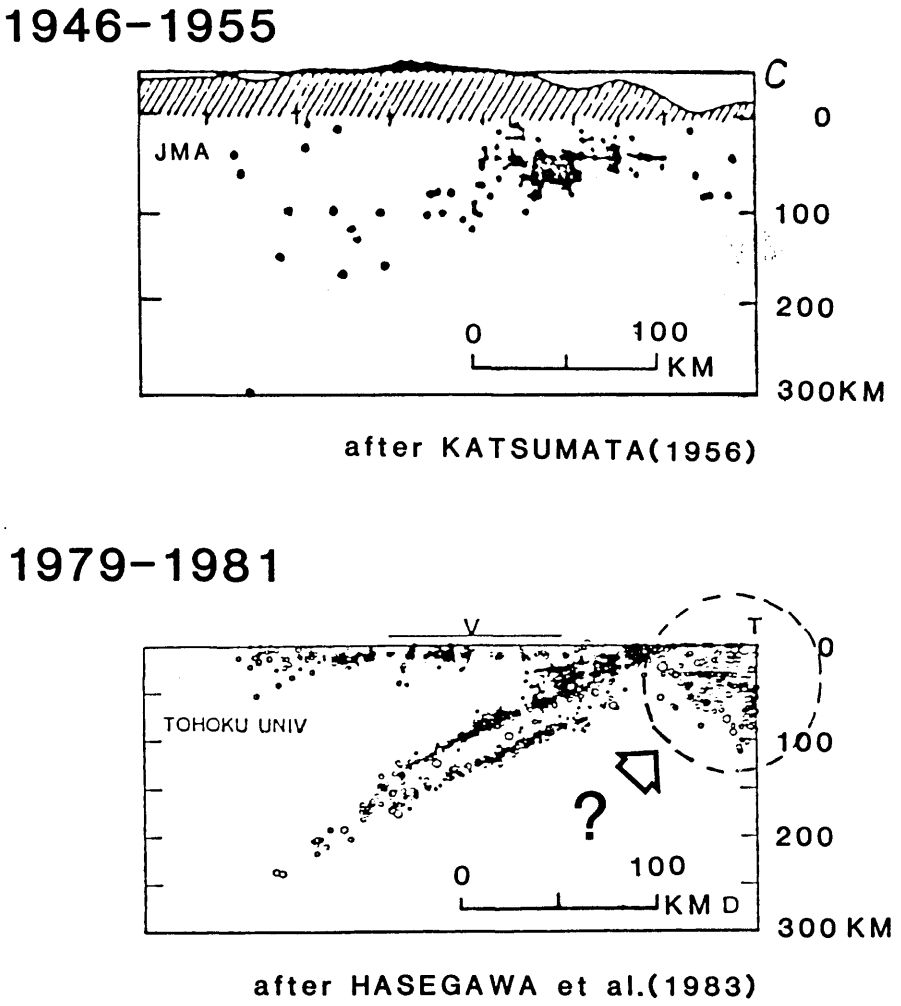

Fig.1-1 Vertical seismic sections determined from land observations. The accuracy of hypocenter location has been remarkably improved. However the seismic activity largely scattered beneath the trench axis is quastionable.

2 Observations

2-1 Introduction

There are three main reasons why observations of natural earthquakes by OBSs are needed in the trench area; the first is that steady state microseismicty which can not be monitored by land networks should be observed by seismogaphs in the vicinity of the trench area where the oceanic plate is believed to start subducting. The activity of microearthquakes would be related to the plate motion or the stress field in the lithospher. The second is that large earthquakes often occur in the area between the coast line and the trench axis. For detailed study of focal process of a large eathquakes, near field observations with good azimuthal coverage are necessary; observations not only from the direction where the land networks are located but also from the opposite direction where the Northwest Pacific Basin is situated. The third reason is closely related to the second one; on-site observations are needed to determine a three-dimensional spatial distribution of aftershocks associated with the large earthquake beneath the sea area.

The first reason is applicable to observations in other geophysically interesting regions which are located far from land networks such as the areas of spreading ridges and offsetting transform faults (eg., Francis and Poter, 1972; Lilwall, Francis and Poter, 1981; Hyndman and Rogers, 1981; Project Rose Scientists, 1981; Ouchi et al., 1982). To monitor the small seismic activities in the sea area, however, we need long period

observations or stationary observations by permanent stations as in the land network. Since it costs very much to operate permanent stations on the ocean bottom, at present, only one permanent OBS system with four seismpographs is in operation in the world on the continental shelf off the south coast of Tokai area, central Honshu by the Japan Meteorological Agency (JMA) (M.R.I,1979; Hamada, 1983). Under the limitation of technology in the present stage, repetition of temporal observations by off-line OBSs in a particular area is one of the most realistic approach to investigate the general feature of seismicity especially in a deep sea area.

To observe large earthquake by OBSs we have to prepare OBS systems much different from those for observation of steady state microseismicity; we need many OBSs whose observational period is much longer than that for study of microseismiciy, because the large earthquake occurs much less frequently than small earthquakes. An off-line OBS system with a long observational period (for expamle, one year or more) requires a special trigger mechanism which save current consumption of electronics used in the system. Such a kind of OBS system has not yet been available. At present we can observe the large event only if it occurs by chance during the period of observation. The rare example is the observation of the 1982 Ibaraki-oki earthquake (M=7.0) off the eastern coast of the Ibaraki Prefecture (Hirata et al.,1984). Although the OBS array was deployed for investigating seismicity off the Fukushima Prefecture, the OBS array recorded by chance the whole sequence of foreshocks, the main shock and aftershocks.

The third purpose of observations essentially requires quick deployment of OBSs in the aftershock area. The first observation of aftershocks by an OBS array was carried out by the University of Tokyo immediately after the 1978 Miyagi-oki earthquake (M=7.4) off the Tohoku District (Yamada et al., 1978; Matsu'ura et al., 1978; Yamada, 1980). The recent development of the OBS system enables us to use a compact OBSs which is so small and easy to handle as to deploy immediately after the occurrence of the main shock by a small and non-equipped ship or even by an aircraft.

Since the designing policiy of OBSs depends on the purpose of the observation, there are and were many kinds of OBS systems(e.g., Ewing and Ewing ,1961; Bradner and Dodds, 1964; Rykunov and Sedov, 1965, 1967; Kishinouye, 1963, 1966). Detailed descriptions on the history of developement of the OBS system can been found in Asada and Shimamura (1974,1976), Nagumo and Kasahara (1976), Ouchi (1978) and Yamada (1980). In breif, the number of OBSs to be deployed in an array becomes larger and the signal-to-noise ratio of the recording system of each OBS becomes much better. These two are essential both in natural earthquake studies and in explosion studies.

2-2 Instrumentation

In this sectiom, we presents a brief review on the OBS systems which are used in the present study. These systems have been developed at Geophysical Institute, Faculty of Science, The University of Tokyo and at Ocean Bottom Seismological Laboratory, Faculty of Science, Hokkaido University by Asada, Shimamura and

Kanazawa (Asada and Shimamura, 1971a,1971b; Shimamura et al., 1970; Yamada, 1980).

2-2-1 Type of OBS

Since the beginning of the 1970's (Asada and Shimamura ,1971a, 1971b), continuous efforts to improve the OBS system have been made by the cooperation of the University of Tokyo and Hokkaido University (Asada and Shimamura,1975; Yamada, 1980). The efforts have been made to accomplish the system with a high signal-to-noise ratio, a compact form and a low cost. At the present time, three types of OBS system are available; a tethered type OBS system, a timed-release pop-up system and an acoustic-release pop-up sytem.

The OBS sytem originated in the tethered one; the OBS on the bottom of the sea is tethered by nylon ropes and polypropylen ropes to surface buoys. An example of the system is illustrated in Fig.2-1, where that used in the 1980 experiment is shown. In this system, the pressure case of the OBS, an alluminum cylinder, sinks in the soft sediment of the bottom almost completely, and so the noises induced by the bottom water current are reduced considerably. Although the system has been improved so as to be simple and easy to handle, it takes about one hour for deployment if the water depth is about 5000 m and about 2 hours for retr@i)val.

The second type of OBS system, the timed-release pop-up system, has advantages of its compactness and easiness of handling. As is showm in Fig.2-2, the whole instrument of OBS

including geophones, a recorder, batteries and other electronics is housed in a commercially available glass sphere with an outer diameter of 43 cm. The weight is 78 kg in air. The size is less than one meter in cubic. Thus it takes less than 10 minutes to launch the OBS. Although the time for the recovery of the OBS onto the ship is generally short, it depends on the maneuverability of the ship. The point is that any ship without any special rig can handle the OBS. Also the system has experience to be launched by a helicopter. The release mechanism for anchors is the electrical corrosion with a timer set before the deployment (Urabe and Kanazawa, 1984). The weak point of the timed-release system is indeed that we have to decide the schedule of making the OBS come up to the sea surfce without regard to the sea condition; it may happen to be very bad because of an unexpected typhoon just on time of OBS retrieval.

The disadvantage of the timed-release system has been overcome by the third type of the OBS sytem. This is equipped with an acoustic transducer which recieves a signal from the ship to release an anchor. Although the size and the weight of the acoustic-release OBS system are larger than those of the timed-release system, it is easier to handle than the tethered type OBS system because of no mooring system with a large length of ropes. The size of the acoustic-release OBS system is mainly restricted by that of the transducer. The pressure case of this system is the same as used for the tethered type.

2-2-2 Seismograph

Each OBS is equipped with one vertical geophone with natural frequency of 3.0 Hz and one horizontal geophone with that of 4.5 Hz. The geophones are mounted on gimbal mechanisms. Two types are used for a cylindrical pressure case and a spherical one. The outputs are recorded by four channels of continuous direct analogue recorder (DAR) with the Phillips cassette mechanism (Yamada et al., 1976). The DAR has the highest packing density of record among frequency modulation (FM) recording and pulse code modulation (PCM) recoring.

The frequency response of the recorder which runs at a speed of 0.13 mm/s is flat from 2 to 30 Hz (3 dB points). The tape speed corresponds to 11 days continuous recording on a C-90 cassette tape. If we make the tape speed a half, the recording period becomes twice, and the highest end of the frequency band becomes a half. We have used the recorders which can record continuous signals for about 11 days and those for 25 days in the present study. The vertical geophone signals are recorded on low and high gain channels, which enable to record signals with total dynamic range of 74 dB. The remaining channels are used for a horizontal component and a time code generator (TCG).

The TCG has a temperature-compensated crystal oscillator with an accuracy of 5 X 10 for the temperature range of 0 - 40 C (Inatani and Furuya,1980). The TCGs are calibrated on ship by the calibrator with the 10 crystal (Shimamura, 1977) before and after the operation. Total clock errors were kept within 0.05s for the whole period of the experiment.

2-3 Observations in the vicinity of the Japan Trench and the Kuril Trench

A series of experiments to study seismicity and a velocity structure of the oceanic lithosphere has been conducted since 1980 in the Northwest Pacific Ocean off Japan (Table 2-1). Each experiment included a natural earthquake observation, a long-range explosion study, a short-range explosion study with small charges and an air-gun profiler study. For the study of seismicity, the following has been considered: Throughout the entire observation, we intended to obtain the general feature of steady state microseismicity for the first reson in 2-1. The length of each period of observation was restricted mainly by the width of frequency band in recording as discussed in 2-2-2. Since we need up to 20-30 Hz to analyze data of microearthquakes, the upper limit of the recording period is about one month if we record signals continuously on a C-90 type cassette tape. This restriction made us repeat the observations in almost the same area to understand the steady state microseismicity. Furthermore, since we also want to study as large area as possible, we have slightly shifted the observation site at each experiment. All the experiments were accomplished in summer season because the sea condition near Japan is better than that in other seasons.

Five OBS arrays were conducted to study seismicity during 1980-1984. Four of them are located in the vicinity of the trench, which are shown in Fig.2-3. The remaining one array was located off Fukushima Prefecture; it observed the 1982 Ibaraki-oki earthquake as was mentioned before (Fig. 2-4). In the

present study, the data from the northern four OBS arrays, which are situated in the vicinity of the trench axis, are analyzed to investigate the seismicity in the trench areas.

(1) The 1980 experiment

In the 1980 experiment, the northern part of the Japan Trench area, at about 40°N, was extensively covered by an OBS array with 10 OBSs. Except for the observations with a small number of OBSs at the early stage by Nagumo (1970a, 1976), this is the first observation by an OBS array with many OBSs in the vicinity of the Japan Trench. As was discussed before, one of the main purpose of this observation is to elucidate the depth distribution of microrathquakes beneath the Japan Trench. Although, to acomplich this, the OBSs are slightly too much separated as compared with an optimal configuration of an array for locating shallow events, a wide aperture seismic array covering the both sides of the trench axis was necessary to obtain the first general picture of the seismicity of this region.

Since the acoustic-release pop-up system had not been developed at the time of the 1980 experiment, the tethered type OBS sytems (T) and the timed-relese pop-up systems (P) were deployed as shown in Fig. 2-5. Eight OBSs were available for analyses. Three of them, P9, P10 and P12 were located on the Northwest Pacific Basin with the sea depth of about 5000 m. OBSs, T3 and T7 were situated nearly at the bottom of the trench deeper than 7000 m, while T11 was placed on the shoulder of the Erimo

Seamount at the junction of the Japan Trench and the Kuril Trench. The remaining two, P4 and P6, were on the continental slope at a depth of 3000-4000 m. Positions of OBSs were determined by the Navy Navigation Satellite System with an accuracy of 0.1 n.m. They are tabulated in Table 2-2 with period of recording. Shorter recording period for P10 and P12 are due to the schedule of ship time and a premature release of the preset timer for P12. P9 was recovered by a fisherman on April 13 in 1982, one year and nine months after launching.

The seismic velocity structure near the OBS array has been studied by Ludwig et al. (1966), Murauchi et al. (1973), Murauchi and Ludwig (1980), Nagumo et al.(1980), Matsuzawa et al., (1980) and Tamano et al. (1980). Moreover we have conducted an air-gun refraction survey over most of our OBSs to obtain the local structure beneath each OBS (Shimamura et al., 1983). These studies show that normally a low velocity sedimentary layer lies beneath an ocean; the thickness of this layer may vary among OBS sites. Furtheremore, our OBS array lay just over a continent-ocean transition region where the oceanic lithosphere is likely to start subducting.

(2) The 1981 Experiment

Almost the same area but slightly west of the observation area of the 1980 experiment was covered by an array with 14 OBSs in the 1981 experiment (Fig. 2-6). The configuration of the array was so arranged as to improve the resolution of location of microearthquakes especially in depth. Furtheremore, one of the

OBSs, P10, was deployed just on the inner wall of the Japan Trench, the area with water depths of between 4000 and 6000 m, where a seismicity gap has been suggested from the data obtained by the 1980 experiment.

The locations and recording periods of OBSs are listed in Table 2-3, where the types of the OBS are designated by T (tethered) and P (timed-release pop-up). Nine pop-up type OBSs and one tethered type OBS were recovered. Date from 8 OBSs out of the 10 OBSs were successfully used for analyses. They are shown in Fig. 2-6. Troubles on other OBSs are as follows; one of the tethered type OBS was estimated to be lost due to fishery works and the other tethered type OBS was due to a strong water current at a very shallow portion of the sea. The OBS P7 had a recording period of only 13 hours because of a premature release of the preset timer. This trouble was caused by the damage to a pressure case of the timer on launching. Although the exact reason of failures in recovery is not known, we suppose some of them are due to a trouble in a timed-release mechanism. OBS P14 had trouble in a TCG and was not used in the present study.

(3) The 1982 experiment

The area covered by the 1982 experiment has two interests; the area is adjacent to those of the previous observations, and the 1982 Urakawa-oki earthquake (M=7.1) occurred slightly north of the present area on March 21, 1982 . The array was located at the junction of the Japan Trench and the Kuril Trench. The area off Urakawa is one of the most active area in seismicity among

those around the junction.

The acoustic-release type OBSs (S) and the timed-release type OBSs were deployed as shown in Fig. 2-7. All the OBSs were retrieved by the second cruise one month after the first cruise for launching of OBSs and a refraction study by explosions and an air-gun. The recording period (about 25 days) of 9 OBSs (P1, P2, P3, P4, P5, P6, S7, S8 and S9) was longer than that in the previous observations (about 11 days) as tabulated in Table 2-4.

Three OBSs were deployed at the Erimo Seamount where microseismicity seemd to be high from the 1980 data. Unfortunately, however, one of them surffered damage in release mechanism maybe on launching and recorded signals for only one day. Records from the other two OBSs were too noisy to analyze; they seems to drag their anchors whole the observational period. Thus, the data from 6 timed-release type OBSs and one acoustic-release type OBS, S11, were used for the present analysis.

The velocity structure in the vicinity of the present OBS array has been investigated by the former refraction and reflection study (Asano et al., 1979). A thick sedimentary layer beneath the sea bottom off Hidaka is found. A predominant negative gravity anomaly off Hidaka (Tomoda, 1973) is interpreted in terms of this thick sediment.

At the second cruise an OBS array with 5 acoustic-release type OBSs was deployed off Fukushima Prefecture. These OBSs were recovered by the third cruise, one and a half month after the deployment. This array was intended for the investigation of

seismicity in the area off Fukushima Prefecture, which is one of the most active areas in seismicity off the coast of Tohoku. As was mentioned before, this array happened to observe the 1982 Ibaraki-oki earthquake on July 23, 1982 (Fig.2-4). The whole sequence of the forshocks, the main shock and the aftershocks associated with this earthquake was recorded. Particuraly, the remarkable foreshock activity recorded by the array was successfully analyzed; the forshocks occurred in a very narrow region of a few km in width (Hirata et at., 1984).

(4) The 1983 experiment

The Kuril Trench area off Tokachi was covered by two OBS array in the 1983 experiment. One is for the refraction and reflection study and the other for the seismicity study, which is the first observation in this area; the former OBS array was deployed and retreived by the first cruise and the latter OBS array was deployed by the first cruise and retrieved by the second cruise two months after launching. The results of the refraction study by an air-gun is reported by Nishizawa et al. (1984a, 1984b). Data from the latter OBS array were used in the present study to investigate the seismicity. Locations of the OBSs for the seismicity study are tabulated in Table 2-5 with their recording periods . All the OBSs were an acoustic-release pop-up type. In the area near the 1983 array, an investigation of the velocity structure is made by Den et al. (1971) but no study on seismicity by an OBS array has been carried out so far.

2-4 Aftershock observations by an OBS array

In this section we review observations of aftershocks by an OBS array. The compact and reliable OBS systems enable quick deployment immediately after the main shock. Four observations of aftershocks associated with large earthquakes ($M \geq 7$) have been successfully carried out by OBS arrays so far, which are tabulated in Table 2-6. It should be noted that OBSs were deployed by very small ships, one of which was a fishing boat of 17t, or helicopters. In general, it is difficult to use a large ship in case of emergency because a schedule of the large ship is usually fixed several month or more before her cruise. Further, it is better to start observations of aftershocks as soon as possible because the number of aftershocks decreases with time and the aftershock area usually extends from an area of the main fracture with time. Hence the quick deployment by the small ship or the aircraft was an essential factor of the OBS system for the aftershock observation.

The observation of aftershocks of the 1978 Miyagi-oki earthquake is the first observation by an OBS array. The observation by 3 tethered type OBSs revealed a hypocenter distribution with better accuracy than the land observation (Yamada et al., 1978; Matsu'ura et al., 1978; Yamada, 1980). Their studies show that the focal depths of aftershocks determined by the land observation have a systematic error to be shallower by 15-25 km than those by the OBS observation.

The OBS array in the aftershock area of the 1982 Urakawa-oki earthquake elucidated the fracture geometry of the earthquake;

the distribution of the aftershocks shows the two conjugate fault planes (Iwasaki et al., 1983).

A helicopter was for the first time used to deploy OBSs on the sea bottom in the observation of aftershocks of the 1982 Ibaraki-oki earthquake. Unfortunately, because of a typhoon coming, the helicopter could not take off until 22 days after the occurrence of the main shock. However, although the OBS array was located about 100 km off the coast, it took only 3 hours for the deployment of the 4 OBSs including a round trip flight to the observation site from the Tokyo heliport; the maneuverability of an aircraft has been clearly demonstrated.

Five timed-release OBSs were deployed by a helicopter only 3 days after the occurrence of the 1983 Japan Sea earthquake. A precise aftershock distribution determined from the OBS data shows that the aftershocks concentrate in the depth range of 8-21 km. The general trend of the aftershock distribution shows that the main fault plane of the earthquake is an eastward dipping one with a low angle (about 15°). Furthermore, westward dipping distributions with a high angle were found (Urabe et al.,1984).

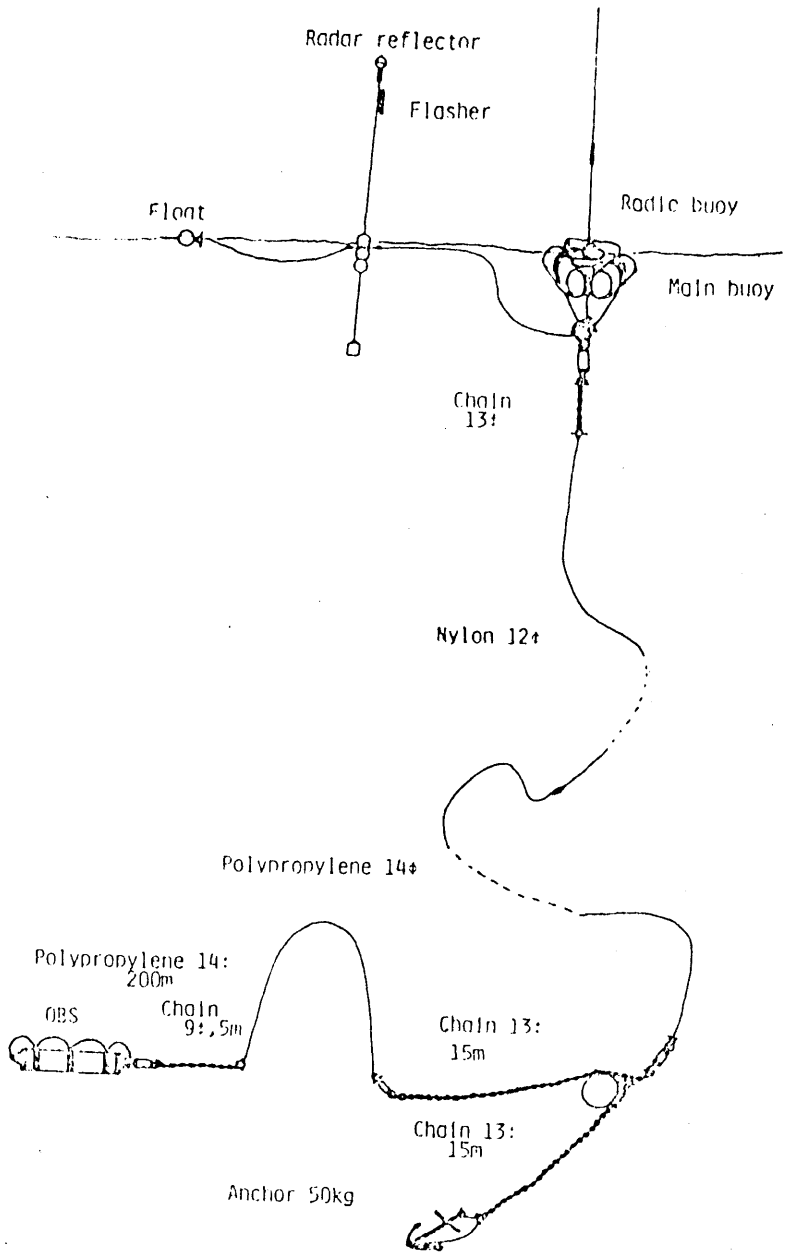

Fig.2-1 Tethered type OBS system.

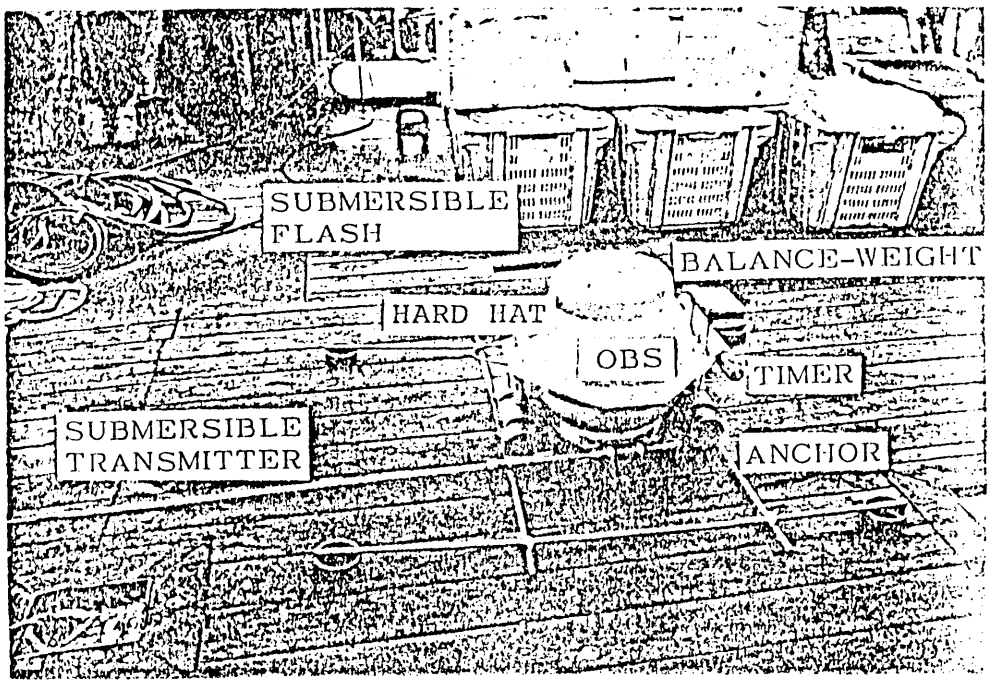

Fig.2-2 Timed-release pop-up OBS system

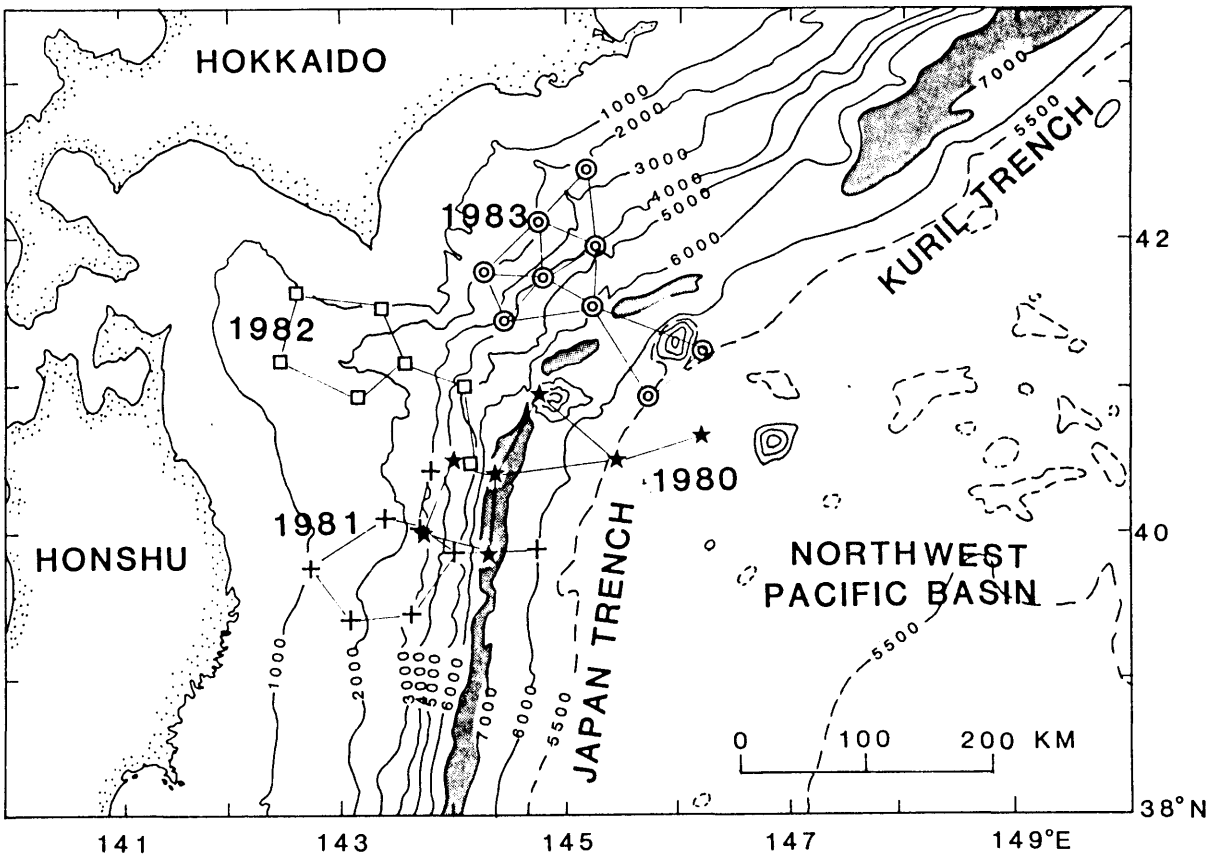

Fig. 2-3 Map of the major bathymetric features in the vicinity of the junction of the Japan Trench and the Kuril Trench, showing the site of OBS arrays operated in 1980, 1981, 1982 and 1983. Positions of the OBSs are represented by stars (1980), crosses (1981), squares (1982) and double circles (1983). Isobaths are in meters. Areas deeper than 7000 m are shaded, indicating the trench axis.

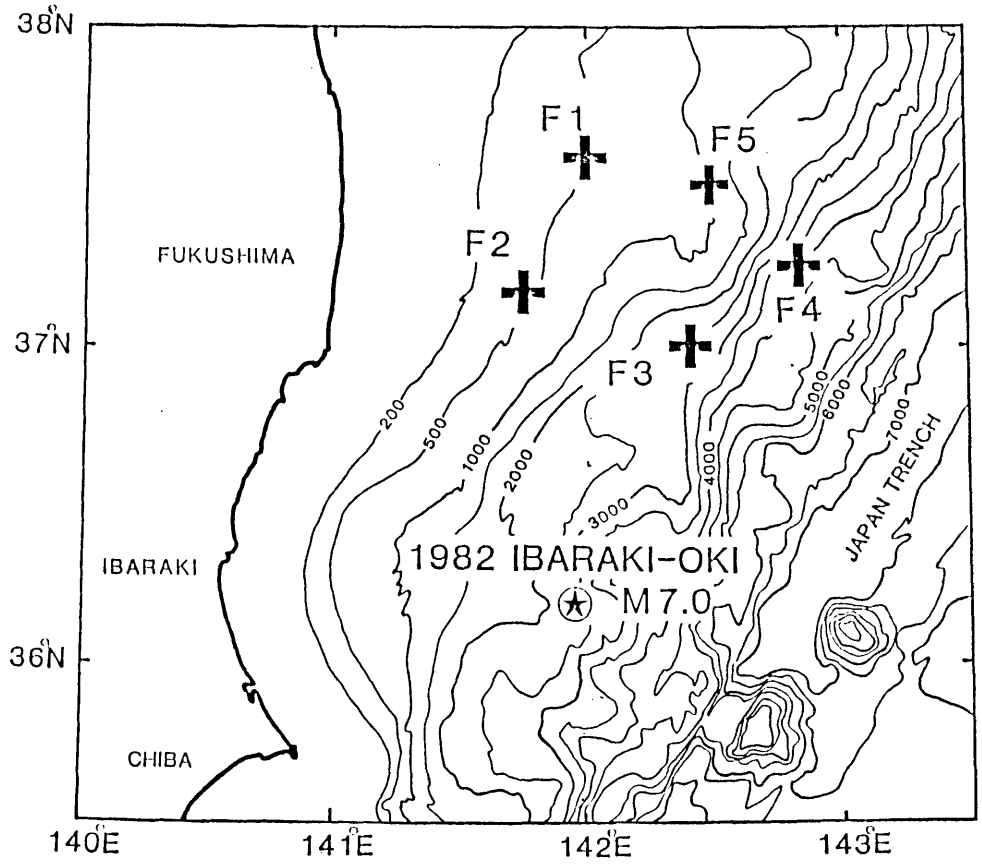

Fig.2-4 Position of the 1982 OBS array off Fukushima.

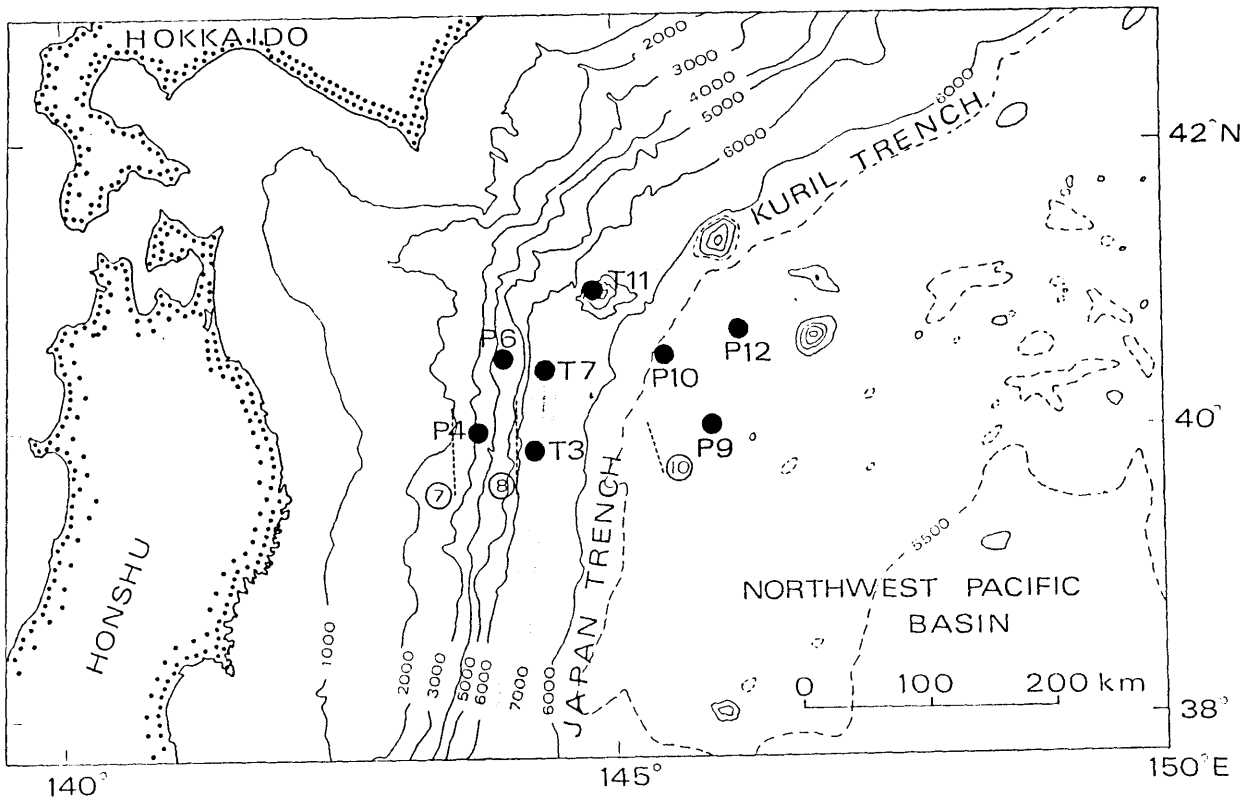

Fig.2-5 Location map showing the site of the 1980 OBS array. The solid circles represents the positions of the OBSs. Broken lines with numerals 7, 8 and 10 show the locations of seismic refraction profiles operated by Ludwig et al. (1966).

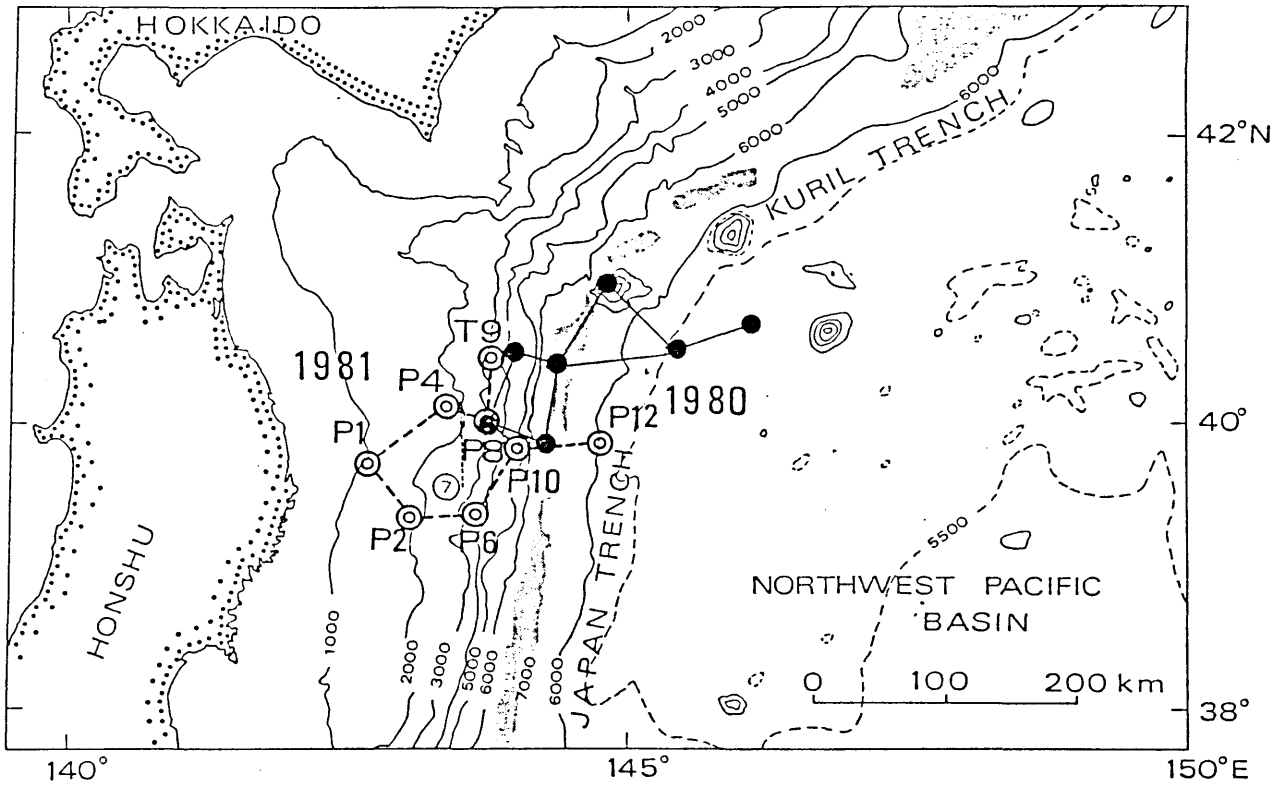

Fig.2-6 Location map showing the site of the 1981 OBS array. The solid circles represents the positions of the OBSs. The broken line with numeral 7 shows the location of seismic refraction profile 7 operated by Ludwig et al. (1966).

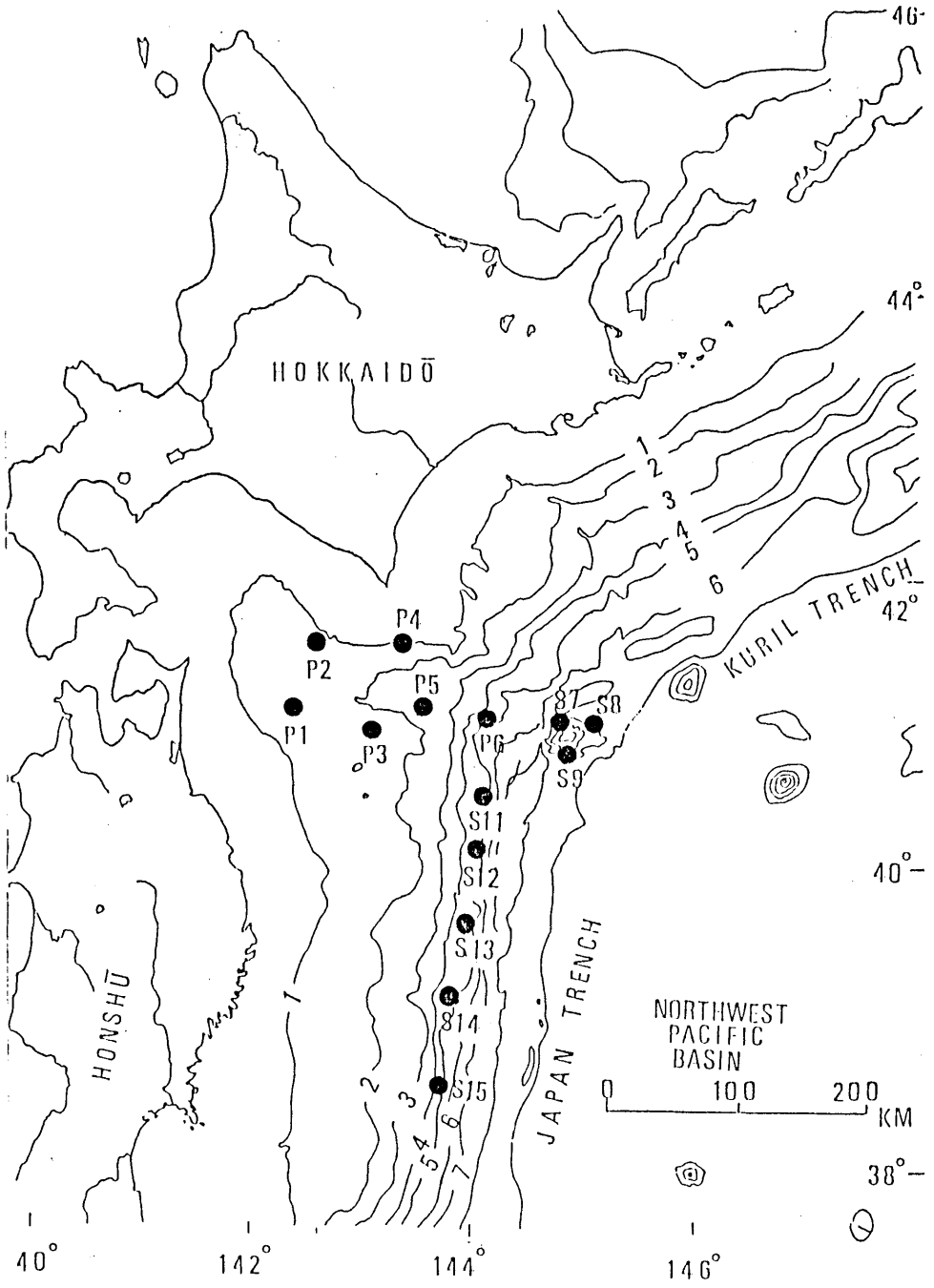

Fig.2-7 Location map showing the site of the 1982 OBS array. The solid circles represents the positions of the OBSs.

YEAR	AREA OF OPERATION	CRUISE ---- SHIP	DEPLOYMENT	RETREIVAL	NUMBER OF OBS'S* T	P	S	: TOTAL
1980	Off Sanriku the Japan Trench	Jul.20 - Aug.6 R/V Ocean Discoverer	Jul.21-24	Jul.30-Aug.4	3 (0)	7[a] (1)	0 (0)	: 10 (1)
1981	Off Sanriku the Japan Trench	Jun. 8 - Jun.25 R/V Ocean Discoverer[+]	Jun. 9-11	Jun.19-23	3 (2)[b]	11 (2)	0 (0)	: 14 (4)
1982	Junction of the Japan Trench and the Kuril Trench	Jun.13 - Jun.27 R/V Sakuramaru Jul. 7 - Jul.16 R/V Tokyomaru	Jun.15-17	Jul. 9-14	0 (0)	6 (0)	8 (0)	: 14[c] (0)
	Off Fukushima	Sep. 1 - Sep. 8 R/V Tokyomaru	Jul.14-15	Sep. 2- 3	0 (0)	0 (0)	5 (0)	: 5 (0)
1983	Off Tokachi the Kuril Trench	Jun.28 - Jul.18 R/V Kaikomaru NO.25 Sep.14 - Sep.18 R/V Kaikomaru No.25	Jul.14-17	Sep.15-17	0 (0)	0 (0)	10 (1)	: 10 (1)

*. T:tethered type OBS; P:timed-release pop-up type; S:acoustic-release pop-up type. Number of OBSs lost is in parentheses.
+. five timed-release pop-up type OBSs were deployed by R/V Hakuhomaru.
a. including 3 OBSs recovered not on schedule due to premature release.
b. maybe due to fishery work and due to strong water current.
c. including 4 OBSs for explosion studies and one recorverd not on schedule.

Table 2-1 Ocean bottom seismograph arrays

Instrument	Latitude (N)	Longitude (E)	Depth (m)	Recording period (JST)
T3	39°51.6'	144°16.4'	7100	2120 Jul.21 to 0350 Aug.1
P4	40° 0.1'	143°45.1'	0300	0250 Jul.22 to 1200 Aug.1
P6	40°30.0'	144° 0.3'	4400	1340 Jul.22 to 1950 Aug.1
T7	40°25.2'	144°22.3'	7080	1240 Jul.22 to 2100 Aug.1
P10	40°30.5'	145°28.5'	5200	3000 Jul.23 to 2350 Jul.29
T11	40°58.5'	144°49.3'	4200	2150 Jul.23 to 0130 Aug.3
P12	40°40.4'	146°10.9'	5180	0720 Jul.24 to 2100 Jul.29

Table 2-2 Ocean bottom seismograph stations operated in 1980

Ocean bottom seismograph stations

Instrument	Latitude (N)	Longitude (E)	Depth (m)	Recording period * (JST)
P1	39° 45.1′	142° 42.9′	1190	1405 Jun. 10–1930 Jun. 23
P2	39° 24.9′	143° 4.0′	1900	1550 Jun. 11–0900 Jun. 15
P4	40° 07.0′	143° 22.0′	1360	0130 Jun. 11–0700 Jun. 21
P6	39° 27.0′	143° 38.0′	3340	2050 Jun. 9–2140 Jun. 19
P7	39° 45.0′	143° 39.8′	3210	1125 Jun. 11–0420 Jun. 12
P8	40° 02.0′	143° 41.9′	2670	0855 Jun. 11–0730 Jun. 21
T9	40° 26.2′	143° 45.5′	3280	2035 Jun. 10–0935 Jun. 20
P10	39° 52.0′	144° 0.1′	4370	0840 Jun. 10–0330 Jun. 20
P12	39° 54.0′	144° 46.3′	6055	2340 Jun. 8–0005 Jun. 19
P14	39° 59.7′	144° 56.4′	5705	1940 Jun. 8–0045 Jun. 20 **

* Period from bottoming to detachment of OBS.

** Period from launching to retrieval of OBS because of failure of TCG.

Table 2-3 Ocean bottom seismograph stations operated in 1981

Instrument 1982:	Latitude (N)	Longitude (E)	Depth (m)	Recording period# (JST)	Deployment	Retreival
P1	41°10.0'	142°27.9'	1390	1740 Jun.15 to 0030 Jul.11	Jun.15	Jul.12
P2	41°37.5'	142°35.5'	1050	2200 Jun.15 to 0720 Jul.11	Jun.15	Jul.12
P3	40°56.1'	143°07.9'	1770	0340 Jun.16 to 1930 Jul.11	Jun.16	Jul.11
P4	41°31.0'	143°22.0'	1220	0740 Jun.16 to 1740 Jul.11	Jun.16	Jul.11
P5	41°09.1'	143°35.6'	2400	1110 Jun.16 to 1010 Jul.11	Jun.16	Jul.11
P6	41°01.1'	144°06.1'	4700	1440 Jun.16 to 0300 Jul.11	Jun.16	Jul.11
S7 *	40°58.5'	144°48.9'	5200	1820 Jun.16 to 1950 Jun.17	Jun.16	Jul.14
S8 **	40°54.9'	145°04.3'	5400	0230 Jun.17 to 0740 Jun.28	Jun.16	Jul.10
S9 **	40°50.3'	144°51.8'	5800	1130 Jun.17 to 1620 Jul. 2	Jun.17	Jul.10
S11	40°28.1'	144°08.7'	4800	1710 Jun.17 to 2249 Jul. 2	Jun.17	Jul.10
S12***	40°07.6'	144°04.1'	4400	2240 Jun.17 to 0430 Jun.30	Jun.17	Jul. 9
S13***	39°38.4'	143°58.0'	4600	0330 Jun.18 to 1610 Jul. 1	Jun.18	Jul. 9
S14***	39°10.0'	143°52.0'	4900	1050 Jun.18 to 1220 Jul. 1	Jun.18	Jul. 9
S15***	38°35.3'	143°44.3'	4500	1700 Jun.18 to 0820 Jul. 9	Jun.18	Jul. 9

#. Period from bottomong to detachment
*. Failure in release mechanism: not used in the present study.
**. Too noisy record to analyze: not used in the present study.
***. OBS for explosion studies: not used in the present study.

Table 2-4 Ocean bottom seismograph stations operated in the 1982 experiment.

Instrument 1983:	Latitude (N)	Longitude (E)	Depth (m)	Recording period* (JST)	Deployment	Retrieval
S8	42°07.9'	144°46.9'	2120	1410 Jul.14 to 0700 Aug.11	Jul.14	Sep.15
S9	42°21.0'	145°07.1'	2710	0420 Jul.15 to 1750 Aug.12	Jul.14	Sep.15
S11	41°57.0'	145°13.9'	4330	0030 Jul.15 to 1820 Aug.12	Jul.14	Sep.17
S12	41°31.0'	145°11.2'	5420	2050 Jul.15 to 0830 Aug.11	Jul.15	Sep.17
S13	41°12.8'	145°45.2'	6020	0000 Jul.17**	Jul.17	---
SE	41°42.9'	144°45.2'	4010	1920 Jul.14 to 0520 Aug.10	Jul.14	Sep.17
SF	41°24.0'	144°25.9'	3780	1640 Jul.15 to 1120 Aug. 9	Jul.15	Sep.18
SG	41°44.1'	144°15.2'	1820	1430 Jul.15 to 1950 Aug.10	Jul.15	Sep.17
SH	40°55.9'	145°44.3'	5510	1420 Jul.17 to 2010 Aug.14	Jul.17	Sep.16
SJ	41°10.0'	146°09.1'	5570	1130 Jul.17 to 1310 Aug.12	Jul.17	Sep.16

* Period from bottoming to detachment

** Time of deployment because of failure in retreival.

Table 2-5 Ocean bottom seismograph stations operated in 1983

Main shock				Deployment				
Date		Area	M (JMA)	Date (after the shock)		Number of OBSs	Type#	Vehicle
Jun.12	1978	Miyagi-oki	7.4	Jun.29	(17 days)	3	T	Haruna-maru (180 t)
Mar.21	1982	Urakawa-oki	7.1	Mar.29	(8 days)	4	P	Hokushin-maru (17 t)*
Jul.23	1982	Ibaraki-oki	7.0	Aug.14	(22 days)	4	P	Aerospatial SA330J Puma**
Mar.26	1983	Japan Sea	7.7	May.29	(3 days)	5	P	Aerospatial SA330J Puma**

#. T:tethered type OBS; P:timed-release pop-up type.
*. Fishing boat.
**. Helicopter.

Table 2-6 . Observations of aftershocks by an OBS array immediately after the occurrence of the main shock.

3 Data processing of OBS records

3-1 Introduction

The method of direct analogue recording (DAR) has the highest packing density of record among other recording methods, such as frequency modulation recording (FM) and pulse code modulation recording (PCM). If we want to record signals continuously for more than several days, only the DAR method is available. Since records of an OBS generally contain noises which can not be easily distinguished from earthquake signals, we need continuous records to investigate microearthquakes; the event triggered recording has a risk of missing the signals that we really want. Thus, we have used the DAR method for 10-25 days recording. Furthermore, we have to process a large amount of data from an array with many OBSs; for processing the data, we need a special playback system.

The process of playback needs transformation of time axis in the record; data are recorded at an ultra low speed (0.06-0.15 mm/s) and reproduced at a speed of several hundred times of the recording speed. If the reproduction is carried out by an analogue processing, we need a device with a flat frequency response up to more than 10 KHz; an optical oscillograph can realize the flat frequency response. However it requires special recording paper which is not only expensive but also poor lasting quality. Reproduction of records involves a process of choosing earthquake signals from the entire record. This process, which is referred to as an event detection hereafter, has been manually

accomplished so far; to hear the record transformed into audible frequency range by ears. Sometimes a visible monitor record is referred for identification of a particular events. However, such a method costs a great deal of labour, care and time (Kasahara, 1981). Some methods have been tried to process the data in a digital manner using a electronic computer; decoding of a time code, display of a waveform, transformation of the time axis (Katsuyama et al., 1975; Moriya and Takeda, 1979; Kasahara, 1981; Fujii, 1983; Urabe, 1984). However these methods still need the manual processing of identification of earthquakes, reproduction of visual records and filing of waveform data. Since they are clearly inadequate for processing a great number of microeathquake records from an array with many OBSs, it has been hoped to develop an automatic data processinng system.

Following the event detection, measurement of an arrival time of each phase is required, if we want to locate the event. If the signal-to-noise ratio of record is poor, it is very difficult to hold an accuracy of phase-picking in time either manually or automatically. The difficulty can be reduced by comparing records at one station with those at other stations on a common time axis. Such a comparison of records at different stations has been automatically done at present for records from a telemetered seismic array, but not for those from an off-line array. We referred to a set of records arranged on a common time axis as a multi-station record, hereafter. In this section, an automatic playback system for a direct analogue tape recordings from an OBS array is described. The system can produce the multi-station record by digital processing.

It should be emphasized again that special care is required to process the DAR continuous data because the total amount of data is very large (Sugawara et al., 1974). The system developed in the present study, which utilizes a mini-computer with a 78 MB magnetic disk, can realize an automatic processing by a new algorism presented in this chapter.

3-2 A hardware system

A block diagram of the system is shown in Fig. 3-1; the system utilizes a mini-computer (DATA GENERAL, ECLIPSE S/140, a 16-bit CPU with a 256 KB core memory) and a high speed analogue to digital (A/D) convertor.

The most important ability of the present system is its high speed A/D conversion; the minimum sampling interval is 10μs. The A/D convertor has 12-bit resolution and 16 channels of analogue input are available. The convertor works at a speed of 100 K samples/s on writing data in a magnetic disk; the disk has a capacity of 73 MB, in which the waveform data area is 64 MB. To realize the high speed sampling, a special software was made because, in general, we have to avoid those bad areas in the disk which one cannot use.

A 10-channel D/A conversion and analogue outputs are available by using a 3-channel D/A convertor originally installed in the system, an external circuit and a software specially developed in the present study. The system is equipped with a magnetic tape deck (1200 ft, 1600 bpi); about 20 MB records are stored in a tape. A thermal chart recorder with flat frequency

response up to 120 Hz has 8 channels for data and one for a time code signal; this is used to make a visible record.

3-3 Event detection and phase-picking

3-3-1 Flow of process

An outline of the process can be devided into two steps; the first step is filing of waveform data by chooing a part of record which contains an event (Fig. 3-2(a)) and the next is editing of waveform data (Fig. 3-2(b)). Both steps involve transformation of a time axis. The cassette tape record is played back at a tape speed of 4.8 cm/s, which is several hundred times as fast as the recording speed, by a 4-channel tape deck specially designed for OBS records. The signal is recorded by an open-reel tape recorder at 19 cm/s. The open-reel tape is used for further data processing. The record is played back at a speed of 9.5 cm/s, 19 cm/s or 38 cm/s. The compression rate of the time axis on the record corresponding to these speeds is 1/160, 1/320 or 1/640, if the data is recorded for 10 days. A signal of 25 Hz at observation is transformed into 4 KHz, 8 KHz and 16 KHz at playing back with these speeds, respectively.

The first step has two logical blocks: (1) event detection, in a narrow sense, for making an event list and (2) cross-reference of event lists of different stations for distinguishing an earthquake from noises. Both processes are sometimes referred to as event detection in a wide sense. For the

former process (1), a relatively slow speed A/D conversion is carried out for the entire record. A high speed A/D conversion is done for only a part of record wich includes an earthquake. Since the algorism using (1) and (2) has twice A/D conversion, it is referred to as a two-pass approach. As is discussed in the following section, this approach saves computer memories very much.

3-3-2 Event detection and waveform filing

(1) continuous slow A/D conversion and event detection

Since we have to deal with a large amount of data and have only a limitted storage of digital data in the disk, we prefer as slow sampling rate of digitizing as possible. The lower limite of sampling rate is determined by the frequency components contained in the record for avoiding aliasing. OBS records have up to 50 Hz for a 10 days record and 20 Hz for a 25 days record. If we digitize whole the 10 days record with 4 channels at 2x50 samples/sec, we need 350 MWORD (700 MB) per an OBS recording tape. For the detection of events from a record with background noise, however, the entire frequency component is not necessary.

The other constraint comes from decoding of the time code signal recorded on the DAR tape. To read the time code, at least 13 samples/s are needed. The form of signal is corrected in a square wave by an anologue processing before it is fed to A/D convertor. The original waveform of the time code and the corrected one are shown in Fig. 3-3.

In order to reduce the number of samples and to conserve only amplitude information of the signal, the original signal is rectified and low-pass filtered by analogue processing (Sugawara et al., 1974) as shown in Fig. 3-4. A suitable filtering of the signal is needed to enhance the signal-to-noise ratio. Although a cut-off frequency depends on the noise character, usually about 3 Hz high-pass filter is applied before rectification. The envelope of the ground signal and the squre signal of the time code are continuously digitized at a speed of higher than 13 samples/s. About 13.5 days continuous record with two components, the amplitude signal of ground motion and the corrected time code signal, is stored in the disk of the present system at a time.

A short term average (STA) of the signal amplitude and a long term average (LTA) are measured at every instant for the entire record in disk. The average is calculated by the first order recursive filter whose time constant is about 1 s for STA and 500-1000 s for LTA. The STA/LTA ratio is used to detect an event.

We use the 4 parameters Ron, Roff, Toff and Tmin to recognize the event as an earthquake. Ron is a threshold of the STA/LTA ratio for declaring the event starts. Roff is a threshold of the ratio for ending of the event. If the ratio of STA/LTA continues less than Roff during the period Toff, the event is judged to end. The duration time D of the event is the period from the time when the ratio of STA/LTA exceeds Ron to the last time when the ratio becomes less than Roff. If D becomes greater than Tmin, the event is reported as an earthquake on the event list.

An appropriate combination of these parameters selects a set of events which satisfy a desired condition of an earthquake size; Ron and Roff control the lower limit of a signal-to-noise ratio of the record, and Tmin gives an approximate measure of a magnitude of the event, which is useful to reject a spike-like or short duration transient noise.

It takes about 30 minutes to process 13.5 days data in the entire disk. An example of the earthquake event list are shown in Fig. 3-5. The following items are presented in the event list;(1) event number, (2) time of the biginning of the event (day, hour, minute and second), (3) duration time, (4) maximum amplitude, (5) integral of amplitude during the event, (6) decoded identification number of the time code generator, (7) sampling rate which is measured by number of samles in one seconed frame on the record, (8) LTA at at the beginning of the event, (9) and (10) position of that data in disk at which the trigger occured. The event list is used in the next step of processing and also used to output waveforms of all the detected event. The D/A conversion to a 8-channel chart recorder takes only about 20 minites for records of 24 hours in total. The output is used for measurement of S-P times or F-P times.

(2) cross-reference of event lists and high speed A/D conversion

After the event detection for the entire records at all the stations of an array, the event lists are compared with each other to examine the character of the event. An algorism for judging whether the event is an earthquake that we really want to

analyze is schematically shown in Fig. 3-6: An event period determined from the duration time (D) of each station is extended forward and backward by Tpost and Tpre, respectively. If the extended event periods of at least particular number (Nmin) of stations overlap each other, the event is reported in a schedule file for the high speed A/D conversion. A length of the reported event for A/D conversion is determined as shown in Fig. 3-6. An example of the schedule file is shown in Fig. 3-7. Actually, if the separation of two seccessive events is less than a particular period, the two events are connected as one event because of avoiding a dead time in A/D conversion.

A high speed A/D conversion is carried out according to the schedule table which is commonly uesed for all the staions of the OBS array. It takes 90 minites to process the whole data recorded on a C-90 cassette tape. Four channels data in original waveform and a corrected time code signal are fed to the A/D convertor. The system has two processing mode for the automatic A/D conversion; one is the time code decoding mode, in which the computer decodes the corrected time code signal and compares a decoded time with the schedule. In this mode the sampling speed should be as slow as possible because the computer is busy in decoding. If the schedule time has come, the mode is changed to that of high speed sampling. The four channels data can be digitized at the highest speed of 25KHz/channel. If we play back the analogue tape record for 10 days at a speed of 9.5 cm/s, the time axis is compressed at a rate of 1/160 and the corresponding sampling rate converted on recording time is 156Hz. The disk of the present system can store the 14.6 hours 4-channel waveform

data in this case. The difference between the time in the schedule and that at which data is actually sampled is less than a few seconds in time of recording.

The sampled waveform file has index records which is referred to as a record header. The record header is written in ASCII code characters. The contents are the following; (1) event number, (2) time of the biginning of the record, (3) average sampling rate in recording time, (4) amplitude resolution of A/D conversion, (5) block number of data in the disk, (6) number of blocks occupied, (7) number of data in the last block, (8) the identification number of the time code generator, (9) polarity of the time code signal, (10) difference in time of the biginning of the record and that of the schedule. An example of the record header is shown in Fig. 3-8.

The waveform data is stored in a magnetic tape in which the record header file and a file header file are also stored. The file header file has information about whole waveform data such as the name of experiment, the name of station, recording date and so on. In a 1200 ft tape, 20 MB data can be stored. It take 10 minutes to write them by the tape deck used in the present study. The waveform data is used for further processing and they can also transcribed on a 8-channel chart recorder by D/A conversion at speeds of 1-2.5 times as fast as the recording speed depending on the frequency response of the recorder.

3-3-3 Editing of waveform data and phase-picking

The waveform data of all the stations are assembled for each

event with a common time axis (Fig. 3-2(b)). For this process, the sampling interval of all the records should be uniform. The sampling rate of the data recorded by different recorders are different beacuse the recording speeds are not exactly the same among recorders.. Furthermore, even in the data recorded by the same recorder, the sampling rate does not remain constant due to fluctuation of recording and/or playing-back speed. Thus the waveform data are numerically resampled by using the cubic spline function with the time code signals. A new record header is produced by the resampling as shown in Fig. 3-9. It takes 2 hours to uniform the whole record in the 20 MB magnetic tape by the present system.

After the resampling of each record, records of all the station are assembled and rearranged for each event. This process involves correction of the time code signal which is calibrated by a standard clock before and after the field operation. Since a large amount of storage in disk is required, the work is carried out on a large computer (HITAC M200H) in the Computer Center, the University of Tokyo; if we process the data from 5 stations, and if each station has a 20 MB tape data, there are 100 MB input data and also 100 MB output data. The CPU time for the editing of five 20 MB tapes is about 3 s. The output has 20 channels in total with record headerds as shown in Fig. 3-10 in the case of 5 stations. Corrections for the time code signals and inter-channel skews are listed in the header file.

The edited record, that is, a multi-station record is output on the chart recorder by the 10-channel D/A convertor. An example is shown in Fig. 3-11. The advantage of the multi-station record

in idetification of a phase is clear as compared with a single-station record when many successive events occur within a short period as in the example.

3-4 Evaluation

Dependence of the detectability of evnents on the event detection parameters is discussed in terms of actual data. Numbers of events detected by various combinations of SLR (a threshold of STA-to-LTA ratio) and Nmin are shown in Fig. 3-12. The data used in this example is 10 days data at the T3 OBS station in the 1980 experiment. The parameters used for counting the numbers are as follows:

The record was played back at a tape speed of 38 cm/s, and a corrected time code signal and a vertical low gain signal are fed to the A/D convertor. In this case the time length of one second period at recording was 1.533 ms at playing back; the tape speed of playing back is 652 times as fast as the recording speed. A high-pass filter of cut-off frequency of 2.24 KHz (3.4 Hz in recording time) was applied for avoiding low frequency noise. The high-pass signal was rectified and then low-pass filterd with a time constant of 220 us (0.14 s in recording time). The signal is an envelope of the original one as was discussed in 3-3-2. LTA and STA were calculated at every instant of the entire record with a time constant of 1000 s for LTA and 1 s for STA. Both Ton and Toff were set to be 10 s. A ratio of Ron to Roff was fixed to be 1.5.

Then we detected 452 events from the 10 days data at T3 when

Ron (SLRon) was 3. Among them 277 events (61.3%) were detected by at least one more OBS (Nmin=2). Examination of waveforms revealed that the events with Nmin=1 and small SLR (<4) contain both microearthquakes with very small amplitude and transient ground noises. On the contrary, events with Nmin $\geq$ 2 are scarcely noises, although their amplitude may be too small to identify the onset of the signal. The ratio of number of events for Nmin $\geq$ 2 to that for Nmin = 1 is more than 85 % for the events with enough amplitude such as Ron = 5. Thus, although the ratio depends on the distances between OBSs in an array, we can say for this array that the number of events with Nmin = 2 gives an aproximate value of the number of actual eathuakes which can be observed by the OBS. The dependence on Nmin for large SLRon is weak.

About 100 eathquake had enough amplitude to measure thier first arrival times. To make an event set of such earthquakes, for exapmle, we can use parameters Nmin = 5 and SLRon = 5. A relation between D and magnitude M of an earthquake is discussed in chapter 5.

3-5 Discussion

To reduce labor and time in playback of record, we have to process automatically as many parts of processing as possible. For this purpose, the properties of seismic signals and also the noises contained in the record should be ivestigated precisely. The first step for automatic processing is to convert a raw analogue data into a digital waveform data in a well organized format, from which we can produce not only arrival time data for

locating earthquake but also data for investigating characteristics of signals.

The production of waveform records for phase-picking has two logical processes; the event detection and the editing of data. For the event detection, the two-pass approach is employed. This approach has been found to work efficiently.

How to pick up all possible event depends on the properties of earthquakes contained in the record. Exactly speeking, we can know what criterion is optimal for a particulr record only after we have finished the analysis of the record. This is, of cource, unrealistic. Thus our strategy of data processing shoud be much more pragmatic. First rough analysis of the record brings an approximate but total information about the entire record. The next analysis can be more sofisticated by using the knowledge previously obtained. The further analysis goes so on. In the present study, we developed a system which produces the basic data in the well organized format. Furthermore, we realized an automatic playback system for the OBS data of a continuous long term tape record; the process was conventionally performed manually with large amount of time, care and labor. The next step is to improve each algorism of event detection, editing and phase-picking. An analysis in frequency domain, for example, should be employed and an automatic phase-picking from the multi-station record is one of the most important problem remained.

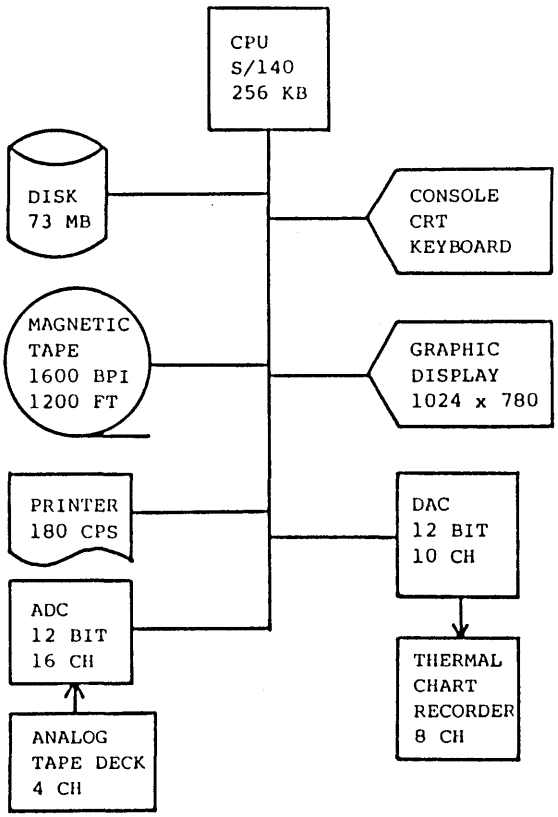

Fig. 3-1 Block diagram of the hardware system.

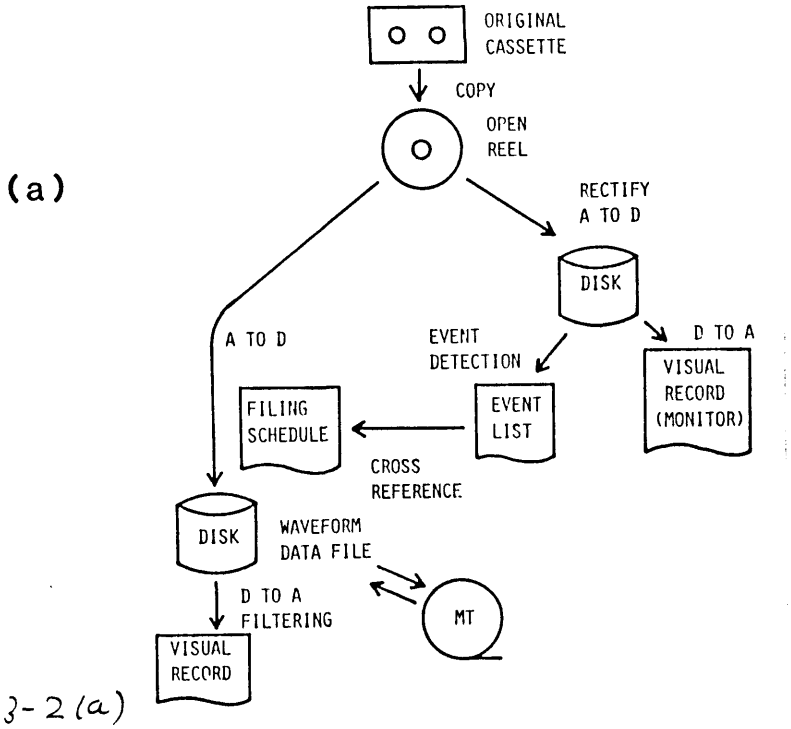

Fig. 3-2 (a)

Flow of data processing (1). From an original analogue cassette tape, a digital waveform data file of earthquakes is created.

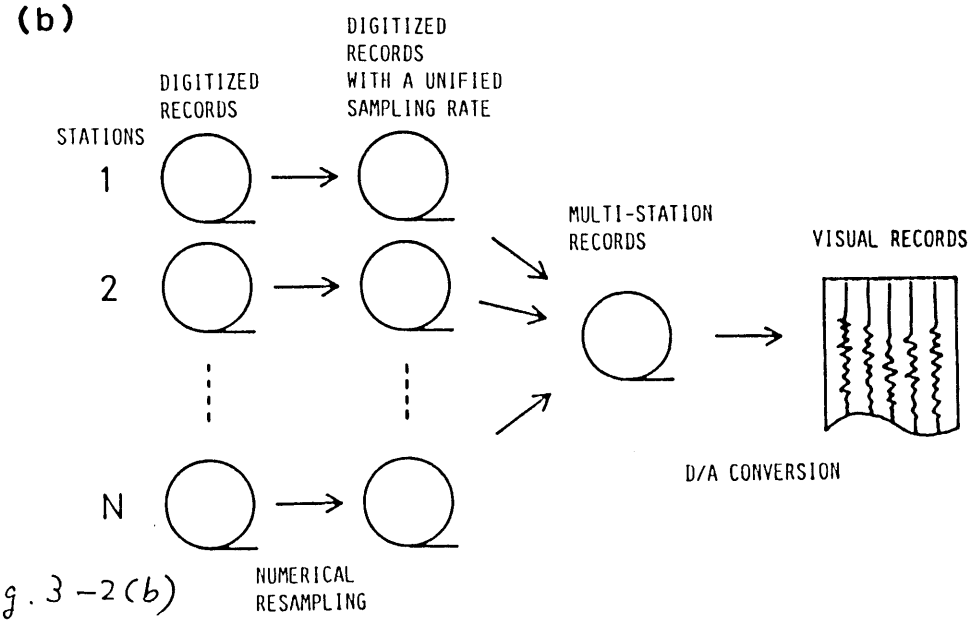

Fig. 3-2 (b)

Flow of data processing (2). The digital waveform data files of all the stations in an OBS network are assembled to make a multi-station file. Visual records are made at last.

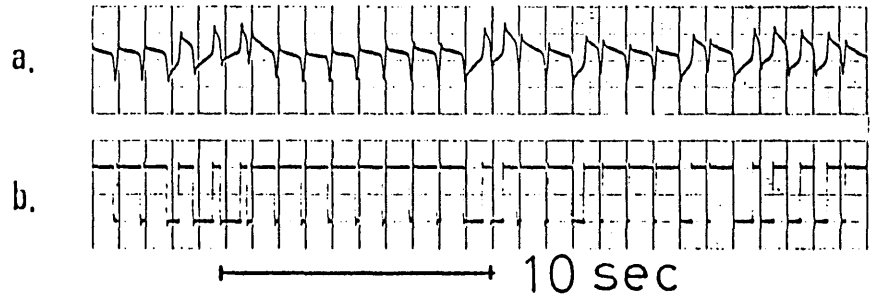

Fig.3-3 (a) An example of a time code signal reproduced from an analogue tape.
(b) Squared signal of (a). This is used to facilitate decoding the time code.

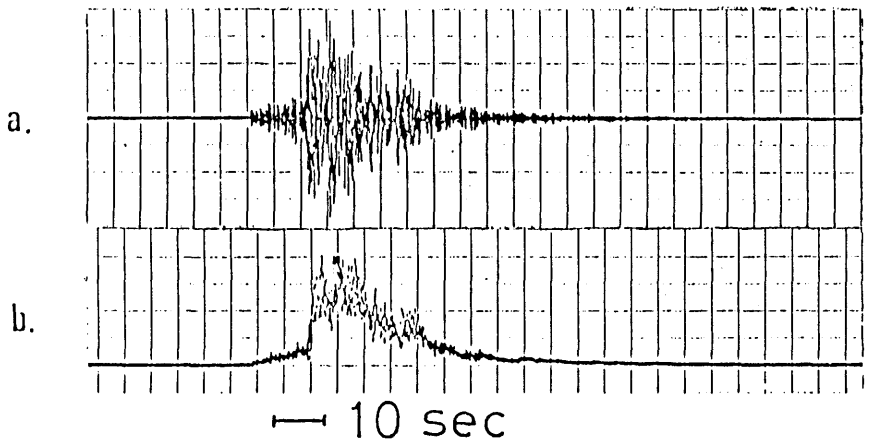

Fig.3-4 (a) An example of a seismogram reproduced from an analogue tape.
(b) Rectified and low-pass filtered signal of (a). The signal is digitized at a low sampling rate for event detection .

(1)	(2)	(3)	(4)	(5)	(6)	(7)	(8)	(9)	(10)
10	16095510	26.8	43.	782.	822401	14.3	14.6	254	84
11	16100955	30.0	107.	1178.	822401	14.4	13.6	260	576
12	16101612	43.2	151.	2011.	822401	14.3	14.0	262	1907
13	16102036	104.1	1009.	17021.	822401	14.3	14.8	264	1624
14	16104901	84.6	96.	2879.	822401	14.3	16.2	276	1657

Fig. 3-5

An example of an event list produced by event detection. Five events are shown. The contents are as follows. (1); event number, (2); time of the beginning of the event (day, hour, minute and second), (3); duration time (s), (4); maximum amplitude, (5); integration of amplitude during the event, (6); identification number of the time code generator, (7); sampling rate (Hz), (8); LTA at the trigger, (9) and (10); block number and data number in which the trigger occurred.

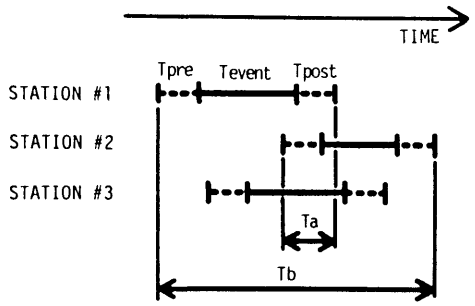

Fig. 3-6

Method of determining an event period by using the event lists of all the stations in an OBS network. Number of the stations are three (named #1, #2 and #3) and Nmin = 3 is assumed. The event periods in the lists are extended backward and forward by Tpre and Tpost, respectively. The period Tb is determined to be an event period of the network because Nmin stations are in event during the period Ta.

(1)	(2)	(3)
19024553	195	1
19032305	108	3
19032835	155	1
19041404	90	3
19045441	113	3

Fig. 3-7

An example of a schedule file for automatic A/D conversion. This is created by cross-referencing the event lists of all stations in an OBS network. Five events are shown. The contents are as follows. (1); time of the beginning of the event (day, hour, minute and second), (2); duration time, (3); gain of A/D converter.

(1)	(2)	(3)	(4)	(5)	(6)	(7)	(8)	(9)	(10)
1	38001635000	105.57	2441	0	9	4096	8201	-1	-4
2	38015615000	105.59	2441	9	9	4096	8201	-1	-3
3	38042443000	105.65	1221	18	9	4096	8201	-1	-3
4	38055309000	105.64	2441	27	9	4096	8201	-1	-1
5	38061615000	105.63	2441	36	9	4096	8201	-1	-2

Fig. 3-8

Examples of record headers produced by automatic A/D conversion. Five records are shown. The contents are as follows. (1); event number, (2); time of the beginning of the record (day, hour, minute, second and milisecond), (3); sampling rate (Hz), (4); amplitude resolution of A/D conversion (uV), (5); block number in the disk, (6); the number of blocks occupied, (7); the number of data in the last block, (8); identification number of the time code generator, (9); polarity of the time code, (10); difference in time of the beginning of the record from that in the schedule.

(1)	(2)	(3)	(4)	(5)	(6)	(7)	(8)	(9)	(10)	(11)	(12)
1	38001636000	100.00	2441	0	9	1632	8201	-1	0	38001635	105.57
2	38015615000	100.00	2441	9	9	2032	8201	-1	0	38015615	105.59
3	38042443000	100.00	1221	18	9	2032	8201	-1	0	38042443	105.65
4	38055310000	100.00	2441	27	9	1632	8201	-1	0	38055309	105.64
5	38061615000	100.00	2441	36	9	1632	8201	-1	0	38061615	105.63

Fig. 3-9 Examples of record headers produced by numerical resampling. The sampling rates are unified. Five headers are shown. The contents are as follows. (1)-(9); the same as the items with the corresponding numbers in Fig.9, (10); error flag at the resampling, (11) and (12); information prior to the resampling (corresponds to the items (2) and (3) in Fig.9, respectively).

	(1)	(2)	(3)	(4)	(5)	(6)	(7)									
	1	38001635602	100.00	5	0	44	672									
*	1	38001636000	100.00	2441	9	1632	8201	-1	0	38001635	105.57	-397	0	0	0	
*	2	38001638000	100.00	2441	8	2128	8006	-1	0	38001638	104.78	-59	0	0	0	
*	3	38001638000	100.00	2441	8	2128	8020	-1	0	38001636	103.97	160	0	0	0	
*	4	38001638000	100.00	2441	9	1632	8212	-1	0	38001636	105.59	8	0	0	0	
*	5	38001637000	100.00	2441	8	2128	8201	-1	0	38001637	105.05	104	0	0	0	
	2	38015614599	100.00	5	44	44	872									
*	1	38015615000	100.00	2441	9	2032	8201	-1	0	38015615	105.59	-400	0	0	0	
*	2	38015615000	100.00	2441	9	2032	8006	-1	0	38015614	104.89	-59	0	0	0	
*	3	38015618000	100.00	2441	8	2128	8020	-1	0	38015618	103.90	161	0	0	0	
*	4	38015617000	100.00	2441	8	1728	8212	-1	0	38015616	105.54	7	0	0	0	
*	5	38015616000	100.00	2441	9	2032	8201	-1	0	38015615	105.02	104	0	0	0	
										(8)		(9)		(10)		

Fig. 3-10 Examples of record headers of multi-station records produced by assembling single-station records. Two headers are shown. The number of stations are five. The contents are as follows. (1)-(3) and (5)-(7); the same as the items with the corresponding numbers in Fig.10, (4); the number of stations, (8); information prior to the assembly (corresponds to the items (1)-(12) in Fig.10 except for the item (5)), (9); correction for the clock (ms), (10); correction for the inter-channel skew (ms).

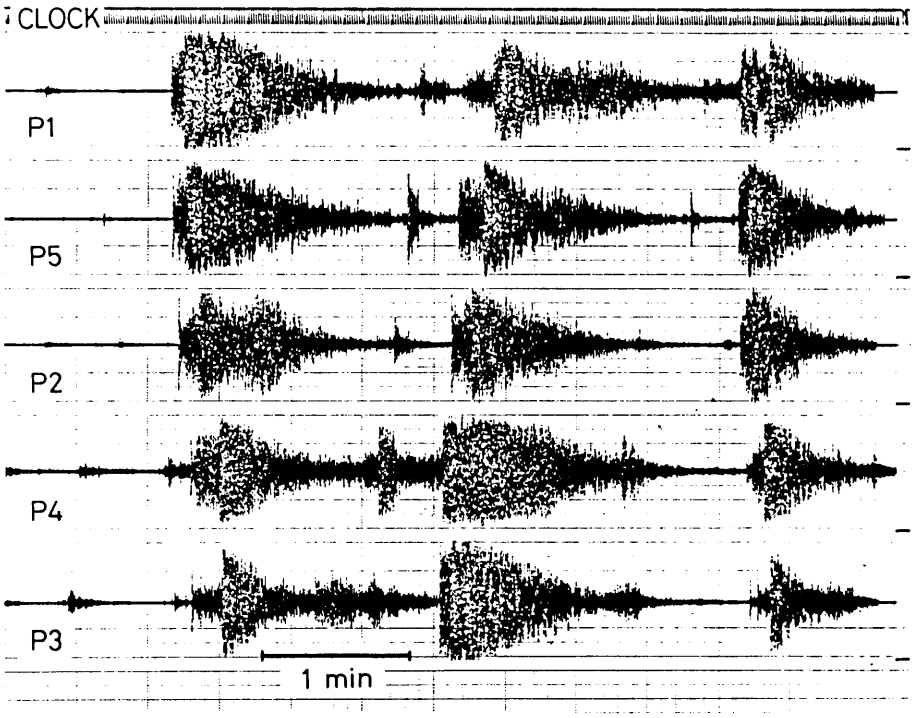

Fig. 3-11

An example of an analogue output of a multi-station record; aftershocks of the 1983 Japan Sea earthquake observed by ocean bottom seismographs. The uppermost trace is a coded clock signal. The lower five traces are the records of the five different stations, P1 to P5.

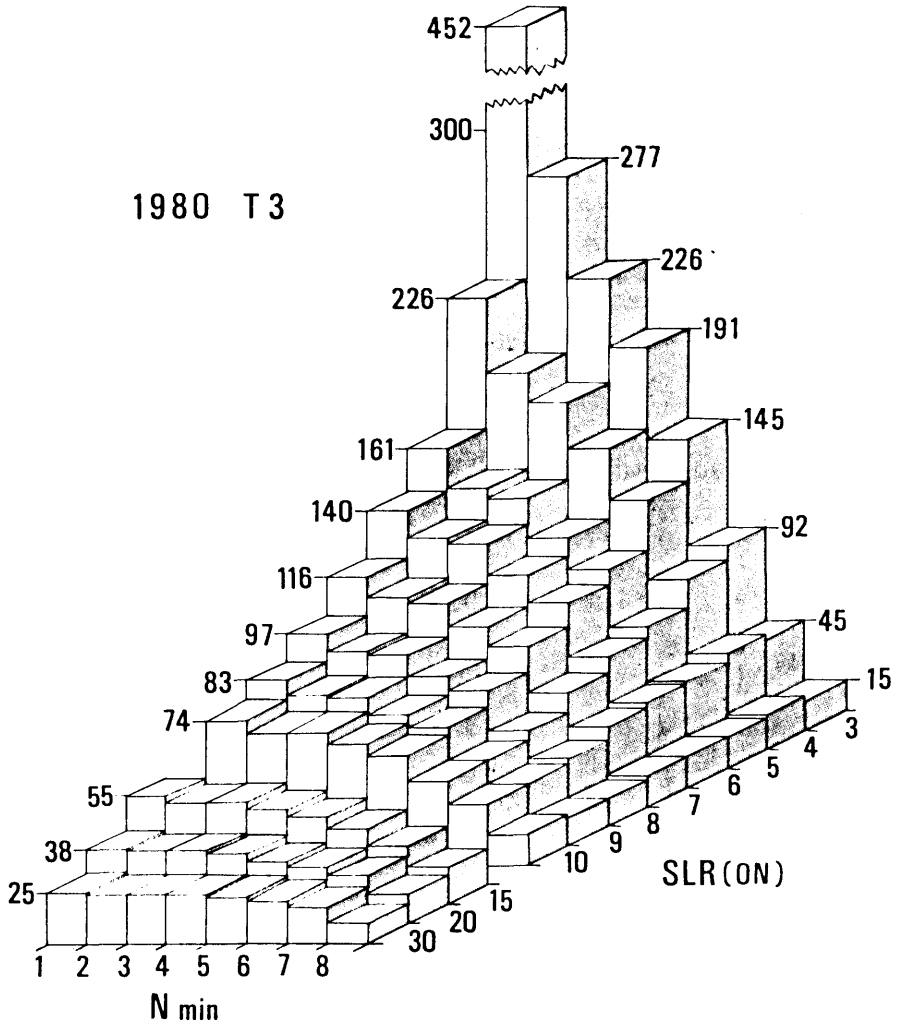

Fig.3-12 Numbers of events detected by various combinations of SLR and Nmin.

4 Hypocenter determination

4-1 Introduction

A method of hypocenter determination is investigated in this chapter. In chapters 1 and 2, we have discussed the necessity of observation near the area concerned. Although the reason seems to be intuitively clear, only quantitative discussion shows how many OBSs are needed for precise location of microearthquakes and how close to the trench area we should deploy OBSs. Actually, we also have a question similar to that in a land seismic network; how far the OBS array can precisely determine location of microearthquakes.

Widely used computer programs of hypocenter ditermination (eg., Bolt, 1960; Herrin et al., 1962; Aki, 1965) employ a least-squares iterative technique described by Jeffreys (1959) and attributed originally to Geiger (1910). Flinn (1965) discussed a method for evaluatting errors involved in solution and developed the theory for confidence regions presented by Geiger (1910). Peters and Crosson (1972) applied the method of prediction analysis by Wolberg (1967) to the evaluation of estimation errors. This method has been used to investigate the capability of earthquake location by an actual seismic network (Ishii and Takagi, 1978).

The analyses show that error involved in hypocenter solution is large outside the network, especially in depth. For events inside or on the border of the network, theoretical estimate of errors gives a reasonable measure of errors actually involved. On

the contrary, the estimate sometimes fails for events outside the network; the theory leads to the underestimation of errors. James et al. (1969) demonstrated by numerical simulation that the error caused by an inadequate station distribution for a particular event located outside the seismic array is much larger than that caused by random errors in data and by the inadequate modeling of a velocity structure. Lilwall and Francis (1978) and Duschenes et al. (1983) investgated the problem for an OBS array with a small number of stations. They showed that the resolving power of the small size array is poor for outside events and that the theory based on the classical least-squares method cannot predict the actual distribution of errors. Further, they pointed out a demerit of the use of a structure model with velocity discontinuities for the problem of hypocenter determination.

The problem of hypocenter determination is one of the most classical inverse problem in seismology. This problem has been investigated by many authors from various points of view: Buland (1976) applied the QR algorism; Bolt (1970) and Jordan and Sverdrup (1981) used the generalized inverse method. Uhrhammer (1980) discussed the resolving power of a small seismic network in terms of the singular value decomposition of a rectangular matrix for a linear system.

In this chapter, to reduce the strong non-linear effect on solving observation equations, we formulate the problem of hypocenter determination with a velocity structure model without discontinuity. And to solve the observation equation, a new inverse theory is developed; a solution is given for the problem of compromise between the estimation error and the resolution of

the estimate. This problem has been the central subject of the inverse theory (Bucks and Gilbert, 1970; Wiggins, 1972; Jackson, 1972; Matsu'ura and Hirata, 1982).

4-2 A generalized inverse technique for hypocenter determination

4-2-1 Quasi-linear inverse problems

In this section we formulate the problem of hypoceter determination in terms of a generalized inverse theory. The velocity structure is modeled such that velocity varies continuously with depth. Further, we assume the problem is qusi-linear with respect to spatial coordinates of a quake focus. The meaning of the term "qusi-linear" will be described later.

The problem of hypocenter determination is to estimate a set of four unkwon parameters, x,y,z and t, from arrival time data, where x and y are horizontal spatial coordinates of a quake focus, z is a focal depth and t is an origin time. Usually we have arrival time of phases at stations whose number is greater than that of unknown parameters. First we define an unknown vector $\mathbf{X}$ which consists of x,y,z and t as

$$\mathbf{X} = \begin{bmatrix} x \\ y \\ z \\ t \end{bmatrix} , \tag{4-1}$$

and a data vector $\mathbf{Y}$ as

$$\mathbf{Y} = \begin{bmatrix} t_1 \\ \vdots \\ t_i \\ \vdots \\ t_n \end{bmatrix} , \tag{4-2}$$

where t_i is an arrival time at the i-th station. Thus, the observation equation can be written in vector form

$$Y=F(X)+N \tag{4-3}$$

where $\mathbb{F}$ are non-linear functions of $\mathbb{X}$ and $\mathbb{N}$ are random noise in data. Since the origin time t is related to $\mathbb{Y}$ in linear form, we can decompose the functions F into two terms;

$$\mathbb{Y} = \mathbb{T}(x, y, z) + t \begin{bmatrix} 1 \\ \vdots \\ 1 \end{bmatrix} + \mathbb{N} . \tag{4-4}$$

Here, the first term is referred to as travel times.

Usually we have rough estimates of spatial coordinates (hypocenter) of an earthquake. Thus expanding $\mathbb{T}$ into a power series around the initial guess (x^0, y^0, z^0) and neglecting the second- and higher order terms of the series, we can obtaine a set of linear observation equations.

The solution of the linear equation gives a correction vector to the initial guess. To solve the linear system we use a linear inverse theory. The solution to the nonlinear system Eq. (4-4) is obtained by the iteration of linear inversion. This iterative procedure can succeed only if the non-linearity of the problem is weak. When the non-linearity is so weak as to permit the linear theory, the problem is referred to as a quasi-linear problem. The assumption of quasi-linearity makes us to pay attention to the

following two points; to use an appropriate initial guess and to use a strucutre model without velocity discontinuity.

4-2-2 Travel time for a medium with a piece-wise constant velocity gradient

In this section we derive a traval time T for the structure model in which velocity varies continuously with depth.

(a) Velocity structure model and coordinate system

The velocity v in the medium is assumed to be a continuous function of depth z. Further, the function is supposed to have a piece-wise positive constant velocity gradient. By rotating a coordinate system around the z-axis, the problem of finding a ray path in a three-dimensional space can be reduced to a two-dimensional problem. The coordinate system in the two-demensional space and notations for the ray path are illustrated in Fig.4-1, where the ray starts at a point A and ends at B.

(b) Decomposition of a ray path into basic ray paths

The ray which has a take-off angle of $\pi/2$ is referred to as the basic ray, hereafter. Any ray path can be decomposed into basic ray paths;

(1) $0 < \theta < \pi/2$

$$\widehat{AB} = \widehat{AD} + \widehat{DB} \quad , \tag{4-5}$$

(2) $\pi/2 < \theta < \pi$

$$\widehat{AB} = \widehat{DB} - \widehat{AD} \tag{4-6}$$

Thus, it is sufficient to consider the basic ray.

(c) Determination of a path of the basic ray

Here we consider the basic ray path as shown in Fig.4-2, where other notations for the medium with layered structure are also shown. The deepest point D is located in the m+1-th layer and the ending point is in the ℓ -th layer. The reference point of the horizontal distance is on z-axis. A horizontal distance X between D and S is a function of d and Z;

$$X = X(d, Z) . \tag{4-7}$$

Under the condition that the velocity gradient is positive in every layer, d is uniquely related to a ray parameter $p = \frac{\sin\theta_s}{V(Z)}$, where θ_s is a take-off angle of the ray at S, as

$$d = v^{-1}(1/p) , \tag{4-8}$$

where v^{-1} is an inverse function of v(z). Thus X is a function of Z and p;

$$X = X(p, Z) . \tag{4-9}$$

The ray path for a particular velocity structure is determined in terms of the geometrical ray theory by Fermart's principle; the geometry of the ray path is determined so as to have a travel time of stationary with variation of the path.
If the velocity is related to the depth z in the i-th layer as

$$v(z) = b_i(z + \alpha_i) \qquad \text{for } z_{i-1} \le z \le z_i \ , \tag{4-10}$$

then the ray path in the i-th layer is an arc,

$$(x - x_i^0)^2 + (z + \alpha_i)^2 = \frac{1}{(p\,z_i)^2} \qquad \text{for } z_{i-1} \le z \le z_i \ , \tag{4-11}$$

where x_i^0 is an integration constant determined by a condition of the starting point of the ray (e.g.,Officer,1958). Thus, the total horizontal distance X between D to S is described in termes of p and Z as

$$X(p, Z) = \sum_{i=1}^{m+1} l_i \ , \tag{4-12}$$

where

$$l_i = m_i - \frac{z_i + \alpha_i}{z_i + \alpha_{i+1}}\, m_{i+1} \ , \tag{4-13}$$

and

$$m_i = \sqrt{\frac{1}{(p\,b_i)^2} - (z_{i-1} + \alpha)^2} \quad . \tag{4-14}$$

To derive Eqs. (4-12), (4-13) and (4-14) we used the continuous condition on the interface (cf.,Eq.(4-34) in 4-2-4).

(d) A ray path between the given two points

To determine the ray path between the given two points A and B, we use so called shooting method of ray tracing; the method is a usual numerical algorithm for solving a non-linear equation. That is,

(1) give an initial guess of a take-off angle (θ) for the ray from A to B.

(2) decompose the ray path into the basic ray path.

(3) calculate a horizontal distance $X(\theta)$ for the assumed ray path by Eqs. (4-12), (4-13) and (4-14).

(4) calculate a redisual ΔX for the horizontal distance as

$$\Delta X = X(\theta) - X(\widehat{AB})$$

(5) if $\Delta X > \varepsilon$, then assume another θ as

$$\theta_{new} = \theta_{old} + \Delta\theta$$

and go to (2);

if $\Delta X < \varepsilon$, then put $\theta(\widehat{AB}) = \theta$, where ε is a certain small value.

To find $\Delta\theta$, we can use Newton's algorithm and the scheme of succesive divisions.

From (AB) determined by iterating (1) through (5), the travel time T(AB) from A to B can be caluculated as

$$T(\widehat{AB}) = \sum_{i=l}^{m+1} t_i \quad , \tag{4-15}$$

where

$$t_i = \frac{1}{2b_i} \ln \left| \frac{(x_{i-1} - x_i^0 + 1/(pb_i))(x_i - x_i^0 - 1/(pb_i))}{(x_{i-1} - x_i^0 - 1/(pb_i))(x_i - x_i^0 + 1/(pb_i))} \right| . \tag{4-16}$$

4-2-3 Linearization and Standardization of the problem

Fisrt we guess most plausible values of unkwown parameters from a priori information. The initial geuss and its uncertanity are referred to as a priori data, hereafter. The most plausible solution prior to observation is denoted by $\mathbb{X}^0$ and its probable error in a statistical sence is by $\mathbb{M}$. When the function $\mathbb{F}(\mathbb{X})$ is quasi-linear, $\mathbb{F}(\mathbb{X})$ can be linearized by expanding at $\mathbb{X} = \mathbb{X}^0$ in a power series and discarding all the second- and higher-order terms as

$$Y = Y^0 + B(X - X^0) + N \tag{4-17}$$

with

$$Y^0 = F(X^0), \qquad B = \text{grad } F(X)|_{X=X^0}, \tag{4-18}$$

where B is a rectangular matrix of n rows and m (=4) columns.

The statistics of the probable error $\mathbb{M}$ in the initial guess and the random noise $\mathbb{N}$ in the data are generally described in terms of an m x m covariance matrix $\mathbb{C}[\mathbb{M}]$ and an n x n covariance

matrix $\mathbb{C}[\mathbb{N}]$, respectively. Since each of these matrices is symmetric and positive definite in itself, they can be rewritten as

$$C\{M\}=W_M\Sigma_M\tilde{W}_M, \qquad C\{N\}=W_N\Sigma_N\tilde{W}_N, \tag{4-19}$$

and then

$$C^{-1}\{M\}=W_M\Sigma_M^{-1}\tilde{W}_M, \qquad C^{-1}\{N\}=W_N\Sigma_N^{-1}\tilde{W}_N, \tag{4-20}$$

where W_M and W_N are orthogonal eigenvector matrices, and Σ_M and Σ_N are diagonal matrices whose nonzero elements are the eigenvalues of $\mathbb{C}[\mathbb{M}]$ and $\mathbb{C}[\mathbb{N}]$, respectively. According to Kaula (1966), we define weighting matrices, $\mathbb{G}$ in the solution space and $\mathbb{E}$ in the data space, by

$$C^{-1}\{M\}=\tilde{G}G, \qquad C^{-1}\{N\}=\tilde{E}E, \tag{4-21}$$

and obtain

$$\left.\begin{aligned} G&=\Sigma_M^{-1/2}\tilde{W}_M, & G^{-1}&=W_M\Sigma_M^{1/2},\\ E&=\Sigma_N^{-1/2}\tilde{W}_N, & E^{-1}&=W_N\Sigma_N^{1/2}. \end{aligned}\right\} \tag{4-22}$$

By using these weigting matrices, the original linear system in Eq.(4-17) is transformed into the standard form;

$$y=y^0+A(x-x^0)+n \tag{4-23}$$

with

$$\left.\begin{array}{lll} x=GX, & x^0=GX^0, & m=GM, \\ y=EY, & y^0=EY^0, & n=EN, \end{array}\right\} \tag{4-24}$$

and

$$A=EBG^{-1}. \tag{4-25}$$

Here, it shoud be noted that the transformed covariance matrices, C[m] and C[n], become unit diagonal,i.e.,

$$C\{m\}=GC\{M\}\tilde{G}=I_m, \qquad C\{n\}=EC\{N\}\tilde{E}=I_n. \tag{4-26}$$

4-2-4 Partial derivatives of the travel time functions $\mathbb{T}$ with respect to spatial coordinates

In this section we derive the explicit form of the coefficient matrix $\mathbb{B}$ whose components consist of partial derivatives of travel time functions $\mathbb{T}$ with respect to spatial coordinates of an earthquake. The purpose is to demonstrate that the partial derivatives are expressed in a compact form regardless of the velocity structure model because a ray path is determined so as to have a minimum travel time. That is, Fermart's principle ensures that the travel time is stationary to small changes of the ray path.

First we will generally describe the problem in terms of the calculus of variations. Next we apply the result obtained to our problem. Let us define a new coordinate as shown in Fig. 4-3. The

travel time along the ray path $\widehat{AB}$ is expressed as

$$T = \int_a^b \frac{1}{v(\xi,\zeta)} \sqrt{1+\zeta'^2}\, d\xi \quad , \tag{4-27}$$

where $v(\xi,\zeta)$ is a velocity function for the medium which is divided into two parts, region 1 and region 2, by a boundary $\zeta = \varphi(\xi)$, and ζ' is the first derivative of ζ with respect to ξ. T can be regarded as a functional $J[\zeta,a,b]$, i.e.,

$$\begin{aligned} J[\zeta,a,b] &= J_1[\zeta_1, a] + J_2[\zeta_2, b] \\ &= \int_a^c F_1[\xi,\zeta_1(\xi),\zeta_1'(\xi)]\, d\xi \\ &\quad + \int_c^b F_2[\xi,\zeta_2(\xi),\zeta_2'(\xi)]\, d\xi \quad . \end{aligned} \tag{4-28}$$

We shall give our attention to all functions $\zeta(\xi)$ which are continuous and differentiable in each region of 1 and 2. At the point on the bounbary, the function ζ_1 is connected to ζ_2. Taking variation of Eq. (4-28), we obtain

$$\delta J[\zeta] = \delta J_1[\zeta_1] + \delta J_2[\zeta_2] \quad , \tag{4-29}$$

with

$$\begin{aligned} \delta J_1[\zeta_1] &= \int_a^c \left[\frac{\partial F_1}{\partial \zeta_1} - \frac{d}{d\xi}\left(\frac{\partial F_1}{\partial \zeta_1'}\right)\right] \delta\zeta_1\, d\xi \\ &+ \left\{ \left.\frac{\partial F_1}{\partial \zeta_1'}\right|_{\xi=c-0} \cdot \delta\gamma + \left(F_1 - \zeta_1' \frac{\partial F_1}{\partial \zeta_1'}\right)\Big|_{\xi=c-0} \cdot \delta c \right\} \\ &- \left\{ \left.\frac{\partial F_1}{\partial \zeta_1'}\right|_{\xi=a} \cdot \delta\alpha + \left(F_1 - \zeta_1' \frac{\partial F_1}{\partial \zeta_1'}\right)\Big|_{\xi=a} \cdot \delta a \right\} , \end{aligned} \tag{4-30}$$

and

$$\delta J_2[\zeta_2] = \int_c^b \left[\frac{\partial F_2}{\partial \zeta_2} - \frac{d}{d\xi}\left(\frac{\partial F_2}{\partial \zeta_2'}\right)\right]\delta\zeta_2 d\xi$$
$$+\left\{\left.\frac{\partial F_2}{\partial \zeta_2'}\right|_{\xi=b} \cdot \delta\beta + \left(F_2 - \zeta_2'\frac{\partial F_2}{\partial \zeta_2'}\right)\Big|_{\xi=b} \cdot \delta b\right\} \qquad (4\text{-}31)$$
$$-\left\{\left.\frac{\partial F_2}{\partial \zeta_2'}\right|_{\xi=c+0} \cdot \delta\gamma + \left(F_2 - \zeta_2'\frac{\partial F_2}{\partial \zeta_2'}\right)\Big|_{\xi=c+0} \cdot \delta c\right\},$$

where

$$\left.\begin{aligned} \delta\alpha &= \delta\zeta_1(a) + \zeta_1'(a)\,\delta a \quad , \\ \delta\beta &= \delta\zeta_2(b) + \zeta_2'(b)\,\delta b \quad , \\ \delta\gamma &= \varphi'(c)\,\delta c \quad . \end{aligned}\right\} \qquad (4\text{-}32)$$

Fermart's principle states that the functional Eq. (4-29) must vanish for the actual ray path under the boundary conditions of $\delta a = \delta b = \delta\alpha = \delta\beta = 0$. In this case the function $\zeta = \zeta(\xi)$ satisfies the following equations,

(i) Euler's equation;

$$\frac{\partial F_i}{\partial \zeta_i} - \frac{d}{d\xi}\left(\frac{\partial F_i}{\partial \zeta_i'}\right) = 0 \quad , \quad i = 1, 2 \, , \qquad (4\text{-}33)$$

(ii) condition of Weierstrass-Erdman;

$$\left(\left.\frac{\partial F_1}{\partial \zeta_1'}\right|_{\xi=c-0} - \left.\frac{\partial F_2}{\partial \zeta_2'}\right|_{\xi=c+0}\right)\varphi'(c)$$
$$+\left\{\left(F_1 - \zeta_1'\frac{\partial F_1}{\partial \zeta_1'}\right)\Big|_{\xi=c-0} - \left(F_2 - \zeta_2'\frac{\partial F_2}{\partial \zeta_2'}\right)\Big|_{\xi=c+0}\right\} = 0 \, . \qquad (4\text{-}34)$$

The first equation is to be used to determine the ray path in each region. From the second condition it is shown that, if the velocity is continuous at the boundary $\zeta = \varphi(\xi)$, the ray path is

connected smoothly at the buoundary; a tangential vector of the ray is continuous at C. Both the equations of (i) and (ii) were used to derive the ray path in 4-2-2. Therefore, for the ray path which satisfy Fermart's principle, the variation of the functional J with respect to the coordinates of end points A and B is

$$\delta J = -\left\{ \left.\frac{\partial F_1}{\partial \zeta_1'}\right|_{\xi=a} \cdot \delta\alpha + \left(F_1 - \zeta_1' \left.\frac{\partial F_1}{\partial \zeta_1'}\right)\right|_{\xi=a} \cdot \delta a \right\} \qquad (4\text{-}35)$$

$$+ \left\{ \left.\frac{\partial F_2}{\partial \zeta_2'}\right|_{\xi=b} \cdot \delta\beta + \left(F_2 - \zeta_2' \left.\frac{\partial F_2}{\partial \zeta_2'}\right|_{\xi=b} \cdot \delta b \right\} .$$

Next we apply this result to the travel time. Since we want to obtain the partial derivatives of the travel time with respect to spatial coordinate of hypocenter A, only the first term in Eq. (4-35) is to be considered. From Eq. (4-27), we have

$$F_1 = \frac{1}{v(\xi,\zeta)} \sqrt{1+\zeta_1'^2} \quad . \qquad (4\text{-}36)$$

Thus, the partials in the - coordinate systems are given by

$$\left.\begin{aligned} \frac{\partial T}{\partial a} &= -\left(F_1 - \zeta' \frac{\partial F_1}{\partial \zeta_1'}\right)\Big|_{\xi=a} = -\left.\frac{1}{v\sqrt{1+\zeta_1'^2}}\right|_{\xi=a} = -\frac{\sin\theta}{v(a,\alpha)} \quad , \\ \frac{\partial T}{\partial \alpha} &= -\left.\frac{\partial F_1}{\partial \zeta_1'}\right|_{\xi=a} = -\left.\frac{\zeta_1'}{v\sqrt{1+\zeta_1'^2}}\right|_{\xi=a} = -\frac{\cos\theta}{v(a,\alpha)} \quad . \end{aligned}\right\} \qquad (4\text{-}37)$$

In our case the velocity function v depends only on z. Therefore we obtain the final expressions in the original three-dimensional coordinate system in Fig. 4-4 as

$$\begin{bmatrix} \frac{\partial T_i}{\partial x_0} \\ \frac{\partial T_i}{\partial y_0} \\ \frac{\partial T_i}{\partial z_0} \end{bmatrix} = \begin{bmatrix} -\frac{\cos\theta_i \sin\theta_i}{v(z_0)} \\ -\frac{\sin\theta_i \sin\theta_i}{v(z_0)} \\ -\frac{\cos\theta_i}{v(z_0)} \end{bmatrix} . \qquad (4\text{-}38)$$

It should be noted that we have derived Eq. (4-38) without any assumption of explicit form of the velocity function v. Thus, without differentiating the travel time either analytically or numerically, we can easily obtain partial derivatives for any velocity model which depends only on z . It is easy to generalize Eq. (4-38) to an equation which is applicable for the structure model whose velocity depends on not only z but also x and y. The continuity condition of velocity throughout the medium ensures that the first derivative of the ray path is continuous on the entire ray. Therefore the partial derivatives are continuous for the medium with velocity varying continuously. This continuity is a necessary condition for the application of the quasi-linear inverse theory to the hypocenter determination problem.

4-3 Generalized least-squares solutions

4-3-1 Generalized inverse matrix $A^{\dagger}$

In order to solve the observation equation Eq.(4-23), we analyze an arbitrary linear system and derive a best solution with the generalized least-squares. The standardized linear

system is to be rewritten as

$$\Delta y = A \Delta x + n \tag{4-39}$$

with

$$\Delta x = x - x^0, \qquad \Delta y = y - y^0, \tag{4-40}$$

According to Lanczos (1961), an arbitrary n x m matrix $\mathbb{A}$ of rank p ($\leq$n,m) can be decomposed into the product of an orthonormal n x n matrix $\mathbb{U}$, a semi-diagonal n x m matrix Λ and a transposed orthonormal m x m matrix $\mathbb{V}$, that is

$$A = U \Lambda \tilde{V} = [U_p | U_0] \left[\begin{array}{c|c} \Lambda_p & O \\ \hline O & O \end{array} \right] \left[\begin{array}{c} \tilde{V}_p \\ \hline \tilde{V}_0 \end{array} \right] = U_p \Lambda_p \tilde{V}_p \tag{4-41}$$

with

$$\left. \begin{array}{ll} U_p = [u_1, \cdots, u_p], & U_0 = [u_{p+1}, \cdots, u_n], \\ V_p = [v_1, \cdots, v_p], & V_0 = [v_{p+1}, \cdots, v_m], \end{array} \right\} \tag{4-42}$$

and

$$\Lambda_p = \begin{bmatrix} \lambda_1 & & 0 \\ & \ddots & \\ 0 & & \lambda_p \end{bmatrix}, \qquad \lambda_1 \geq \lambda_2 \geq \cdots \geq \lambda_p > 0. \tag{4-43}$$

Here, the n-dimensional column vector $\mathbf{u}_i$, the m-dimensional column vector $\mathbf{v}_i$ and the non-zero diagonal elements λ_i are defined by the "coupled eigenvalue equations,"

$$\left. \begin{array}{l} A v_i = \lambda_i u_i \\ \tilde{A} u_i = \lambda_i v_i \end{array} \right\} \qquad (i = 1, \cdots, p), \tag{4-44}$$

for positive eigenvalues, and the "decoupled eigenvalue eqations,"

$$\left.\begin{aligned} Av_i &= 0 \quad (i=p+1, \cdots, m), \\ \tilde{A}u_i &= 0 \quad (i=p+1, \cdots, n), \end{aligned}\right\} \tag{4-45}$$

for zero eigen values. The factorization above is known as a singular value decomposition, and it was developed by Eckart and Young (1939) for general matrices.

Transformations of x, y and $\mathbb{A}$ by $\mathbb{U}$ and $\mathbb{V}$;

$$\left.\begin{aligned} y' &= \tilde{U}y = \begin{bmatrix} \tilde{U}_p y \\ \hline \tilde{U}_0 y \end{bmatrix}, \qquad x' = \tilde{V}x = \left[\begin{array}{c} \tilde{V}_p x \\ \hline \tilde{V}_0 x \end{array}\right], \\ A' &= \tilde{U}AV = \Lambda = \left[\begin{array}{c|c} \Lambda_p & O \\ \hline O & O \end{array}\right], \end{aligned}\right\} \tag{4-46}$$

yield a new linear system equivalent to Eq.(4-39) as

$$y' = \Lambda x', \tag{4-47}$$

or, denoting an arbitrary column vector of m-p components by η,

$$\left.\begin{aligned} y_p' &= \Lambda_p x_p', \\ y_0' &= 0, \qquad x_0' = \eta, \end{aligned}\right\} \tag{4-48}$$

with

$$\left.\begin{aligned} y_p' &= \tilde{U}_p y, \qquad y_0' = \tilde{U}_0 y, \\ x_p' &= \tilde{V}_p x, \qquad x_0' = \tilde{V}_0 x. \end{aligned}\right\} \tag{4-49}$$

These equations show that ,only if the linear system is

well-posed (m=n=p), it has a unique and complete solution. In other cases, the linear system has no unique solution. However, there still exists a unique solution in terms of the generalized least-squares as is discussed later.

From the inverse transformation of Eq.(4-46), we obtaine

$$\left.\begin{aligned} y &= Uy' = U_p y_p' + U_0 y_0' , \\ x &= Vx' = V_p x_p' + V_0 x_0' . \end{aligned}\right\} \tag{4-50}$$

By using the above relations, the residual vector, $r \equiv y - Ax$, can be expressed as

$$r \equiv y - Ax = U_p(y_p' - \Lambda_p x_p') + U_0 y_0' , \tag{4-51}$$

and the squared norm of the redidual vector, $\|r\|^2 = \tilde{r}r$, is given by

$$\|r\|^2 = \|y - Ax\|^2 = \|y_p' - \Lambda_p x_p'\|^2 + \|y_0'\|^2 . \tag{4-52}$$

The least-squares solution, which minimizes $\|r\|^2$, requires

$$x_p' = \Lambda_p^{-1} y_p' \tag{4-53}$$

leaving x_0' free. Thus, we obtain a general expression of the least-squares solution as follows;

$$x = V_p \Lambda_p^{-1} \tilde{U}_p y + V_0 \eta , \tag{4-54}$$

where η is an arbitrary column vector of m-p components.

It should be noticed that the least-squares solution is unique if p=m. When p<m, an aditional condition is required to define a unique solution; the condition is to minimize the squared norm of the solution vector,

$$||x||^2=||\Lambda_p^{-1}\tilde{U}_p y||^2+||\eta||^2 . \tag{4-55}$$

Putting η = 0 in Eq. (4-54), we obtain a unique solution which minimizes both $||r||^2$ and $||x||^2$:

$$\hat{x}=A^{\dagger}y \tag{4-56}$$

with

$$A^{\dagger}=V_p\Lambda_p^{-1}\tilde{U}_p . \tag{4-57}$$

The inverse operator $A^{\dagger}$ was introduced by Lanczos (1961) as the "natural inverse " of matrix A, which is equivalent to the "generalized inverse" of Penrose (1955).

4-3-2 Error analysis

In this section we analyze the linear system Eq. (4-39) in a stochastic framework. Letting H be a linear inverse operator to the problem, the correction vector $\Delta\hat{x}$ is given by

$$\Delta\hat{x}=H\Delta y , \tag{4-58}$$

and then the solution vector $\hat{x}$ is written as

$$\hat{x}=x^0+\Delta\hat{x}=HAx+(I-HA)x^0+Hn \tag{4-59}$$

or, by putting $m=x^0-x$,

$$\hat{x}=x+(I-HA)m+Hn\,. \tag{4-60}$$

The above relations indicate that the estimate $\hat{x}$ depends inevitably on the initial guess x except for the case of HA=I. The covariance matrix of estimation error $\hat{x}$ - x in the standardized system is

$$\begin{aligned} C\{\hat{x}\}&=(I-HA)C\{m\}\widetilde{(I-HA)}+HC\{n\}\tilde{H} \\ &=(I-HA)\widetilde{(I-HA)}+H\tilde{H}\,, \end{aligned} \tag{4-61}$$

supposing that the probale error m in the initial guess and the random noise n in the data are uncorrelated with each other. The first term of the right-hand side of Eq. (4-61) is related to the resolving error resulting from the error in the initial guess, and the second term to the random error from the noise in the data. The matrix is referred to as the total covariance matrix (Jackson, 1979).

Now we take the generalized inverse A^+ of the coefficient matrix A as the linear inverse operator H. Denoting the rank of A by p ($\leq$ n,m), the generalized inverse A^+ produces the correction vector,

$$\Delta\hat{x}_p=A^+\Delta y=V_p\Lambda_p^{-1}\tilde{U}_p\Delta y\,. \tag{4-62}$$

The solution vector and corresponding total covariance matrix are respectively given by

$$\hat{x}_p = Rx + (I-R)x^0 + A^{\dagger}n \tag{4-63}$$

and

$$C\{\hat{x}_p\} = (I-R)\widetilde{(I-R)} + A^{\dagger}\tilde{A}^{\dagger} \tag{4-64}$$

with

$$R = A^{\dagger}A = V_p\tilde{V}_p . \tag{4-65}$$

Here, $\mathbb{R}$ is the resolution matrix introduced by Wiggins (1972). It shoud be noticed that the resolution matrix is unit diagonal if and only if p = m.

The total covariance matrix in Eq.(4-64) can be rewritten in the following form;

$$\begin{aligned} C\{\hat{x}_p\} &= I - V_p\tilde{V}_p + V_p\Lambda_p^{-2}\tilde{V}_p \\ &= V_0\tilde{V}_0 + V_p\Lambda_p^{-2}\tilde{V}_p , \end{aligned} \tag{4-66}$$

or

$$C\{\hat{x}_p\} = VD_p\tilde{V} \tag{4-67}$$

with

$$V = [V_p|V_0] , \qquad D_p = \left[\begin{array}{c|c} \Lambda_p^{-2} & O \\ \hline O & I_{m-p} \end{array}\right] . \tag{4-68}$$

From Eq.(4-66), it is directly found that the noise in the data is active in the Vp-space, while the error in the initial guess

is in the V_0 -space.

The solution produced by the generalized inverse operator A^+ may be regarded as a straightforward extention of the classical least-squares solution. Actually, it minimizes the sum of squares of residuals. For simplicity, we refer to this solution as the "least-squares solution" hereafter. It is clear from the present error analysis that when the coefficient matrix A has a very small eigenvalue, the estimation error becomes tremendously large, and so the least-squares solution losses any physical meaning.

4-3-3 A generalized least-squares solution

The smallest non-zero eigenvalues in Eqs. (4-66), (4-67) and (4-68) sometimes becomes very small in the problem of hypocenter determination. A sensible way to suppress the estimation error so that the solution has a physical meaning is to reconstruct the inverse operator out of the q ($\leq$p) largest eigenvalues and the corresponding eigenvectors in the generalized inverse. To determine the effective number q of degrees of freedom in data, for example, Wiggins (1972) and also Jackson (1972) set a threshold on the eigenvalues such that

$$\sum_{j=1}^{q} (V_{ij}/\lambda_j)^2 \leq \sigma_i^2 \qquad (i=1, \cdots, m), \tag{4-69}$$

where the left-hand side corresponds to the variance of estimate which results from the random noise in data, and the right-hand

side to a maximum allowable variance determined a priori from our requirement for definiteness in the solution. In their formalism, the effect of non-uniqueness due to poor resolution is not strictly taken into account. Thus there remains ambiguity in the determination of the effective number.

In our formalism, the ambiguous problem can be reduced to the definite problem of minimizing that determinant of the covariance matrix which is a measure of the extent of errors in the solution; effective number q is determined as the result of the minimization. A practical approach is as follows:

We consider a linear inverse operator which is constructed out of the k ($0 \leq k \leq p$) largest eigenvalues and the corresponding eigenvectors in the generalized inverse. For the solution $\hat{\mathbf{x}}_k$ produced by this operator, the determinant of the covariance matrix is calculated by

$$s_k^2 \equiv |C\{\hat{\mathbf{x}}_k\}| = \prod_{i=1}^{k} 1/\lambda_i^2 \tag{4-70}$$

with

$$C\{\hat{\mathbf{x}}_k\} = \boldsymbol{V}\boldsymbol{D}_k\tilde{\boldsymbol{V}}, \tag{4-71}$$

It should be noted that the determinant of the covariance matrix $\mathbb{C}[\hat{\mathbf{x}}_k]$ is equivalent to the determinant of the matrix $\mathbb{D}_k$ because of the orthogonality of $\mathbb{V}$. Suppose that the p positive eigenvalues are arranged in

$$\lambda_1 > \lambda_2 > \cdots > \lambda_q \geq 1 > \lambda_{q+1} > \cdots > \lambda_p > 0 . \tag{4-72}$$

Then, a function s of the parameter k takes a minimum at k=q ($0 \leq q \leq p$), i.e.,

$$(s_k^2)_{\min} = s_q^2 = \prod_{i=1}^{q} 1/\lambda_i^2 \leq 1 . \tag{4-73}$$

This indicates that the minimizationof the determinant of the covariance matrix is realized by mearly truncating those eigenvalues which are smaller than unity.

Adopting the integer q as the effective number of degrees of freedom in data, a best linear inverse operator is defined by

$$A_q^{\dagger} = V_q \Lambda_q^{-1} \tilde{U}_q . \tag{4-74}$$

The inverse operator $\mathbb{A}_q^{\dagger}$ produces the correction vector,

$$\Delta \hat{x}_q = A_q^{\dagger} \Delta y , \tag{4-75}$$

and the solution vector and the corresponding covariance matrix are respectively written as

$$\hat{x}_q = A_q^{\dagger} A x + (I - A_q^{\dagger} A) x^0 + A_q^{\dagger} n \tag{4-76}$$

and

$$C\{\hat{x}_q\} = V D_q \tilde{V} \tag{4-77}$$

with

$$D_q = \left[\begin{array}{c|c} \Lambda_q^{-2} & O \\ \hline O & I_{m-q} \end{array}\right] . \tag{4-78}$$

According to Matsu'ura and Hirata (1982), we refer to the solution as the "generalized least-squares solution" hereafter, to distinguish it from the least-squares solution in Eq.(4-63). The solution and covariance matrix in the original system is

$$\Delta\hat{X}_q=G^{-1}\Delta\hat{x}_q\,,\qquad \hat{X}_q\equiv X^0+\Delta\hat{X}_q=G^{-1}\hat{x}_q\,, \tag{4-79}$$

and

$$C\{\hat{X}_q\}=G^{-1}C\{\hat{x}_q\}\tilde{G}^{-1}\,. \tag{4-80}$$

If we assume the Gaussian distribution both for the probable error $\mathbb{M}$ in the initial guess and the random noise $\mathbb{N}$ in the data, a confidence region for the solution is defined by an inequality,

$$\widetilde{(X-\hat{X}_q)}C^{-1}\{\hat{X}_q\}(X-\hat{X}_q)\leq\gamma^2\,, \tag{4-81}$$

which represents the region enclosed by a generalized second-order surface (hyperellipsoide) in the m-dimensional solution space. If $\gamma=1$, Eq. (4-81) gives a confidence region corresponding to one standard error, if $\gamma=2$, that to two standard errors and so on.

The m-dimensional volume $\mathbb{L}^m(\hat{\mathbb{X}}_q)$ of the confidence region is evaluated by

$$L^m(\hat{X}_q)=\kappa|C\{\hat{X}_q\}|^{1/2}=\kappa|C\{\hat{x}_q\}|^{1/2}|C\{M\}|^{1/2} \tag{4-82}$$

with

$$\kappa=\gamma^m\times\begin{cases}\dfrac{\pi^{m/2}}{(m/2)!} & (m \text{ is even}),\\ \dfrac{\pi^{(m-1)/2}2^m((m-1)/2)!}{m!} & (m \text{ is odd}).\end{cases} \tag{4-83}$$

Denoting the m-dimensional volume of the confidence region of the initial guess by $\mathbb{L}^m(\mathbb{X}^\circ)$, we obtain

$$L^m(\hat{X}_q)=s_q L^m(X^0)\leq L^m(X^0), \tag{4-84}$$

where it is noticed that the factor s_q, which is defined in Eq. (4-73), represents a contraction rate of the confidence region. Namely, the generalized inverse process always decreases the confidence region.

4-3-4 Comparison with a minimum variance solution

The least-squares solution and the generalized least-squares solution are compared with a minimum variance solution in terms of the variance and the residual. First we define the minimum variance solution presented by Jackson (1979) in our notations.

Consider a set of the obseved data equations and the a priori data equations in the standardized system, i.e.,

$$\left.\begin{aligned} y&=Ax+n\\ x^0&=x+m\end{aligned}\right\} \tag{4-85}$$

with

$$C\{m\}=I_m, \qquad C\{n\}=I_n, \tag{4-86}$$

where x^0 is the initial guess obtained from a priori data, and m and n indicate the probable errors in the initial guess and the random noise in the observed data, respectively. Rewriting Eq.(4-85) as

$$\left.\begin{aligned} \Delta y &= A\Delta x + n \\ 0 &= \Delta x + m \end{aligned}\right\} \tag{4-87}$$

with

$$\Delta x = x - x^0, \qquad \Delta y = y - y^0, \qquad y^0 = Ax^0, \tag{4-88}$$

and combining these two linear systems, we obtain a matrix equation to be solved as follows,

$$\begin{bmatrix} \Delta y \\ 0 \end{bmatrix} = \begin{bmatrix} A \\ I \end{bmatrix} \Delta x + \begin{bmatrix} n \\ m \end{bmatrix}. \tag{4-89}$$

Since the above linear system is essentially over-determined, we may apply the classical least-squares procedure to solve it. Denoting the inverse operator by $\mathbb{H}$, and the correction vector by $\Delta\hat{x}_m$, the result is given by

$$H_m = (\tilde{A}A + I)^{-1}[\tilde{A} | I_m], \tag{4-90}$$

and

$$\Delta\hat{x}_m = H_m \begin{bmatrix} \Delta y \\ 0 \end{bmatrix} = (\tilde{A}A + I)^{-1}\tilde{A}\Delta y. \tag{4-91}$$

Thus the solution vector $\hat{x}_m$ and the covariance matrix of estimation error $\hat{x}_m - x$ are written as

$$\hat{x}_m = x + (\tilde{A}A + I)^{-1} m + (\tilde{A}A + I)^{-1} \tilde{A} n \tag{4-92}$$

and

$$C\{\hat{x}_m\} = (\tilde{A}A + I)^{-1} . \tag{4-93}$$

In the special case of $x^0 = 0$, as pointed out by Jackson (1972), the solution Eq.(4-92) is formally identical to the best linear solution of Franklin (1970) which minimizes the total variance in Eq.(4-61). For this reason, we refer to the solution in Eq. (4-92) as the "minimum variance solution" hereafter.

Decomposing the covariance matrix $\mathbb{C}[\hat{x}]$ and the residual vector $r = y - A\hat{x}$ into standard form,

$$\left.\begin{aligned} C\{\hat{x}\} &= V D \tilde{V} , \\ r &= U S \tilde{U} \Delta y , \end{aligned}\right\} \tag{4-94}$$

the matices $\mathbb{D}$ and $\mathbb{S}$ are expressed as follows: for the least-squares solution $\hat{x}_p$,

$$D_p = \left[\begin{array}{c|c} \Lambda_p^{-2} & O \\ \hline O & I_{m-p} \end{array}\right], \qquad S_p = \left[\begin{array}{c|c} O_p & O \\ \hline O & I_{n-p} \end{array}\right], \tag{4-95}$$

for the generalized least squares solution $\hat{x}_g$,

$$D_q=\left[\begin{array}{c|c} \Lambda_q^{-2} & O \\ \hline O & I_{m-q} \end{array}\right], \qquad S_q=\left[\begin{array}{c|c} O_q & O \\ \hline O & I_{n-q} \end{array}\right], \tag{4-96}$$

and for the minimum variance solution $\hat{x}_{mv}$,

$$D_m=\left[\begin{array}{c|c} (\Lambda_p^2+I_p)^{-1} & O \\ \hline O & I_{m-p} \end{array}\right], \qquad S_m=\left[\begin{array}{c|c} (\Lambda_p^2+I_p)^{-1} & O \\ \hline O & I_{n-p} \end{array}\right]. \tag{4-97}$$

The above expressions clarify properties of each solution. That is, the generalized least-squares solution tends to the least-squares solution when the effective number q approaches to p (=m), and these solutions agree completely with each other if q=p. On the other hand, the minimum variance solution also tends to the least-squares solution when q approaches p, but they never agree with each other even if q=p. Here, it should be noted that the effective number q approaches p if the a priori constraints on model parameters become weak. When the a priori constraints are infinitely weak ($\mathbb{C}[\mathbb{M}]\to\infty\mathbb{I}$), the minimum variance solution agrees with the least-squares solution and also the generalized least-squares solution.

4-3-5 Succesive iteration of linear inversion

In quasi-linear inverse problems, model parameters are optimized by the successive iteration of linear inversion. At the k-th ($k\geq 2$) step of the successive iteration, the starting model $X^{(k-1)}$ is given by the estimate $\hat{X}^{(k-1)}$ of one step earlier. The statistics of its probable error $\mathbb{M}^{(k-1)}=\hat{X}^{(k-1)}-X$ is expressed by the

covariance matrix of the previous step,i.e.,

$$\left.\begin{aligned} X^{(k-1)}&=\hat{X}^{(k-1)}, \\ C\{M^{(k-1)}\}&=C\{\hat{X}^{(k-1)}\}. \end{aligned}\right\} \tag{4-98}$$

Now the probable error $\mathbb{M}^{(k-1)}$ in the starting model statistically depends on the random noise $\mathbb{N}$ in data; the covariance matrix of estimate in the k-th step includes the cross term of $\mathbb{M}^{(k-1)}$ and $\mathbb{N}$.

In the original system, for example, the estimate of the second step and the corresponding covariance matrix are written as follows;

$$\hat{X}^{(2)}=X+(I-B_{(2)}^{\dagger}B_{(2)})(\hat{X}^{(1)}-X)+B_{(2)}^{\dagger}N, \tag{4-99}$$

and

$$\begin{aligned} C\{\hat{X}^{(2)}\}=&(I-B_{(2)}^{\dagger}B_{(2)})C\{M^{(1)}\}\widetilde{(I-B_{(2)}^{\dagger}B_{(2)})} \\ &+B_{(2)}^{\dagger}C\{N\}\tilde{B}_{(2)}^{\dagger}+(I-B_{(2)}^{\dagger}B_{(2)})B_{(1)}^{\dagger}C\{N\}\tilde{B}_{(2)}^{\dagger} \\ &+B_{(2)}^{\dagger}C\{N\}\tilde{B}_{(1)}^{\dagger}\widetilde{(I-B_{(2)}^{\dagger}B_{(2)})} \end{aligned} \tag{4-100}$$

with

$$\left.\begin{aligned} B_{(1)}&=E^{-1}AG, & B_{(1)}^{\dagger}&=G^{-1}A_{q_1}^{\dagger}E, \\ B_{(2)}&=E^{-1}A'G', & B_{(2)}^{\dagger}&=G'^{-1}A_{q_2}'^{\dagger}E, \end{aligned}\right\} \tag{4-101}$$

and

$$C\{M^{(1)}\}=C\{\hat{X}^{(1)}\}=(I-B_{(1)}^{\dagger}B_{(1)})C\{M\}\widetilde{(I-B_{(1)}^{\dagger}B_{(1)})}+B_{(1)}^{\dagger}C\{N\}\tilde{B}_{(1)}^{\dagger}, \tag{4-102}$$

where the matrices $\mathbb{E}$ and $\mathbb{G}$ are the same as those in Eq. (4-21), and $\mathbb{G}'$ indicates the new weighting matrix defined by

$$C^{-1}\{M^{(1)}\}=\tilde{G}'G' . \tag{4-103}$$

In Eq.(4-100), the third and fourth terms correspond to the cross term of $M^{(1)}$ and N.

Substituting the following expressions of A, A_{g1}^{+}, A', $A_{g2}^{'+}$, and G',

$$\left.\begin{aligned} A&=U\Lambda\tilde{V}, \quad & A_{q_1}^{\dagger}&=V_{q_1}\Lambda_{q_1}^{-1}\tilde{U}_{q_1}, \\ A'&=U'\Lambda'\tilde{V}', \quad & A_{q_2}^{'\dagger}&=V'_{q_2}\Lambda'^{-1}_{q_2}\tilde{U}'_{q_2}, \end{aligned}\right\} \tag{4-104}$$

and

$$G'=D_{q_1}^{-1/2}\tilde{V}G, \tag{4-105}$$

into Eqs.(4-100,101), the covariance matrix can be rewritten in a simple form,

$$C\{\hat{X}^{(2)}\}=G'^{-1}V'D'_{q_2}\tilde{V}'\tilde{G}'^{-1}, \tag{4-106}$$

where

$$D'_{q_2}=\left[\begin{array}{c|c} D'_{11} & D'_{12} \\ \hline D'_{21} & D'_{22} \end{array}\right] \tag{4-107}$$

with

$$\left.\begin{aligned} D'_{11}&=\Lambda'^{-2}_{q_2}, \quad & D'_{22}&=I_{m-q_2}, \\ D'_{12}&=\tilde{D}'_{21}=[\Lambda'^{-1}_{q_2}\tilde{U}'_{q_2}U_{q_1}|O]V_0' . \end{aligned}\right\} \tag{4-108}$$

Then the determinant of the covariance matrix is evaluated as

$$|C\{\hat{X}^{(2)}\}|=|D'_{q_2}||C\{M^{(1)}\}| \tag{4-109}$$

with

$$|D'_{q_2}|=|D'_{11}||D'_{22}-D'_{21}D'^{-1}_{11}D'_{12}|\,. \tag{4-110}$$

Here, it should be noted that the matrix product $\mathbb{D}'_{21}\mathbb{D}'^{-1}_{11}\mathbb{D}'_{12}$ can be expressed by using the eigenvector matrices as

$$D'_{21}D'^{-1}_{11}D'_{12}=\tilde{V}'_0\left[\begin{array}{c|c}\tilde{U}_{q_1}U_{q_2}\tilde{U}_{q_2}U_{q_1} & O\\ \hline O & O_{m-q_1}\end{array}\right]V'_0\,. \tag{4-131}$$

When the problem is linear, the original coefficient matrix in the second step is exactly the same as that in the first step, and so the above process does not affect the solution at all. When the problem is nonlinear but weakly nonlinear, that is $\mathbb{B}_{(2)}\approx\mathbb{B}_{(1)}$, the singular value decomposition of the standardized coefficient matrix A' in the second step becomes

$$A'\approx U\Lambda' I\,. \tag{4-112}$$

Then, from the comparison of the above expression with Eq.(4-104), we obtain the approximate relation of $\mathbb{U}'\approx\mathbb{U}$ and $\mathbb{V}'\approx\mathbb{I}$. This indicates that the effects of the cross term $\mathbb{D}'_{12}$ and $\mathbb{D}'_{21}$ are negligible, and so the matrix $\mathbb{D}'_{\beta 2}$ in Eq.(4-106) may be replaced by the diagonal matrix $\mathbb{D}_{\beta 2}$ in Eq. (4-78), if the nonlinearity is weak.

In a case of the weak nonliniearity, discarding the cross term of the probable error in the starting model and the random noise in data, the generalized inversion at each step of the successive iteration is carried out in the same way as describe in the previous sections. Since the generalized inversion always reduce the confidence region for the solution, the iteration yields

$$L^m_{\min} \leq \cdots \leq L^m(\hat{X}^{(k)}_{q_k}) \leq L^m(\hat{X}^{(k-1)}_{q_{k-1}}) \leq \cdots \leq L^m(X^0) \tag{4-113}$$

with

$$L^m(\hat{X}^{(k)}_{q_k}) = s_{q_k} L^m(\hat{X}^{(k-1)}_{q_{k-1}}) , \tag{4-114}$$

where $\mathbb{L}^m_{min}$ indicates the m-dimensional volume of confidence region. The effective number q decreases step by step as the confidence region contracts; the contraction rate s_q approaches to unity exponentially (Fig.4-5). In fact, $q \approx m$ and $s_q \ll 1$ if the confidence region for a starting model is extremely large, while $q \approx 0$ and $s \approx 1$ if the confidence region is very small. Therefor, we can use the contraction rate s to judge the convergence of the iteration process. Denoting a certain threshold by ε, the convergence criterion is given by

$$1 - s_q < \varepsilon . \tag{4-115}$$

4-4 Numerical examples

The generalized least-squares solution is applied to the hypocenter determination. As was discussed in the previous sections, the solution is controlled by both the data and the initial guess if the resolving power of the data set is poor. In this section, by some numerical simulations, the dependence of spatial distribution of stations and initial guesss on the solution is discussed.

Figure 4-6 shows locations of stations which recieve signals from three earthquake whose epicenter are located at C with depths at 10, 30 and 60 km. First we calculate travel times for each station using a velocity structure as shown in Fig.(4-7). We use those calculated travel times as data to which random errors with a mean of 0 s and a standard deviation of 0.05 s are added. The initial guess of epicenter is located at a few tens km from the true solution. Errors in the initial guess is set as the same order of magnitude as that of the difference between the initial and the true value; 5 s for an origin time, 25 km for an epicenter and 30 km for an depth.

Results of hypocenter determinations by the method presented in this chapter are shown in Figs.(4-8) and (4-9) with different combinations of stations used in calculation. From these examples, the dependences of the array configuration and the initial guess are clear; if the stations are distributed poorly in azimuthal coverage, the resolving power of the arrival time data is poor and then the solutions strongly depend on the initial guess.

Figures 4-10, 4-11,4-12 and 4-13 show the process of successive iteration with the contraction of confidence regions. The confidence regions are defined by the total covariance matrices in Eq.(4-81) with γ=1. A projection of the hyperellipsoid for one standard error onto a particular plane is represented by a ellipsis, which is referred to as an error ellipsis hereafter. On each plane of these figures, successive steps of linear inversion for the weak nonlinear problem are displayed by error ellipses; cross terms in Eq.(4-106) are not taken into acount as was discussed in 4-3-5.

4-5 Discussion

The problem of hypocenter determination was investegated in a framework of the generalized inverse theory. We have developed the theory and derived a new solution for the least-squares problem with a priori information. To derive the solution, a new criterion has been introduced. The criterion eliminates ambiguity in determinating the effective number q of degrees of freedom in data; the presented criterion is to minimize the determinant of the total covariance matrix. The theory provides a basis on the "sharp cutoff approach" of Wiggins (1972) and Jackson (1972). On the other hand, the minimum variance solution of Franklin (1970) and Jackson (1972), which gives another generalization of the classical theory, provides a theoretical basis on the "tapered cutoff approach" of Levenberg (1944) and Marquardt (1968). These two solutions, the generalized least-squares solution and the minimum variance solution, agree with each other if the a priori

constraints on model parameters are infinitely weak.

The present theory revealed that an ill-posed linear system can be reduced to a well-posed system if we employ sufficient a priori information about unknown parameters. In other word, if we have data which has poor resolving power, we can know only those solutions which depend strongly on the initial guess.

We have applied the generalized least-squares solution to the problem of locating earthquakes in terms of the quasi-linear inverse theory. A computer program has been developed for a velocity model varying continuously with depth; the program can automatically control compromise between errors due to random noise in data and those due to poor resolution.

Investigations of the resolving power of data in the problem of hypocenter determination is quite important; sice we analyze as many event as possible, we have to locate those small events whose signals are detected by only three or four stations in the array. Thus, the effective configuration of the array does not remain constant. Therefore, we have to estimate resolution of each data on locating events. Application of the method to actual OBS data is discussed in the following chapters.

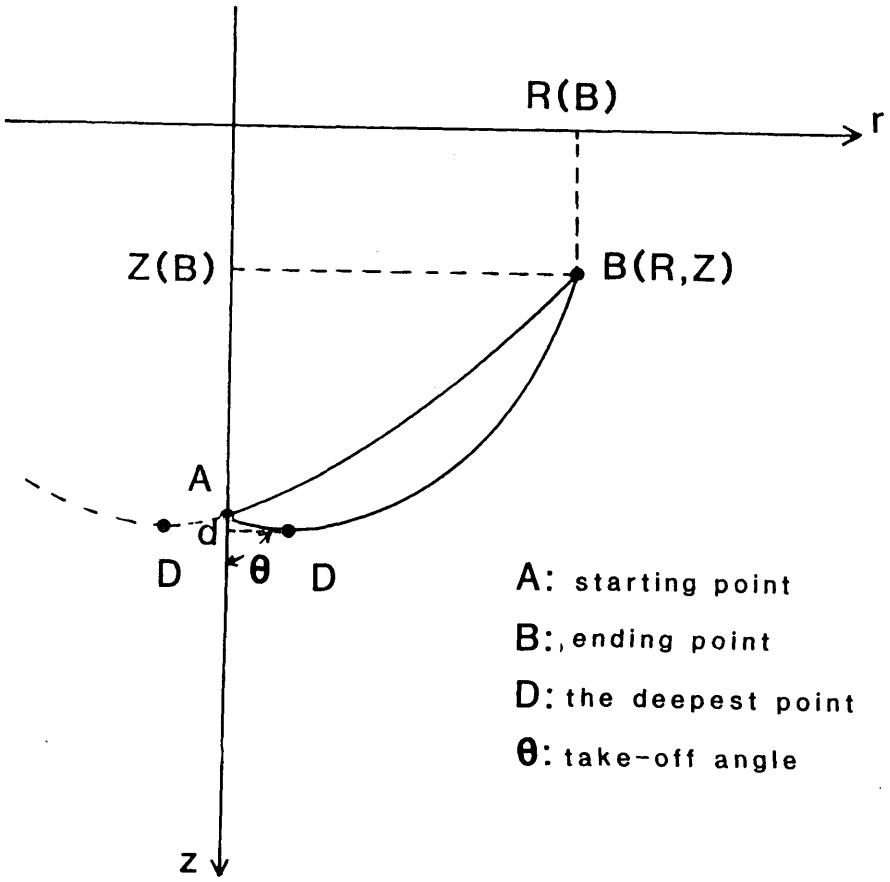

Fig.4-1 Coordinate system and notations for a ray path

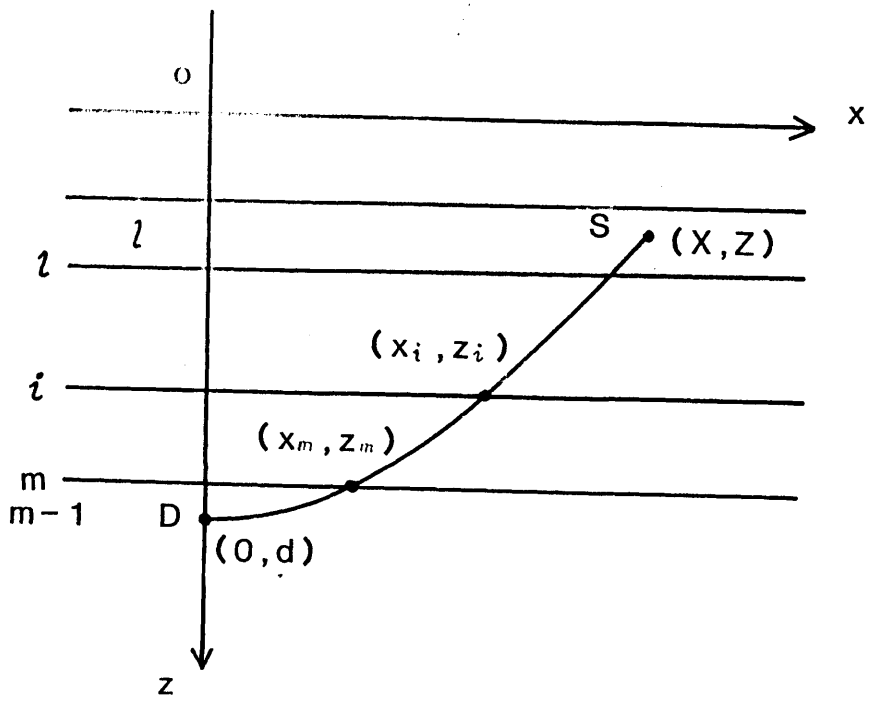

Fig.4-2 Basic ray in a layered structure. D: the deepest point. S: ending point.

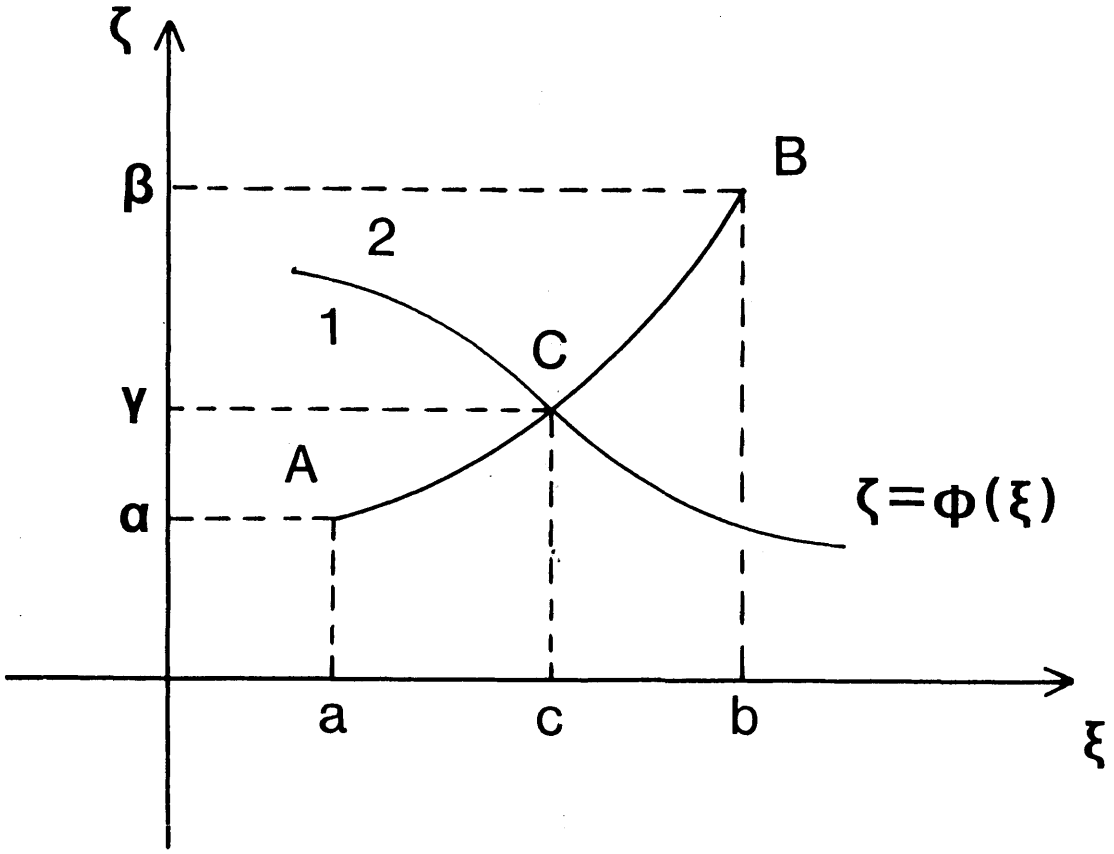

Fig.4-3 Coordinate system for the medium which is divided into two parts, region 1 and region 2, by a boundary $\zeta=\varphi(\xi)$.

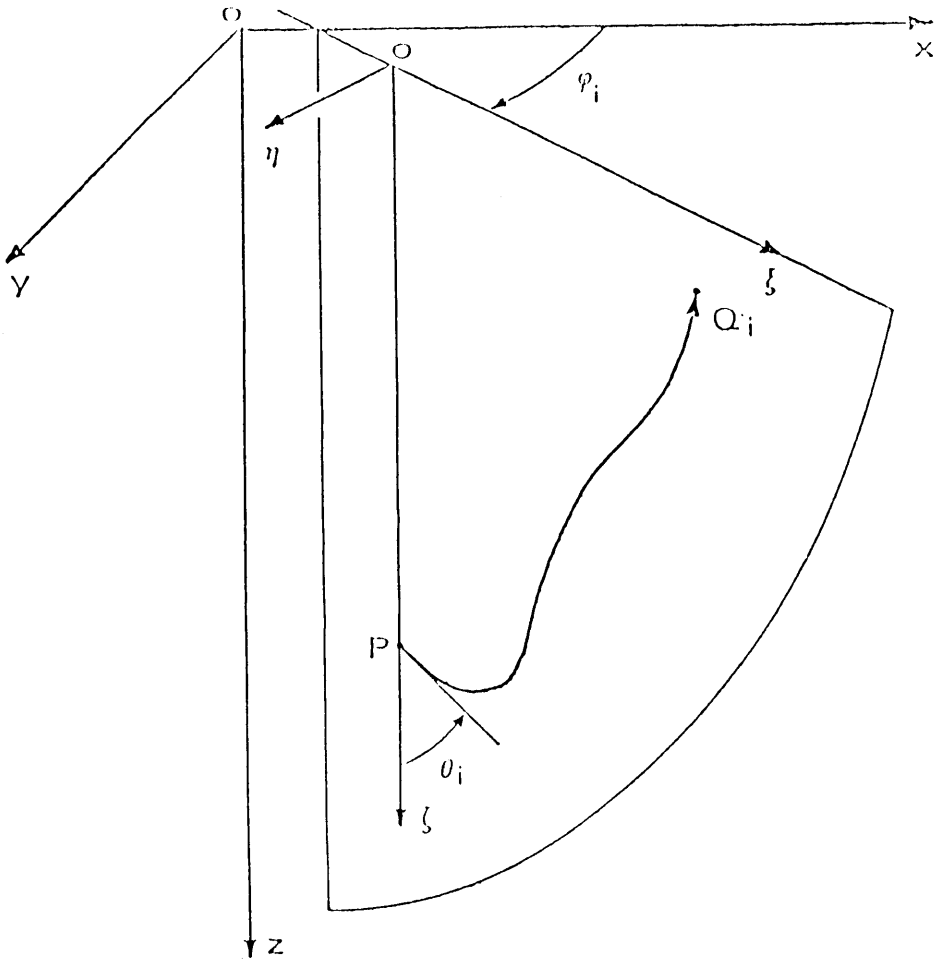

P [x_o, y_o, z_o] : Hypocenter

Q_i[x_i, y_i, z_i] : Station

Fig.4-4 Three-dimensional coordinate system in which a hypocenter and a staion are located.

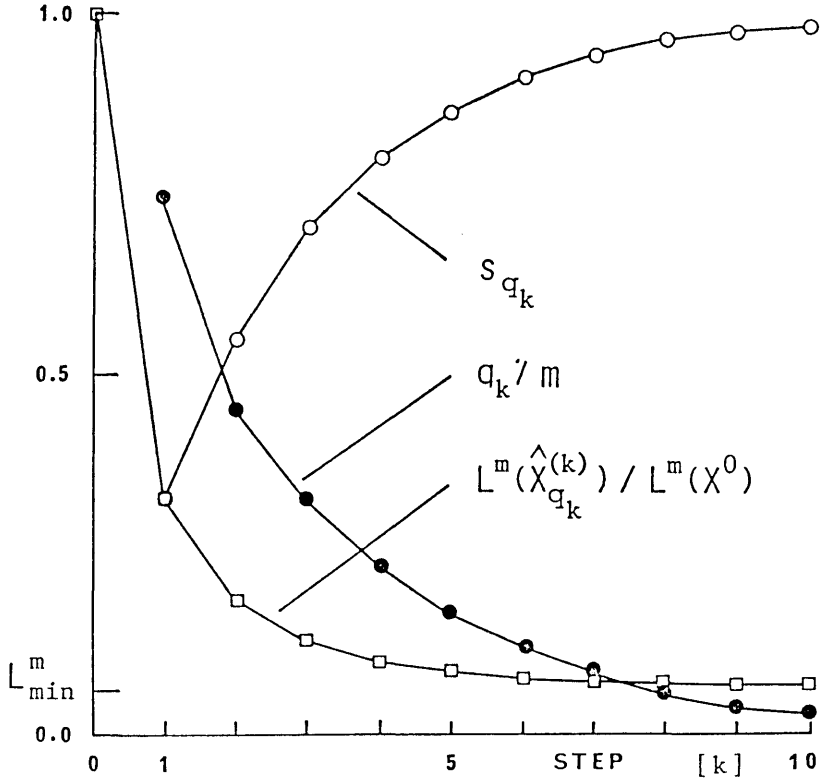

Fig. 4-5 Schematic diagram showing variations of the effective number q_k, the contraction rate s_{q_k} and the m-dimensional volume $L^m(\hat{X}^{(k)}_{q_k})$ of a confidence region in the successive iteration process of linear inversion. The normalizing factors, m and $L^m(X^0)$, are the number of independent model parameters and the m-dimensional volume of the initial confidence region, respectively.

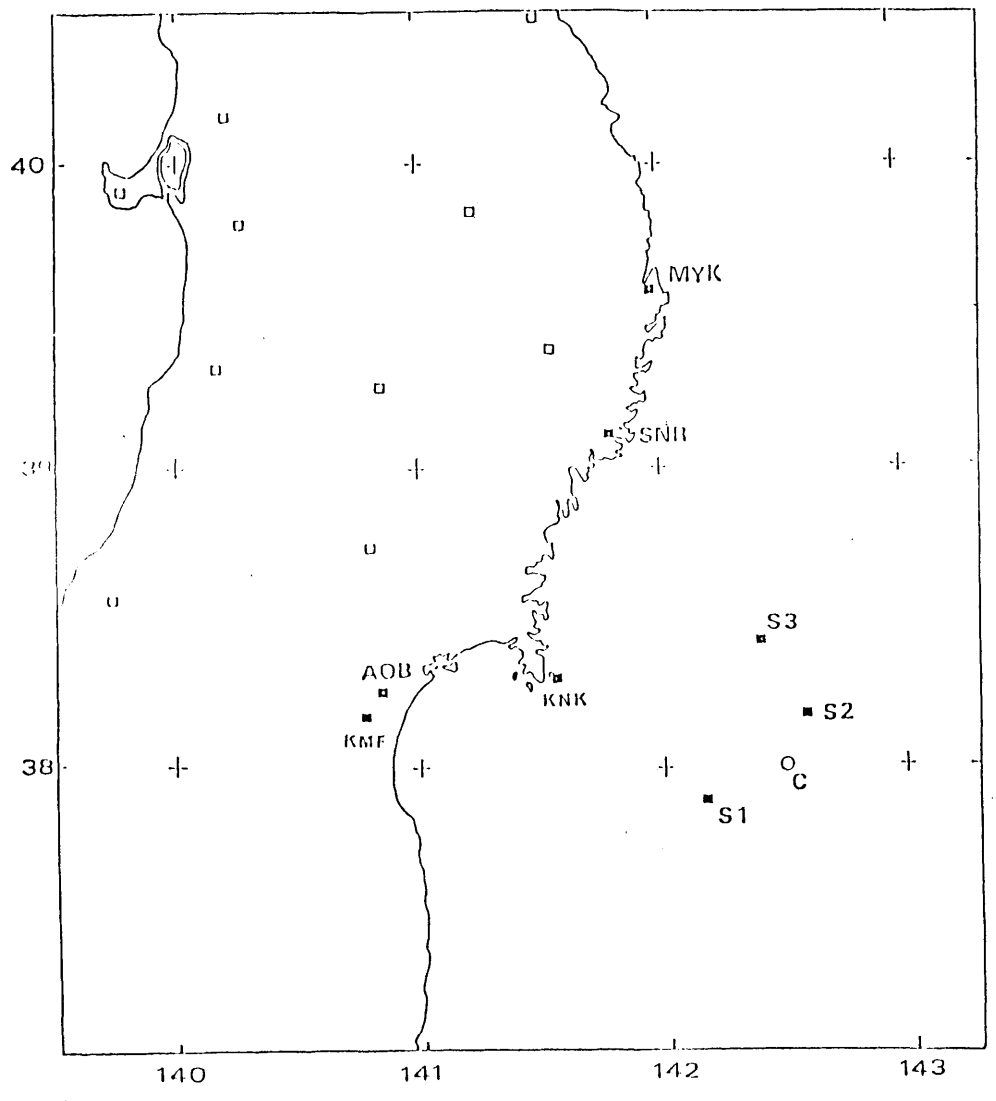

Fig.4-6 Locations of stations for numerical simulations. The stuation is the same as in case of observation of aftershocks of the 1978 Miyagi-oki earthquake. Earthquakes are assumed to be located at C with depths at 10, 30 and 60 km.

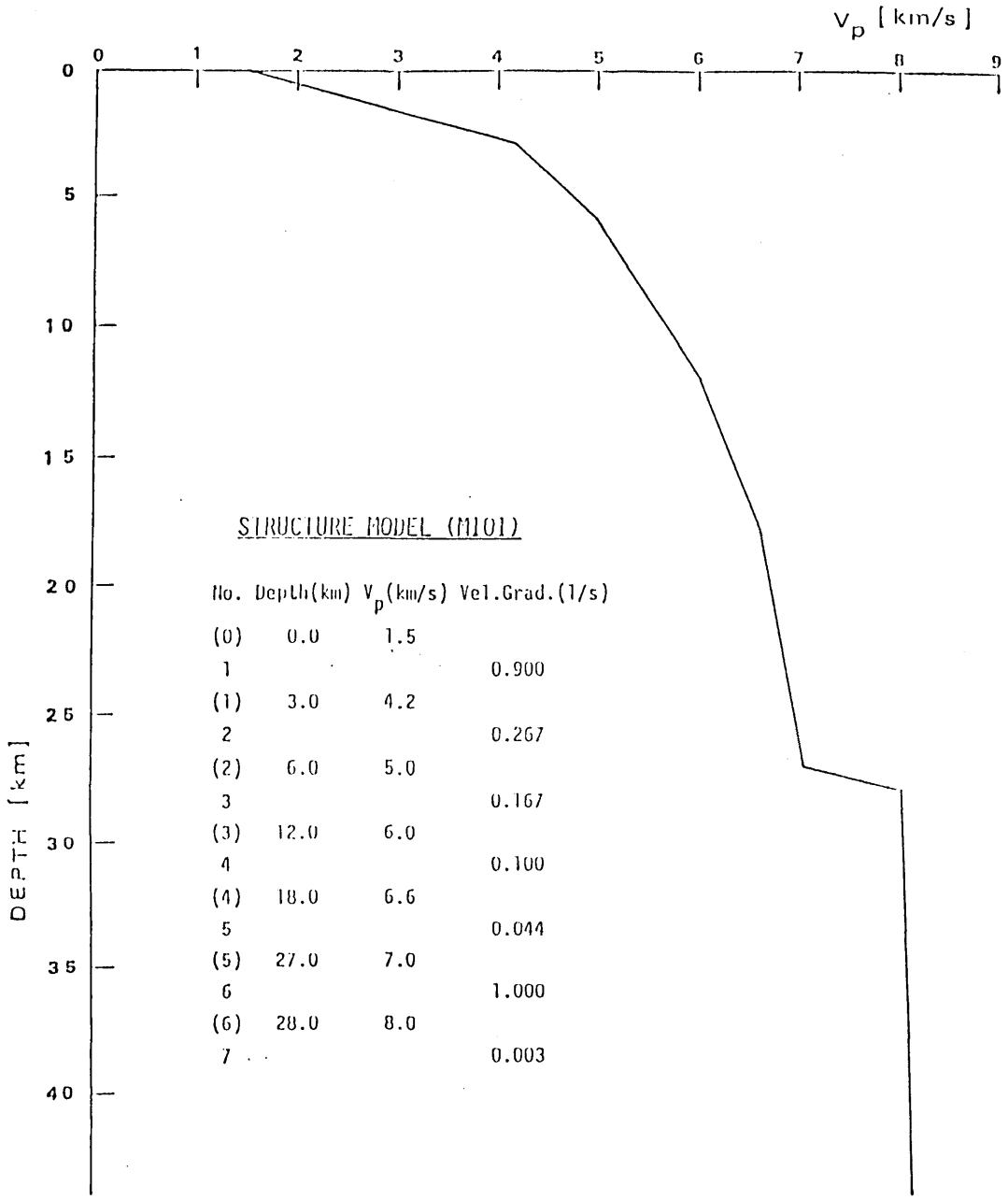

Fig.4 / Velocity structure used for numerical simulations.

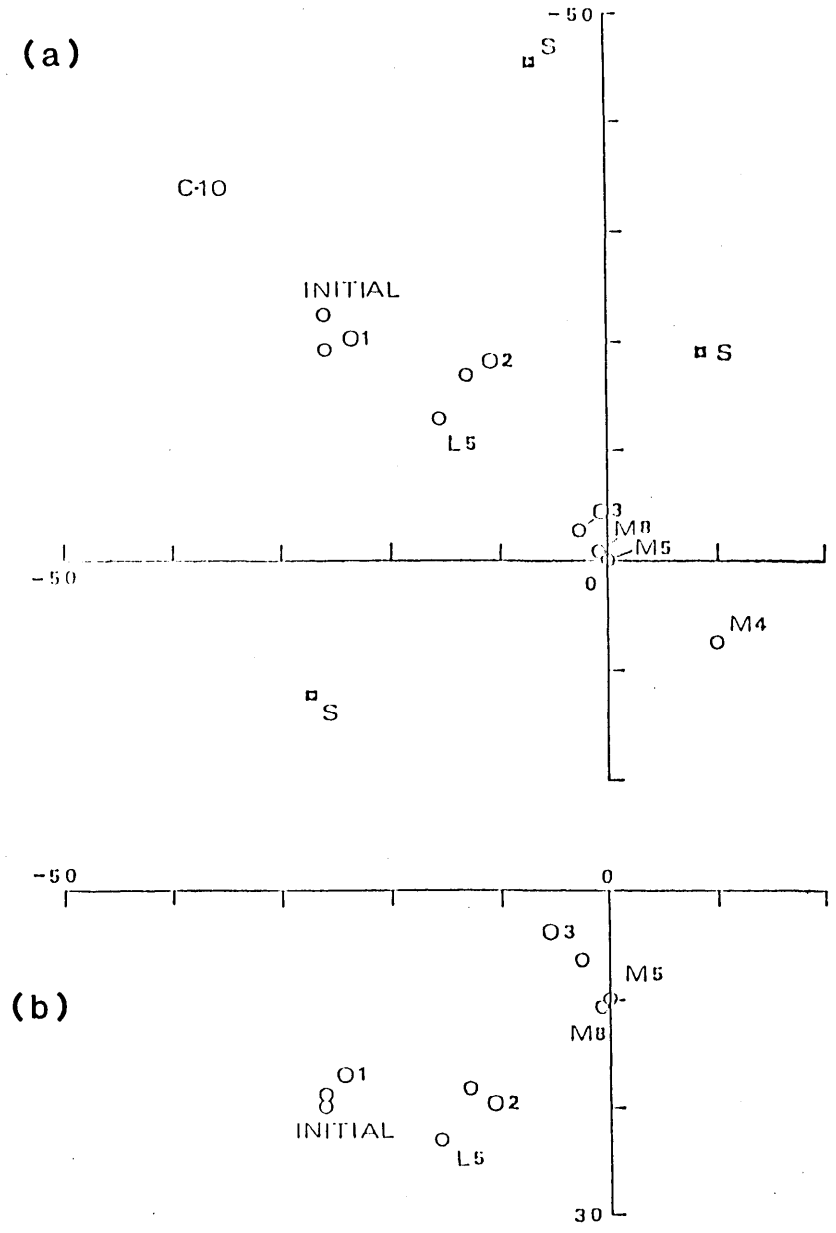

Fig.4-8 Calculated hypocenters for an event located at a depth of 10 km. (a) epicenters for various combinations of stations are shown. Open squares indicate positions of stations in the sea area (S1, S2 and S3). The true solution is located at the origin and the initial hypocenter is located at (-25,-25). An epicenter labeled L5 is a solution when 5 land stations are used and that with O2 when 2 stations in sea area. Epicenters with M show solution when both sea and land stations are used. (b) depths.

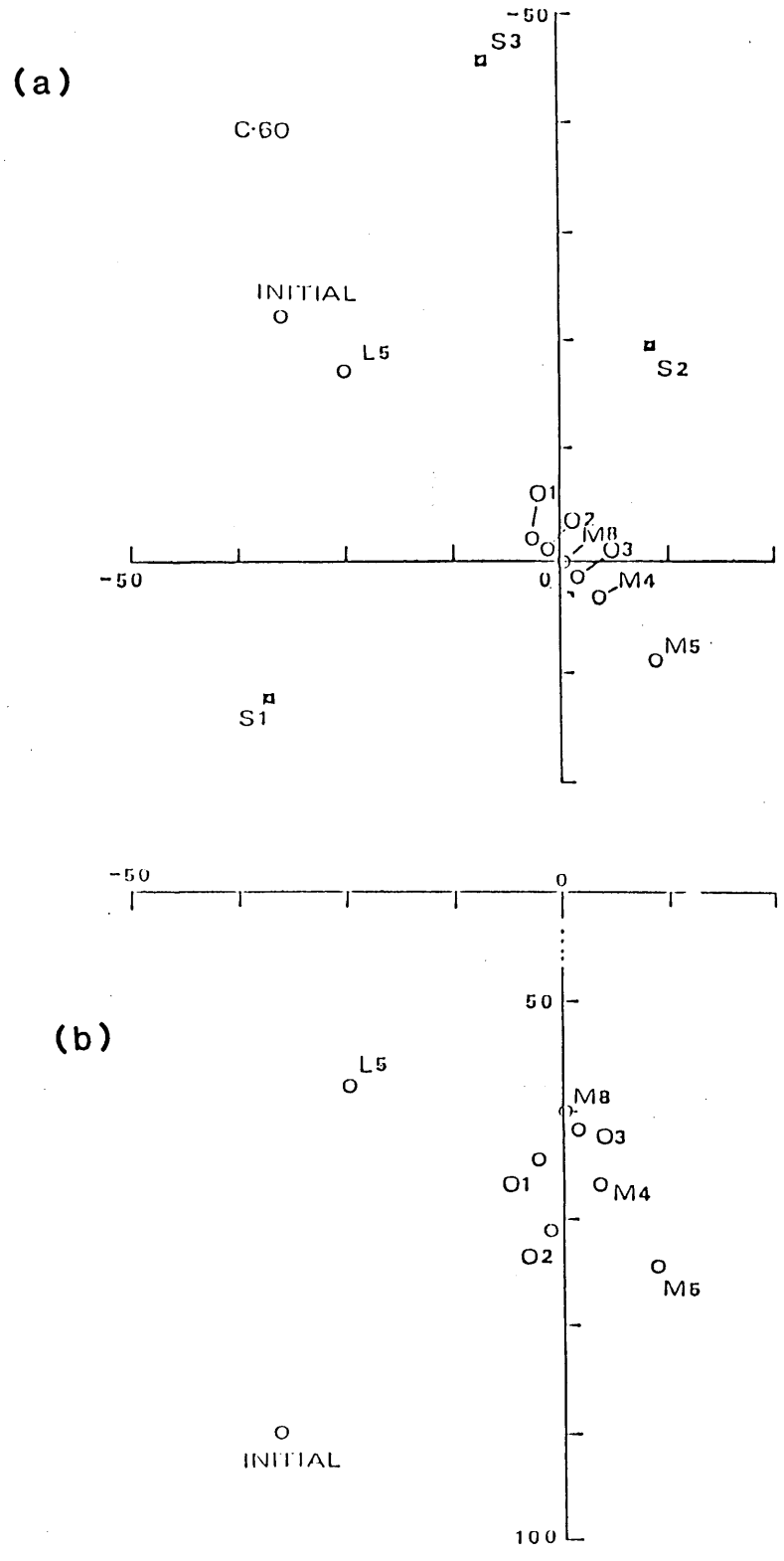

Fig.4-9 Epicenters (a) and depths (b) for the event with depth of 60 km.

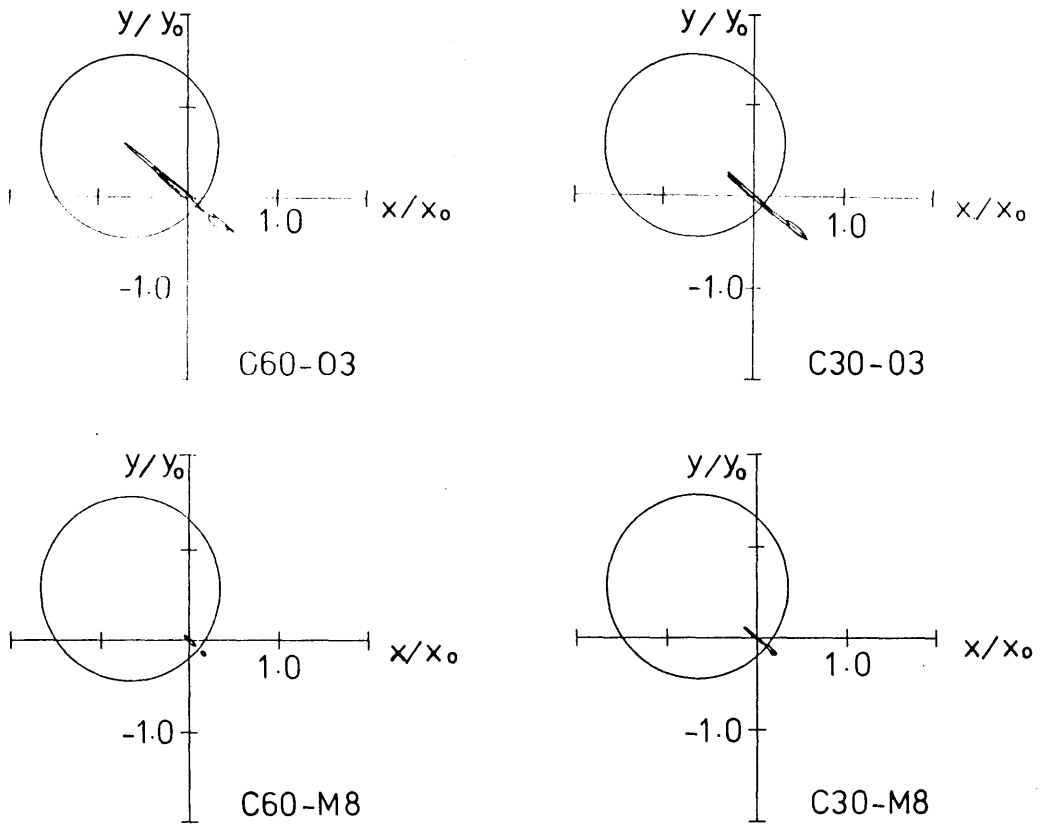

Fig.4-10 Process of successive iteration with the contraction of confidence regions. Projections of the hyperellipsoid for one standard error on a x-y plane in the coordinate in Fig. 4-4. Ellipses are normalized by the errors in the initial guess.

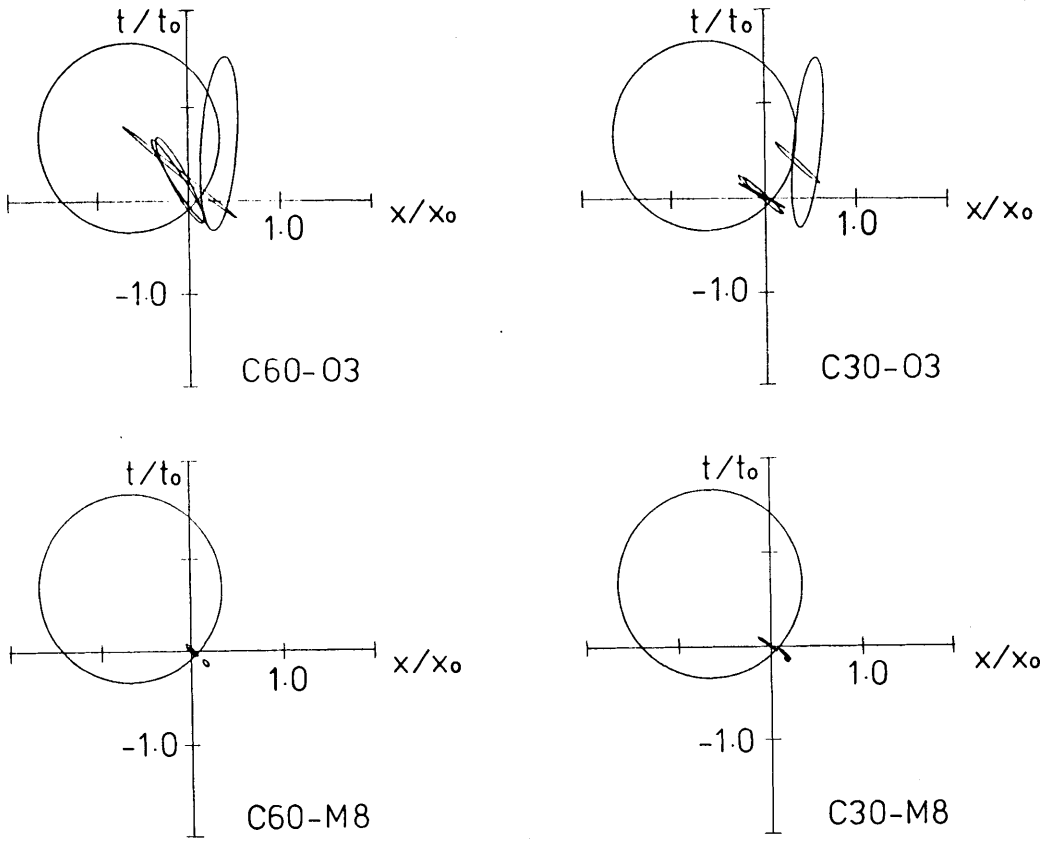

Fig.4-11 Projections onto x-t plane. See the caption of Fig.4-10.

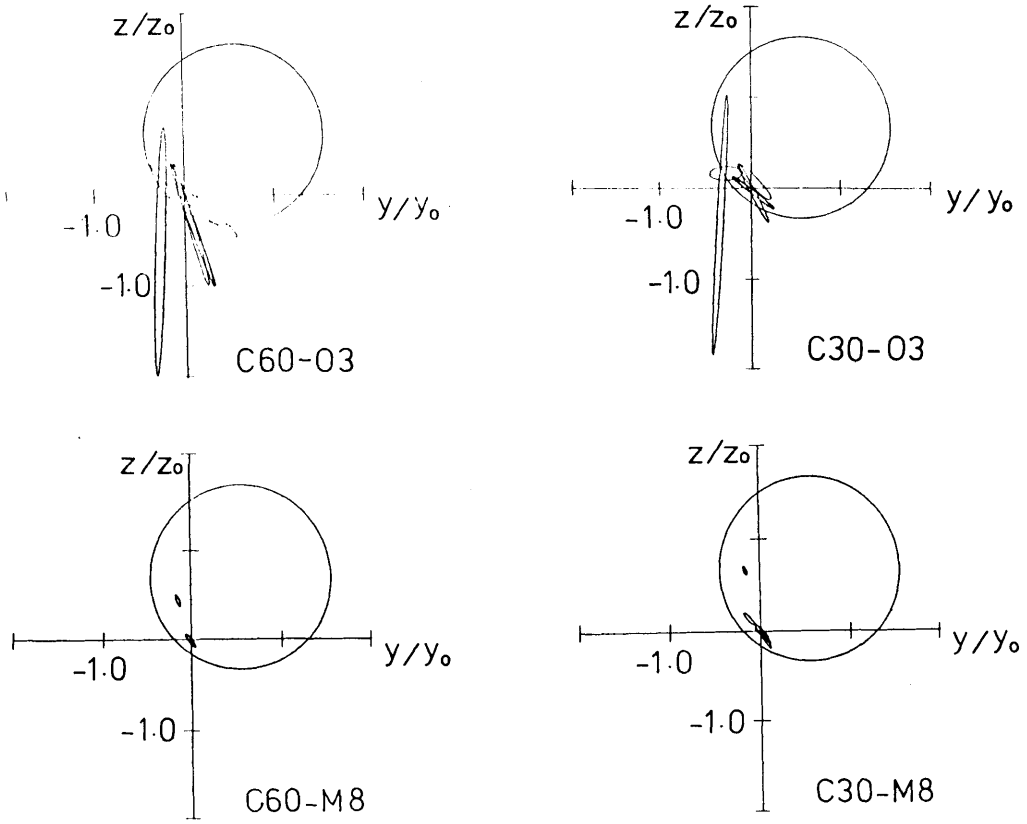

Fig.4-12 Projections onto y-z plane. See the caption of Fig.4-10.

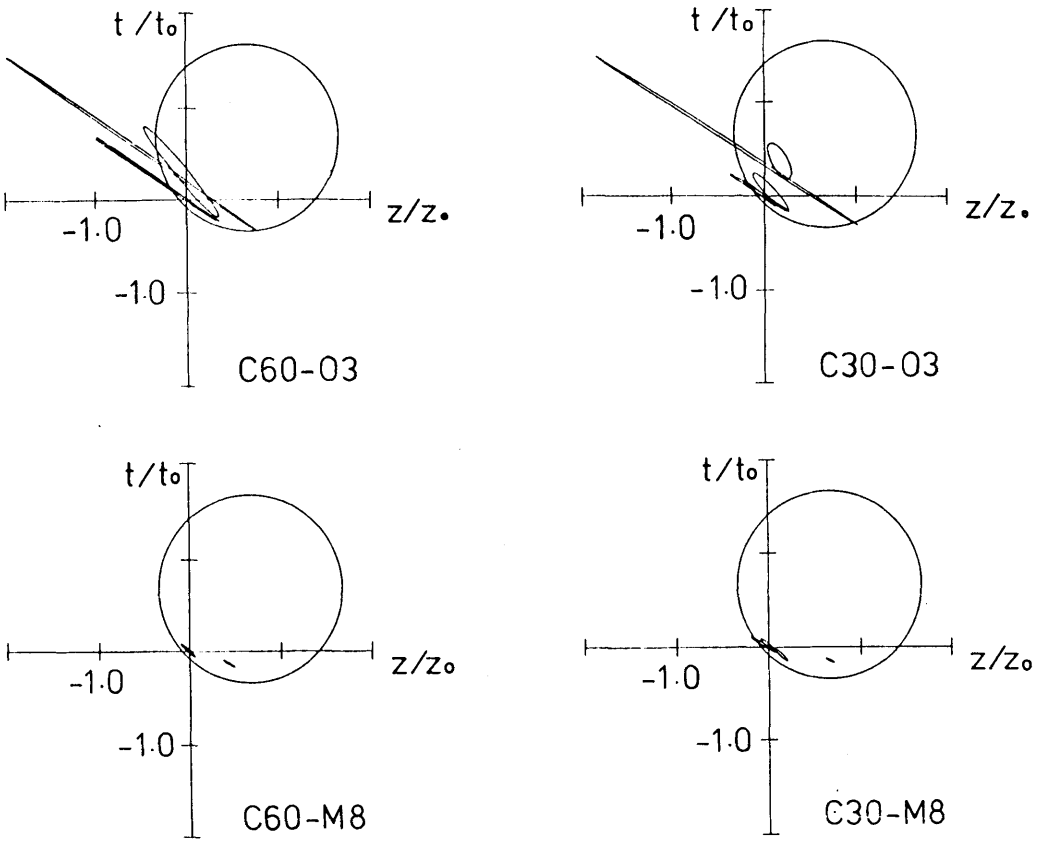

Fig.4-13 Projections onto z-t plane. See the caption of Fig.4-10.

5 Earthquake data

5-1 Number of events detected by the OBS observation

The number of earthquakes detected by an OBS increases as the threshold of the amplitude of a signal decreases. The threshold of a STA-to-LTA ratio (SLR), which is introduced in chapter 3 for the event detection, determines the lower bounds of the signal amplitude. Figure 5-1 shows a typical distribution of the number of detected events with respect to R_{ON} (SLR at the biginning of event), where the ratio of R_{ON} to SLR at the end of event is fixed to be 1.5. The data are the same as in Fig. 3-12. From Fig. 5-5, we can find that the number of events with amplitude greater than R_{ON} is inversely proportional to R_{ON}:

$$N(R_{ON}) = N_0 / R_{ON} \quad . \tag{5-1}$$

Thus the number density n of the event whith maximum amplitude A is proportional to A^{-2},

$$n(A) = n_0 A^{-2} \quad . \tag{5-2}$$

This relation corresponds with the case of m=2 in the Ishimoto and Iida's relation (Ishimoto and Iida, 1939);

$$m(A) = n_0 A^{-m} \quad . \tag{5-3}$$

As was pointed out by Asada et al. (1951), m is related to the b value as

$$m = b + 1 , \tag{5-4}$$

where b is a coefficient in Gutenberg-Richter's formula,

$$\log n(M) = a - bM . \tag{5-5}$$

To derive Eq. (5-4), we suppose that log A is linearly related to magnitude M. Supposing the linear relation between log A and M as

$$\log A = \alpha M - \beta(r) , \tag{5-6}$$

where $\beta(r)$ is a function of epicentral distance r, we have

$$m = \frac{b}{\alpha} + 1 . \tag{5-7}$$

This is identical to Eq. (5-4) when $\alpha=1$. Therefore the data in Fig. 5-1 indicates that Gutenberg-Richter's formula with $b=\alpha$ is appricable for the events whose signals are at least foure times as large as ground noise in amplitude.

The number of the events with smaller amplitude (SLR$\leq$4), which were detected by only one OBS, is larger than that expected

from Eq. (5-1). As was discussed in 3-4, the examination of waveforms shows most of such small amplitude signales are not likely signals of an earthquake origin. The number of events for $N \geq 2$ is suitable for the measure of activity near a particular OBS. As far as the evnts for $N \geq 2$, the occurence rate of earthquakes agree well with that expected from Eq. (5-1) at least for the events with a signal-to-noise ratio of greater than 3.0.

On the contrary, the number of those events which were detected by many OBSs ($N \geq 5$) is fewer than the number expected by Eq. (5-1). This can be explained as follows: Events which are detected by many OBSs (e.g.,$N \geq 5$) must be large enough in magnitude. The signals from small events may not be recorded at all stations widely distributed in a region. These small events are dropped out from the set of events for $N \geq 5$. The dependence of the number of events on N varies from site to site, because the distribution of earthquakes is not uniform in space. This problem will be discussed again.

5-2 Steady state activity of microearthquakes

The OBS experiments revealed a high seismic activity near the trench in a steady state. The 1980 array recorded about 50 events per day, though the number varies among OBSs (Fig. 5-2). The other OBS arrays operated in 1981, 1982 and 1983 also recorded a large number of microearthquakes. Another example of daily frequency of events is illustrated in Fig. 5-3. Earthquakes were observed at a rate of 57 event/day by OBS S8 of the 1983 array; the number of events with a signal-to-noise ratio of

greater than 3 amounts to 1599 for 27.8 days. A half of these events were commonly recorded by at least five OBSs and 190 events out of them have S-P time of less than 30 s and enough amplitude to be located from arrival time data. That is to say, one can determine hypocenters of a tenth of the whole number of observed earthquakes.

5-3 Non-uniform distribution of earthquakes in space

Here we investigate how many events can be observed at each station of the OBS array. If earthquakes occur uniformly in space, a number of earthquakes N decrease with the number of stations Ns which can record the event; the number of events which can be recorded at many stations will be small.

Figure 5-4 shows the distribution of N with respect to Ns for each OBS of the 1980 array. At P4 and P6, N decreases with Ns. This means that there were only a small number of events whose amplitudes are large enough to be recorded by distant OBSs but the number of small events near P4 or P6 is quite large. The distribution varies from OBS to OBS; at P9, T11 and P12, N for Ns $\geq$ 5 is greater than N for Ns = 3. T11 has many events for Ns = 1; more than 70 % of total number of events were detected only by T11. This is partly because the noise level of records at T11 is much greater than those at other OBSs. The distributions for P9 and P12 may indicate that the seismic activity is low near these OBSs.

5-4 Magnitude

In the 1980 experiment, only sixteen events were detected both by the OBS array and the Tohoku University land network. The Observation Center for Earthquake Prediction (OCEP), Tohoku University, reported the body wave local magnitudes of these earthquakes (personal communication). The largest event located within the 1980 OBS array area has a magnitude of 4.0.

Duration times of microearthquakes (F-P time) at the OBS station T7 in the 1980 experiment are related to magnitudes determined by the OCEP land network as shown in Fig. 5-5. Duration times of microearthqukes at OBS stations in the 1982 and the 1983 experiments are related to the magnitudes determined by the land network operated by the Research Center for Earthquake Prediction (RCEP), Hokkaido University as shown in Figs. 5-6 and 5-7. Figures 5-5, 5-6 and 5-7 show that the empirical relation of $M = A + B \log(F-P)$ is valid in the case of OBS observation. The F-P times for the 1982 array were measured manually from visual records on a sheet of paper with a chart speed of 1 mm/s. The F-P time for the 1983 array is the event duration time D described in 3-3-2. Although the coefficients A and B take different values for different stations, they are in good agreement (Fig. 5-8).

For the events detected by at least three OBSs of the 1980 array, frequency distribution of the events versus magnitudes is shown in Fig. 5-9. It is found that the 1980 OBS array could detect the events with magnitudes ranging from 1.0 to 4.0. Most events varied in magnitude from 1.5 to 3.0. We can expect that the 1980 OBS array uniformly detect the events with magnitude greater than 2.0 in and near the array. It has been reported that

the land network can uniformly detect events with magnitude greater than 2.9 in this region (Yamamoto and Kono, 1982). Hence the detectability of the 1980 array is about one magnitude greater in range than that of the land network for this trench area.

The earthquakes detected by the 1981 array varied from 1.0 to 4.5 in magnitude. Figure 5-10 shows the number of earthquakes detected by OBS P1 and those by P4 in the 1982 array. The magnitude range of earthquakes detected by the 1982 array is from 0.5 to 5.0.

The number of detected earthquakes varies if we change the criterion for the identification of an event as an earthquake. For example, the number of earthquakes depends on the minimum number of staions (Nmin) which can detect the event as illustrated in Fig. 5-11. About 30% of earthquakes with small magnitude (M = 1) were not commonly detected by 5 OBSs. However, it can be seen that the events with magnitudes of greater than 2 are uniformly detected by the 1983 array.

5-5 Seismograms

An interesting feature of the seismograms recorded by most of the OBSs is that the first arrival of a horizontal component is delayed by 2 - 3 s compared with that of a vertical component (Fig. 5-12). An unconsolidated ocean floor sediment contrasts sharply in velocity with the oceanic crust. The nearly vertical incidence of seismic rays due to the sharp velocity contrast deprive us of a clear P-phase in the horizontal component. The

late arrivals of the horizontal components can be interpreted as P-to-S converted waves at the bottom of the sedimentary layer. The velocity structure of the sedimentary layer is inferred from refraction and/or reflection studies performed near the OBS array. On the contrary, no clear delay of onset in the horizontal component is found in seismograms recorded by OBS T11 (the 1980 array) located on the Erimo Seamount, where the unconsolidated sedimentary layer is quite thin (Fig. 5-13). Quite apart from the delay of first arrival on the horizontal component, the delays of arrivals of P- and S-waves due to the sedimentary layer are so large that careful treatment is needed for locationg earthquakes.

P-waves reflected at the sea surface were observed as later phases by OBSs. P10 and P12 of the 1980 array, on the Northwet Pacific Basin, recorded them clearly.

5-6 Estimation of epicentral distances from amplitude data

It is necessary to estimate epicentral distances of earthquakes which can not be located from arrival time data; the number of events that we can locate is only a tenth of the whole events. As was discussed in 5-3, a magnitude M can be estimated by a signal duration D as

$$M = a_1 + a_2 \log D \qquad (5\text{-}8)$$

where a_1 and a_2 are constants. The magnitude M is also related to

a maximum amplitude Amax in velocity and an epicentral distance Δ as

$$M = b_1 \log A_{max} + b_2 \log \Delta + b_3 \ , \tag{5-9}$$

where b_1, b_2 and b_3 are constants (Watanabe, 1971). From Eqs. (5-8) and (5-9), we obtain a formula,

$$\log \Delta = c_1 \log D + c_2 \log A_{max} + c_5 \tag{5-10}$$

where c_1, c_2 and c_5 are constants to be determined by using the earthquakes whose Δ are knwon from the result of hypocenter determination. However it is not easy to measure accurately the maximum amplitude; signals with large amplitude are sometimes saturated. Thus we use an integrated amplitude (A) during the event instead of Amax to obtain information of signal amplitudes. Furthermore, a long term average of signal amplitude at the biginning of the event (LTA_1) and that at the end of the events (LTA_2) are taken into account, because D depends on the level of the background noise. As a result, we use the following relation among Δ, D, A, LTA_1 and LTA_2 to estimate the epicentral distance Δ;

$$\log \Delta = C_1 \log D + C_2 \log A + C_3 \log LTA_1 + C_4 \log LTA_2 + C_5, \tag{5-11}$$

where C_1, C_2, C_3, C_4 and C_5 are constants determined by using earthquakes whose hypocenters are known from arrival time data: D, A, LTA_1 and LTA_2 are measured from digitized records of amplitide signals as shown in Fig. 5-14.

Coefficients in Eq. (5-11) are determined from the data obtained in the 1983 experiment. An example is given in Fig. 5-15, where the estimated epicentral distances by Eq. (5-11) are compared with the epicentral distances which are calculated from hypocenters determined by arrival time inversion. Figure 5-15 indicates that the relative error in the estimate is about 50 %.

Figure 5-16 shows the distribution of earthquakes with the epicentral distances determined by Eq. (5-15) with $C_1 = 2.6$, $C_2 = -1.0$, $C_3 = 0.7$, $C_4 = 0.4$ and $C_5 = 0.5$. This diagram illustrates that 80% of the total number of earthquakes detected by OBS S8 of the 1983 array are located within 250 km from the OBS. As was mentioned in 5-2, only 190 events were located from arrival time data; the estimation of epicentral distances indicates that many small events are located in or near the array and only 15% of them can be located. Although the estimate involves a large error in indivisual epicenteral distance, we can say that the pattern of earthquake distribution shown in Fig. 5-16 gives a good approximation to a real distribution pattern.

5-7 Discussion and conclusions

Gutenberg-Richter's formula is applicable to the occurrence rate of microearthquakes observed in the trench area at least for events whose signal amplitude is greater than the background noise

level. Each OBS of the arrays during 1980 - 1983 recorded 50-60 events per day and 20-30 events out of them were commonly observed by several OBSs in the array. The data obtained by the 1983 array indicated 80% of the whole detected events occured in or near the OBS arrays. The data also suggested that there were many small events near the OBS; if we deploy OBSs much more densely, we can determine the hypocenters of these small earthquakes.

Our OBS arrays could detect microearthquakes whose magnitude greater than 2 almost uniformly. The 1980 experiment suggests the low seismic activity near the OBSs P9 and P12 located on the Northwest Pacific Basin.

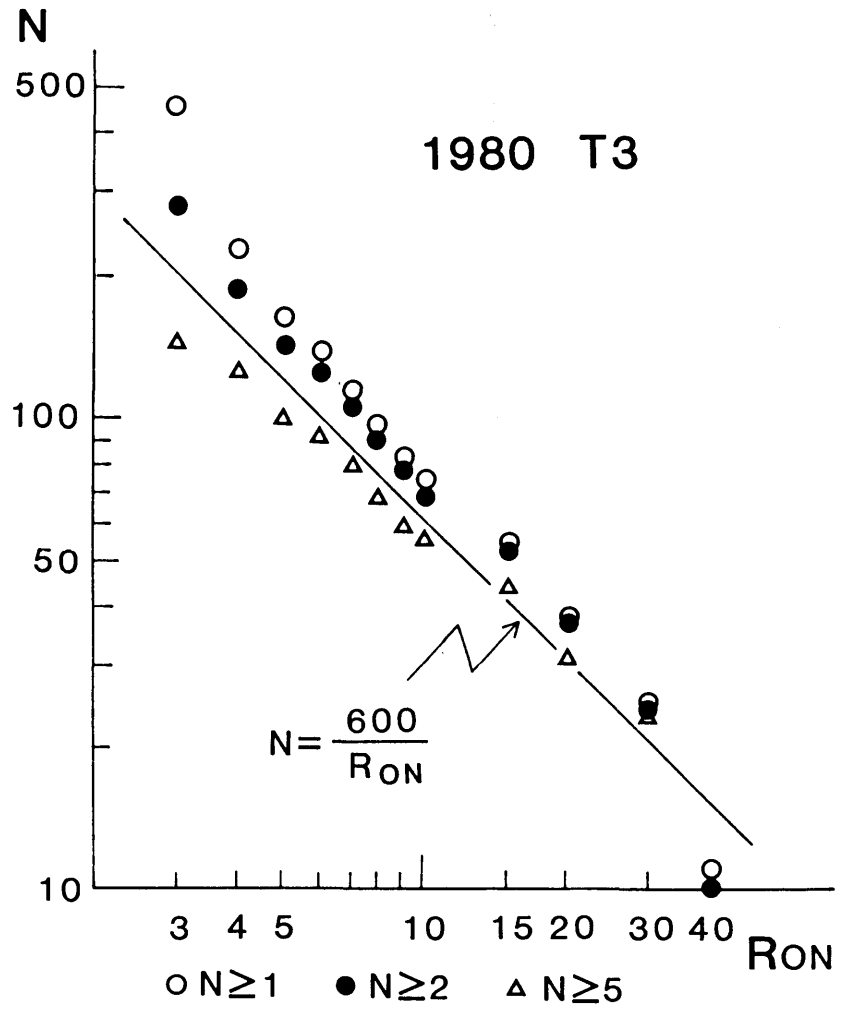

Fig.5-1 Number of detected events N versus SLR at the biginning of event Ron. The ratio of Ron to SLR at the end of event is fixed to be 1.5. The data are the same as in Fig. 3-12. Open circles show numbers of all events detected by OBS T3 (1980). Solid circles indicate those detected by T3 and at least one more OBS. Open triangles are those by T3 and other four OBSs.

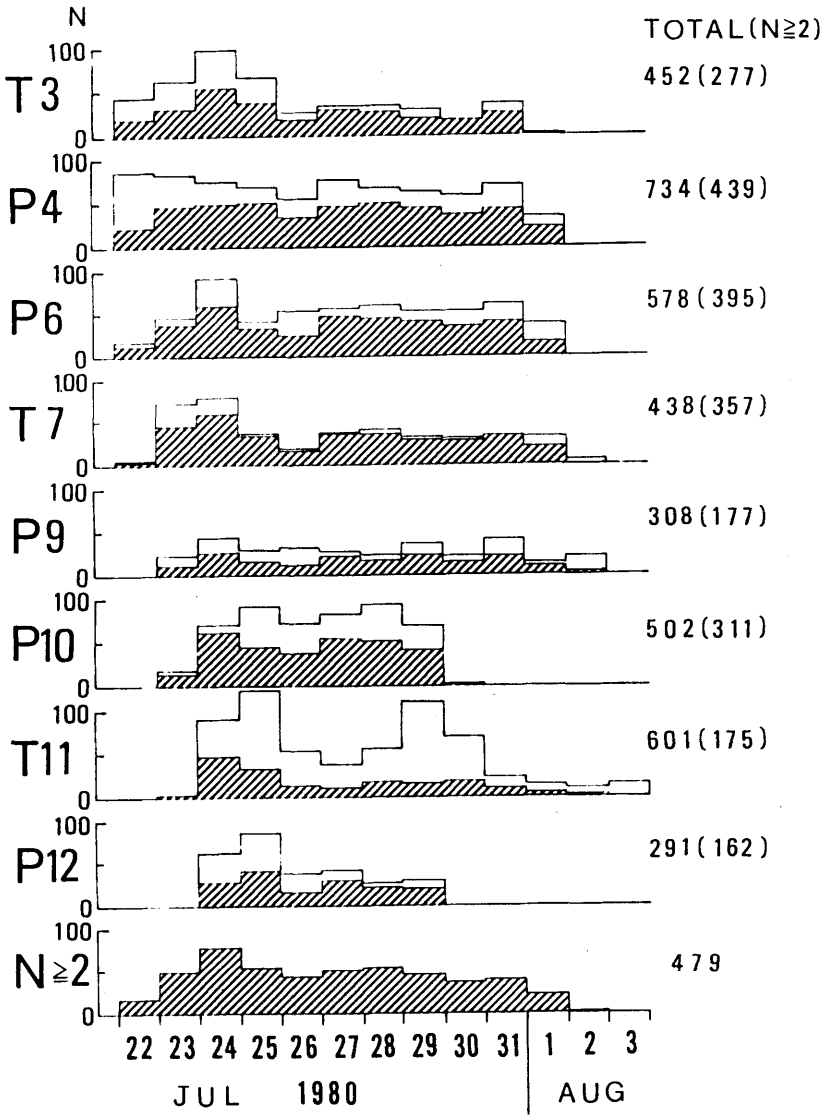

Fig.5-2 Daily frequency of event recorded by the 1980 array. Shaded area indicate numbers of events which are detected at least two OBSs.

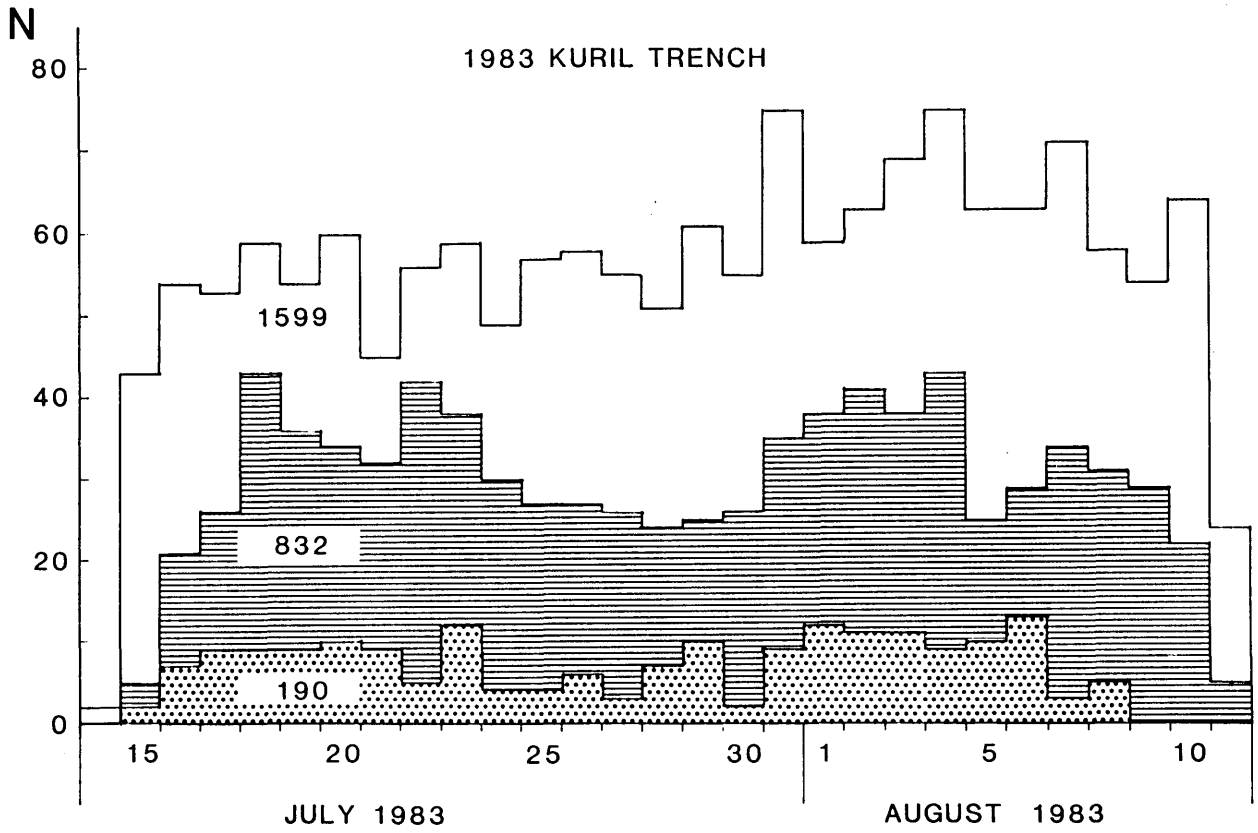

Fig. 5-3 Daily frequency of event recorded by an OBS S8 during the observational period. Events detected by S8 and at least one more OBS are counted. Total number is 1599. A shaded area with lateral stripes indicates number of events detected by S8 and other four OBSs, total of which amounts to 832. A doted are shows the number of event detected by at least five OBSs with S-P time less than 30 sec. Thse 190 events are analized to determine hypocenters.

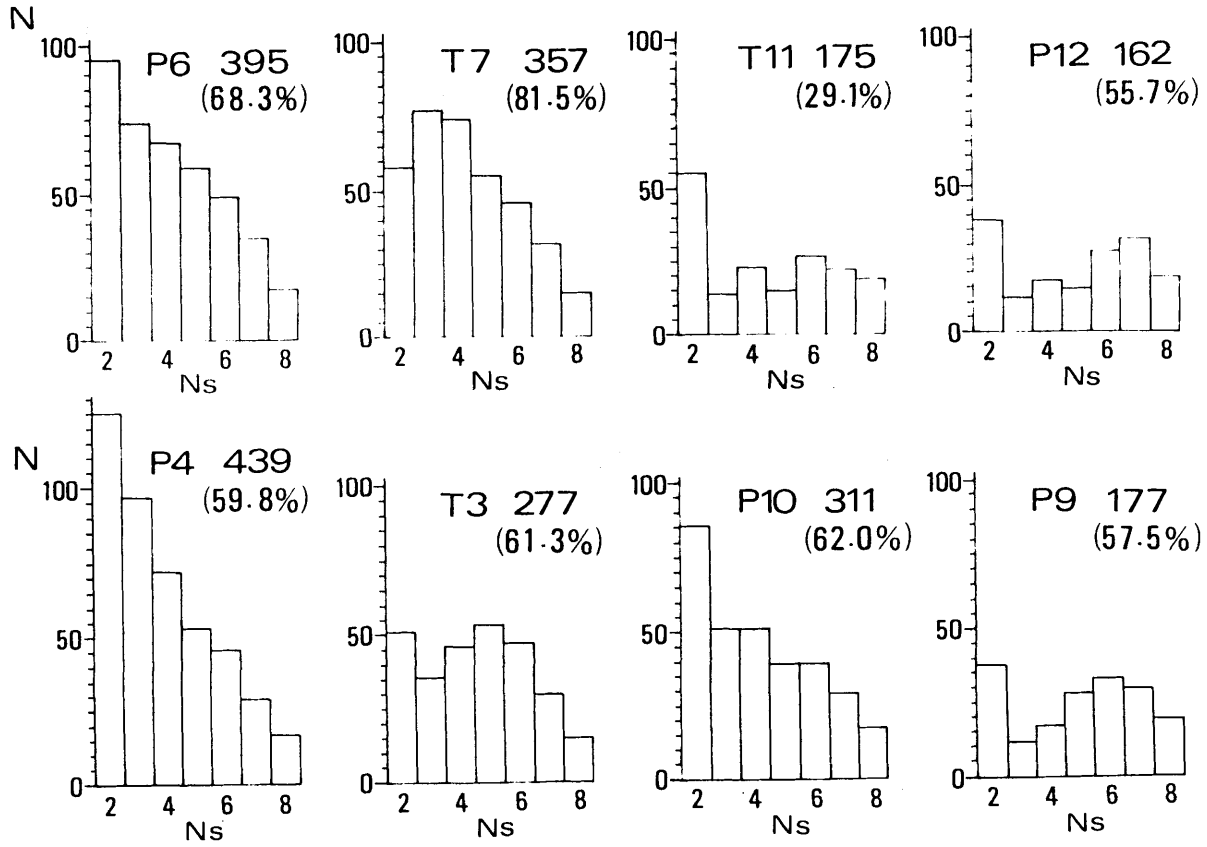

Fig.5-4 Number of earthquakes N versus number of stations Ns which can record the events. Data are obtained by the 1980 OBS array.

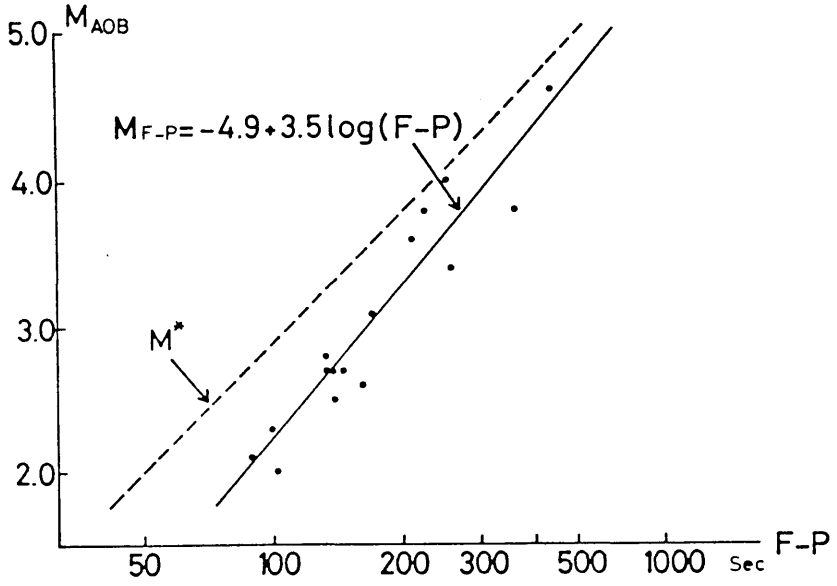

Fig. 5-5 Magnitude–signal duration ($F-P$ time) relation. M(AOB) shows magnitudes determined by the land network operated by OCEP. Sixteen events are used to determine the coefficients of the empirical relation for $M(F-P)$ by means of the least squares method (solid line). The relation, $M^* = -3.1 + 3.0 \log (F-P)$, found by Yamada (1980) for aftershocks of the 1978 Miyagi-oki earthquake is also shown (broken line). The [illegible]

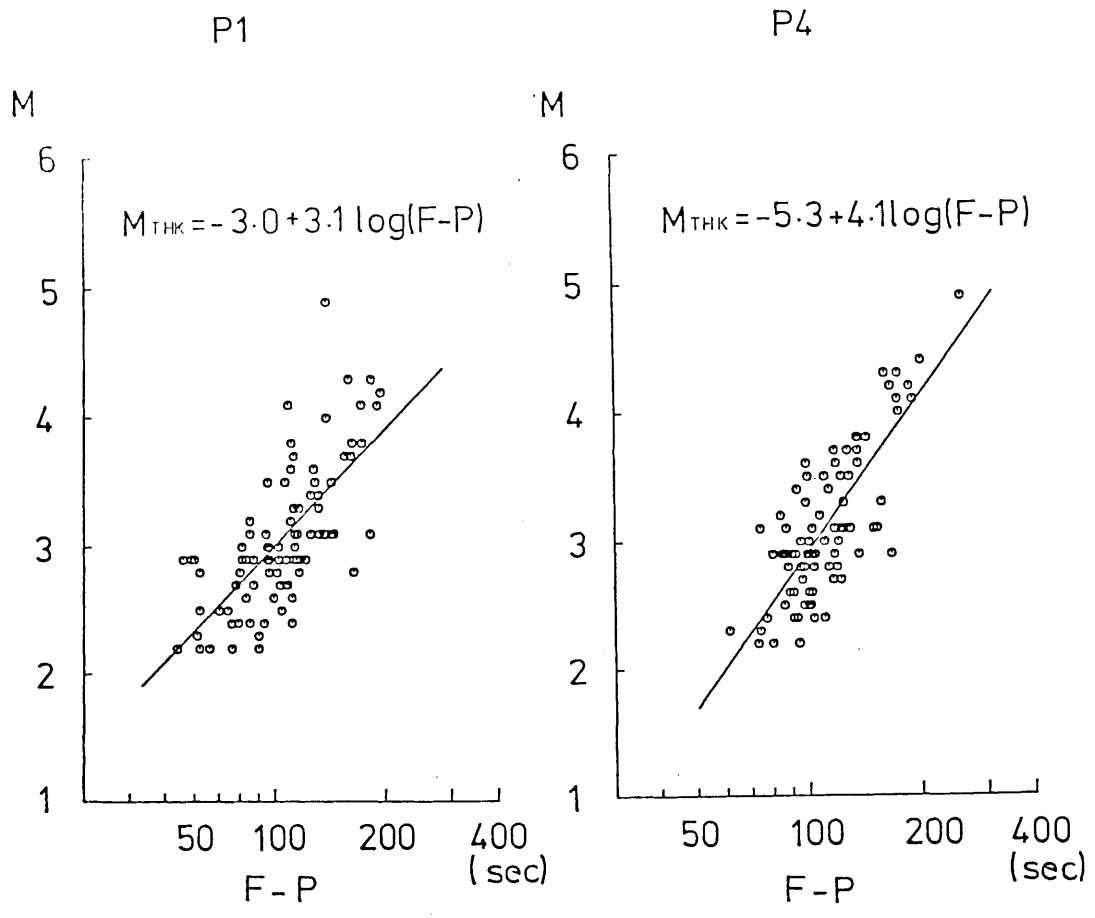

Fig.5-6 Magnitude versus signal duration (F-P time) relation for OBS stations of the 1982. M show magnitude determined by the land network operated by RCEP, Hokkaido University.

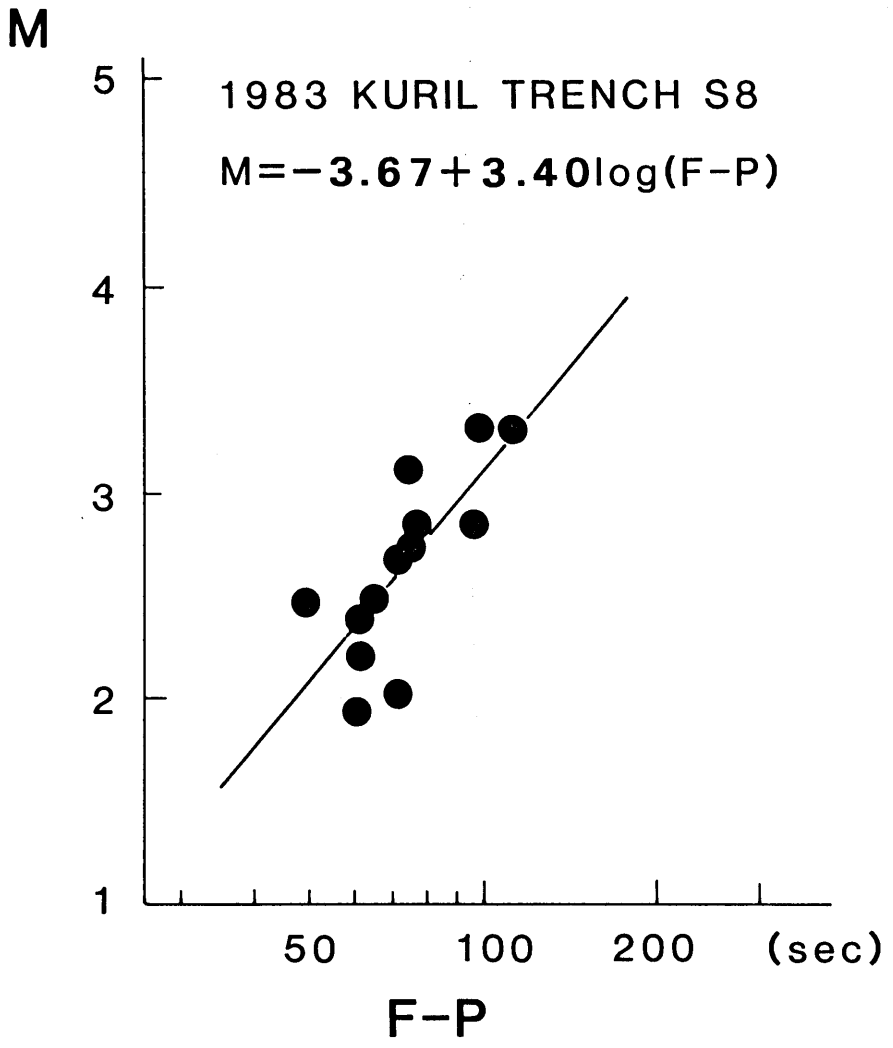

Fig. 5-7 Magnitude versus signal duration (F-P time) relation. M shows magnitude determined by the land network operated by RCEP, Hokkaido University. F-P time is the same as measured from the rectified and low-pass filterd signal as shown in Fig. 5-4. Thirteen earthquakes are recorded commonly by the OBS array and the land network. Coefficients of the empirical relation for M are determined by mean of the least squares method (solid line).

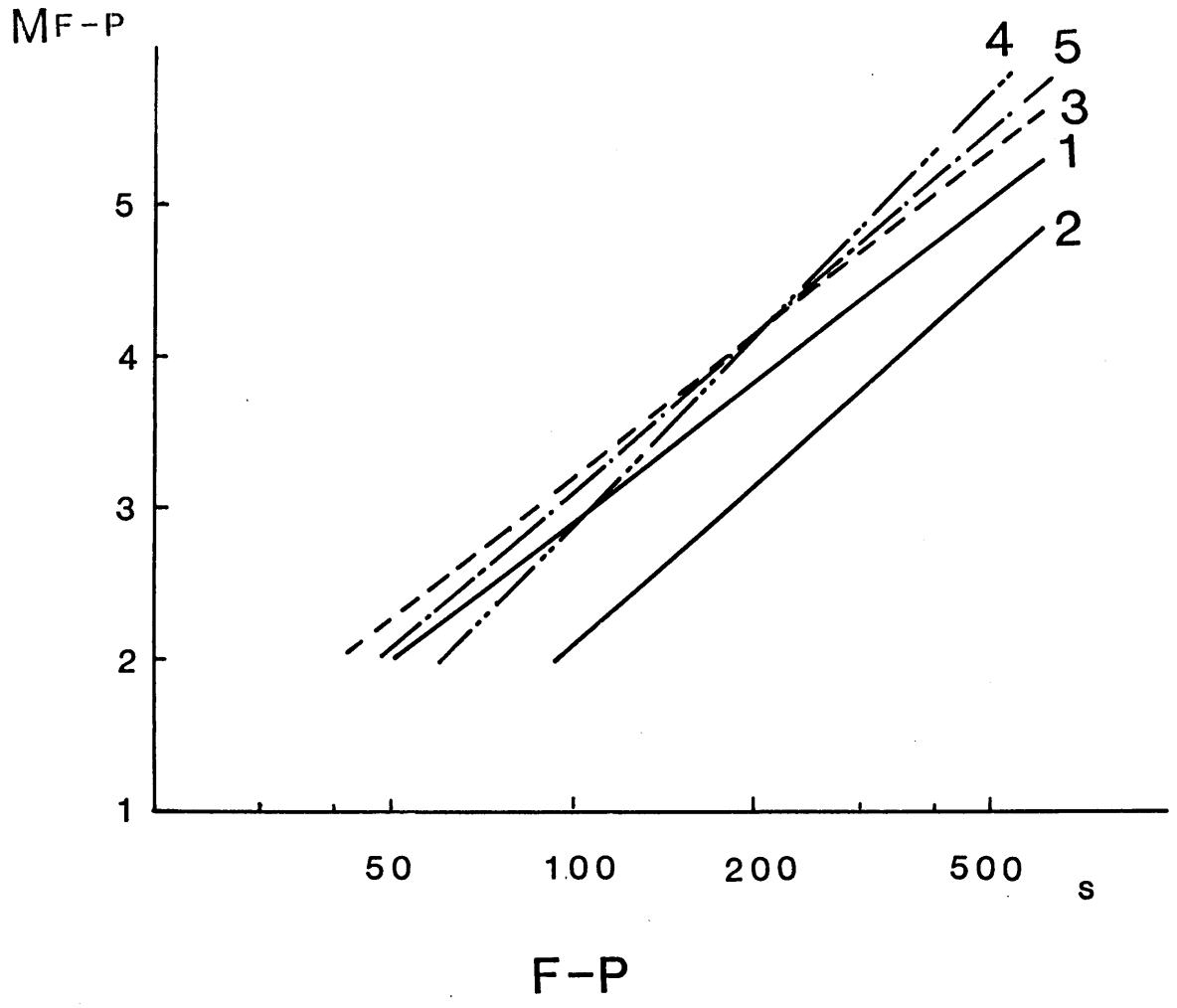

Fig.5-8 Summary of relations between M_{F-P} and F-P time: 1.aftershoks of the 1978 Miyagi-oki earthquake (Yamada,1980), 2. 1980 T7, 3.1982 P1, 4.1982 P4, 5.1983 S8.

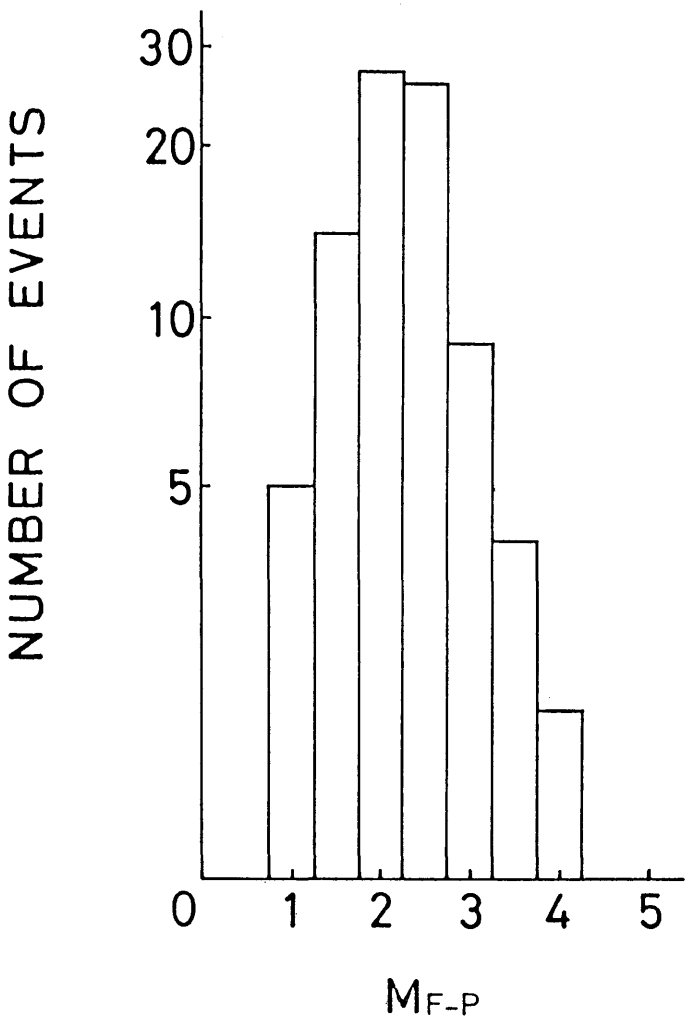

Fig.5-9 Number of events recorded by at least three OBSs of the 1980 array vesus magnitedes. About 100 events are counted. The 1980 OBS array could uniformly detect events with magnitudes greater than 2.0

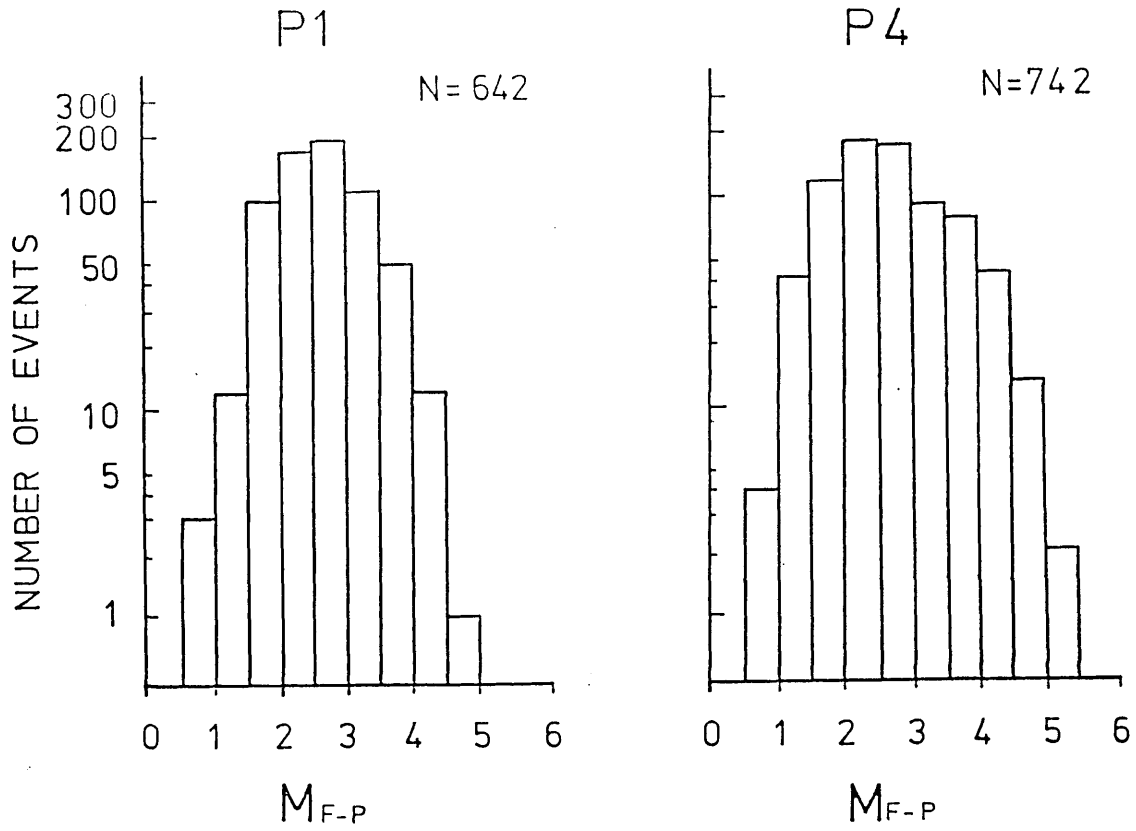

Fig.5-10 Number of events recorded by OBSs P1 and P4 of the 1982 array versus magnitudes.

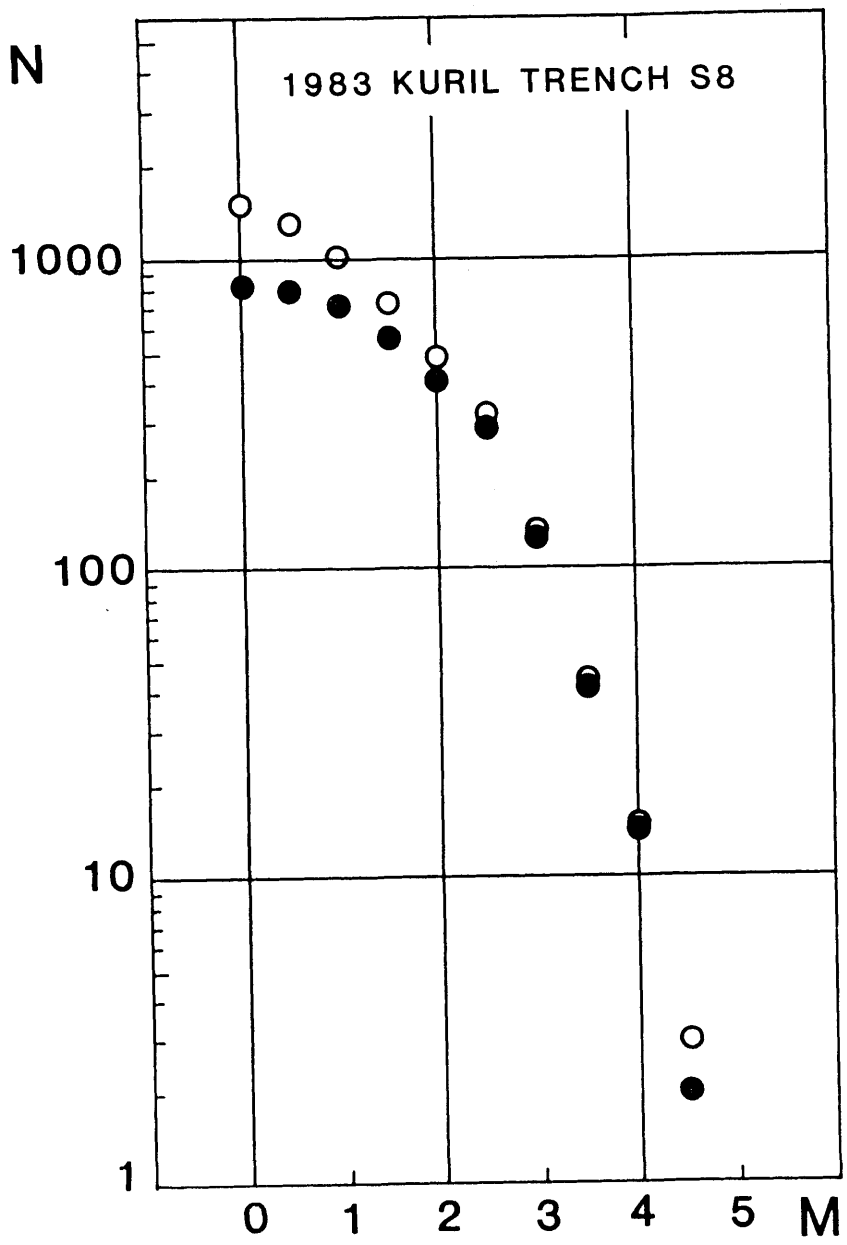

Fig. 5-11 Cumulative number versus magnitude determined from signal duration with the relation as shown in Fig. 5-7. Open circles show numbers of events recorded by both S8 and at least one more OBS . Solid circles are those recorded by S8 and other four OBSs. The OBS array could uniformly detect events with magnitude greater than 2.0

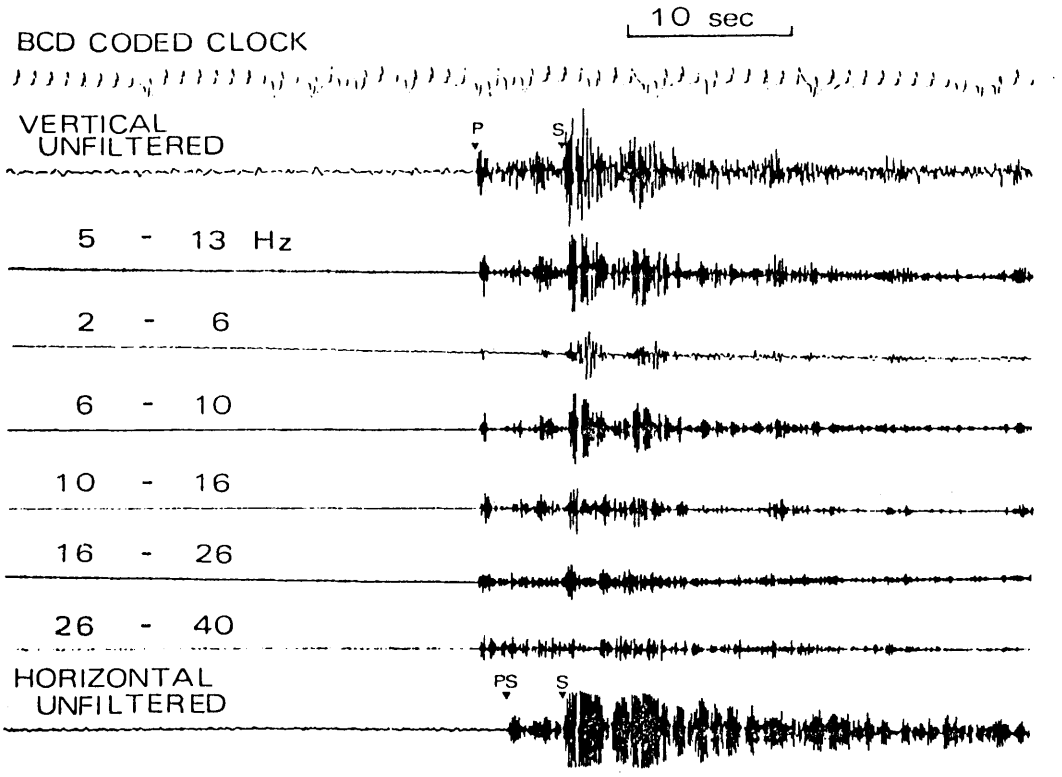

Fig. 5-12 Seismograms recorded by OBS P10 for an event located on the seaward trench wall. The records are band-pass filtered to pick a reliable first arrival with a good SNR. Both filtered and unfiltered seismograms are shown. A clear onset of *P* arrival is seen on the vertical channels and that of *S* on a horizontal channel. The first arrival phase on the horizontal component is an *S*-to-*P* converted wave due to a thick unconsolidated sedimentary layer, which is denoted by *PS*. A *P*-wave once reflected from a sea surface is also identified on the vertical channels of high frequency bands about 7 s after the first *P* arrival. (1980)

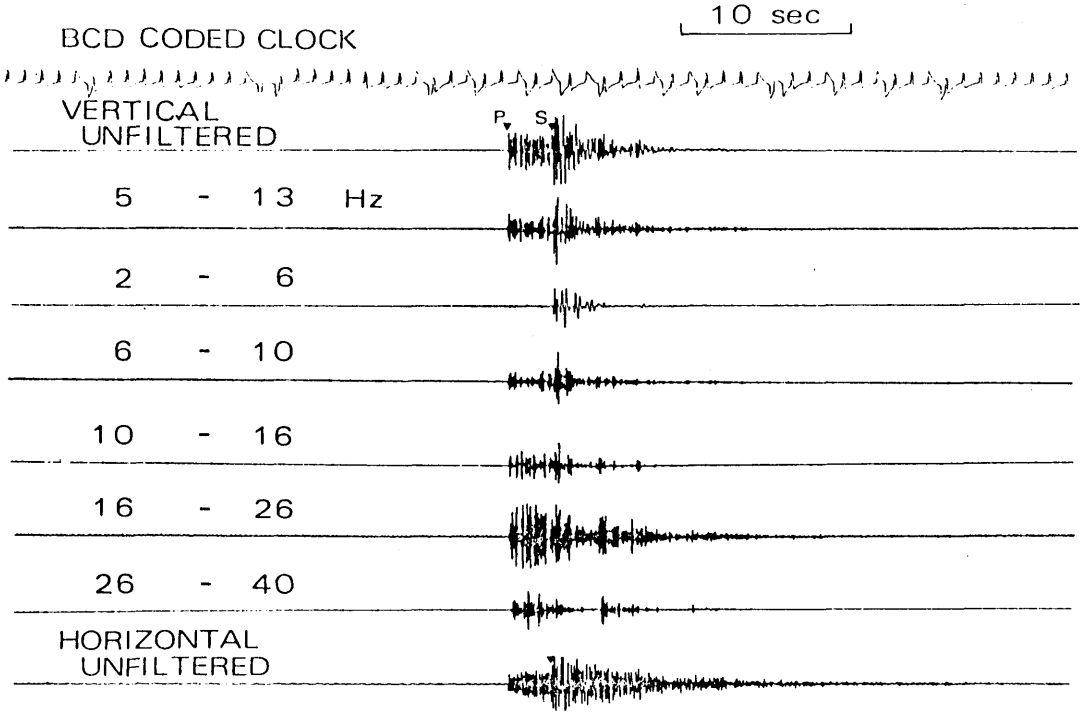

Fig.5-13 An example of microearthquakes near the Erimo Seamount recorded by T11. This OBS registered about 10 events per day which had $S-P$ times shorter than a few seconds, suggesting active seismicity near the seamount. Of these events only two could be located. The event shown in the figure is located at 40.96° N, 145.05° E, just beneath the Erimo Seamount, with a focal depth of 8 km. Clear onsets of P and S arrivals with high-frequency components are shown. No delay in the first arrival on the horizontal channel suggests absence of thick unconsolidated sediment on the seamount. (1980)

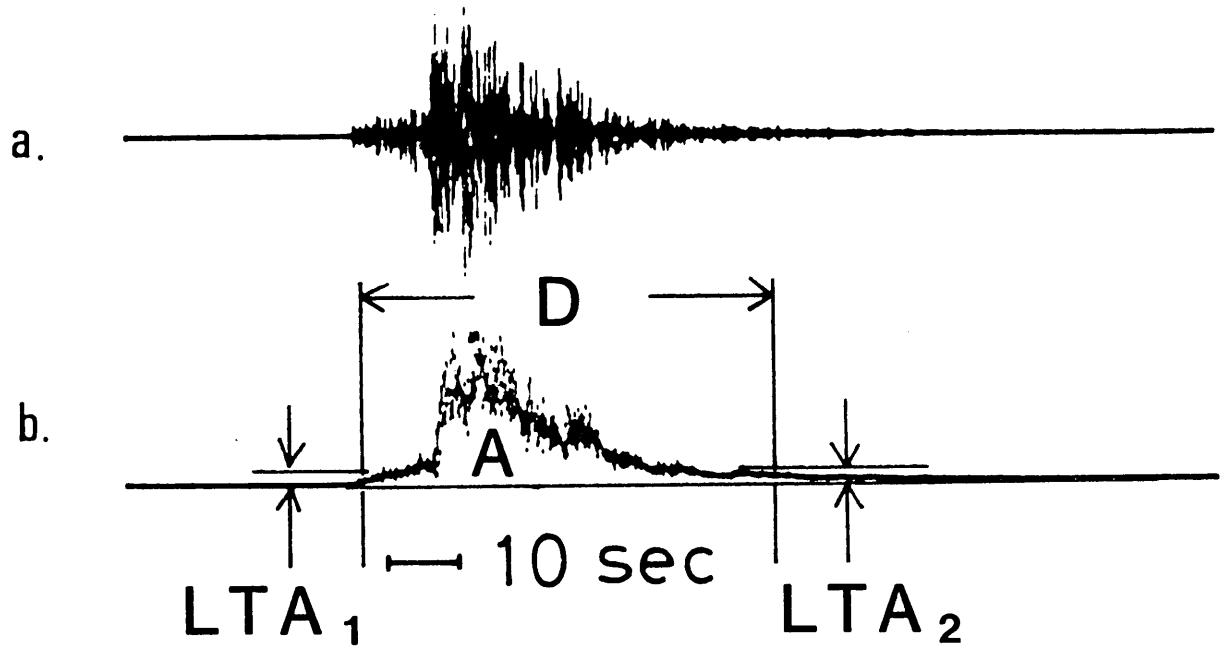

Fig. 5-14 (a) An example of a seismogram reproduced from an analogue tape. (b) Rectified and low-pass filtered signal of the same record as in (a). The signal, which represents the envelope of the original waveform, is digitized at a low sampling rate (10-15 Hz) for event detection. The signal is judged as an event if the STA/LTA exceeds a certain limit. Signal duration time (D), maximum amplitude, integrated amplitude during the event (A), LTA at the beginning of the event (LTA1) and that at the end of the event (LTA2) are measured.

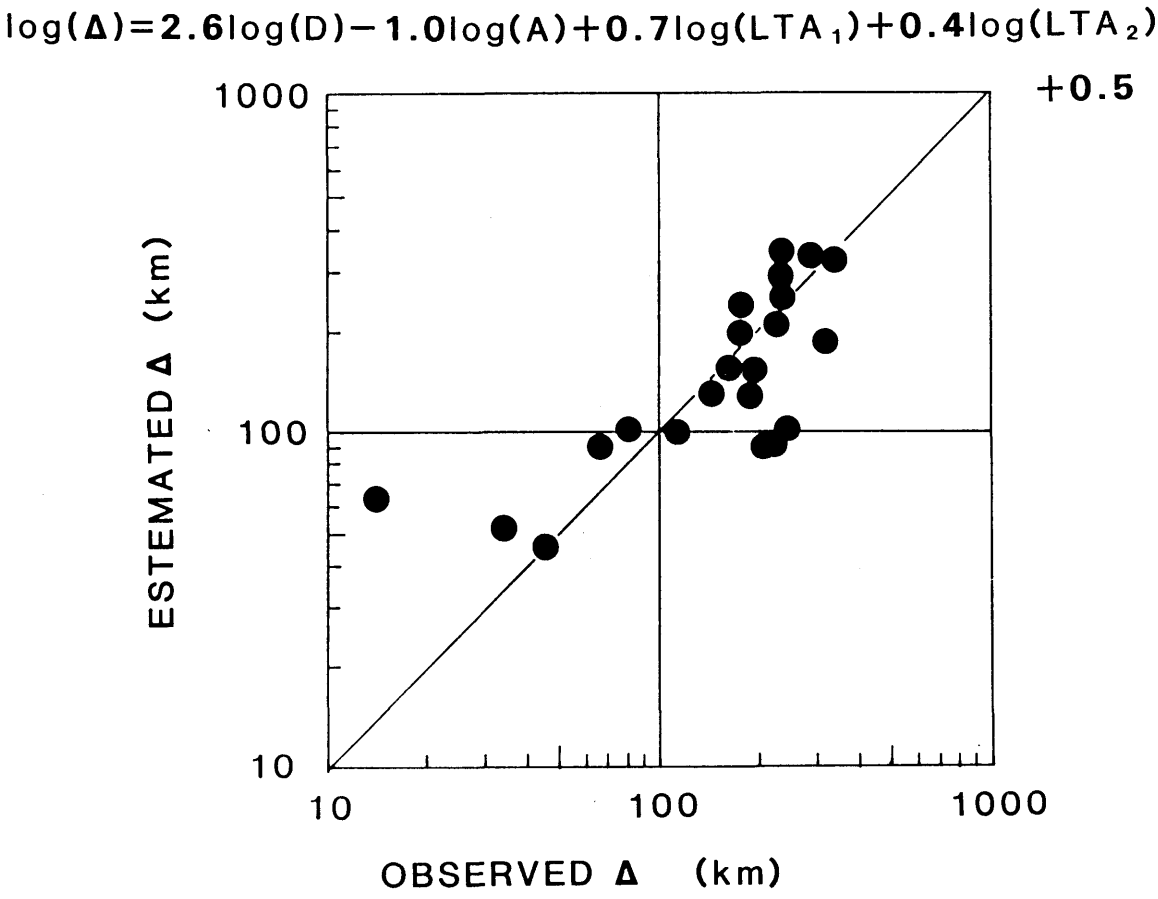

Fig. 5-15 Obseved epicentral distance measured by the hypocenter determination versus estimated epicentral distance obtained by the relation between amplitude and distance. Rough estimate with about 50 % from amplitude and signal duration data can be obatind from the formula. Coefficients are determined from selected 22 data.

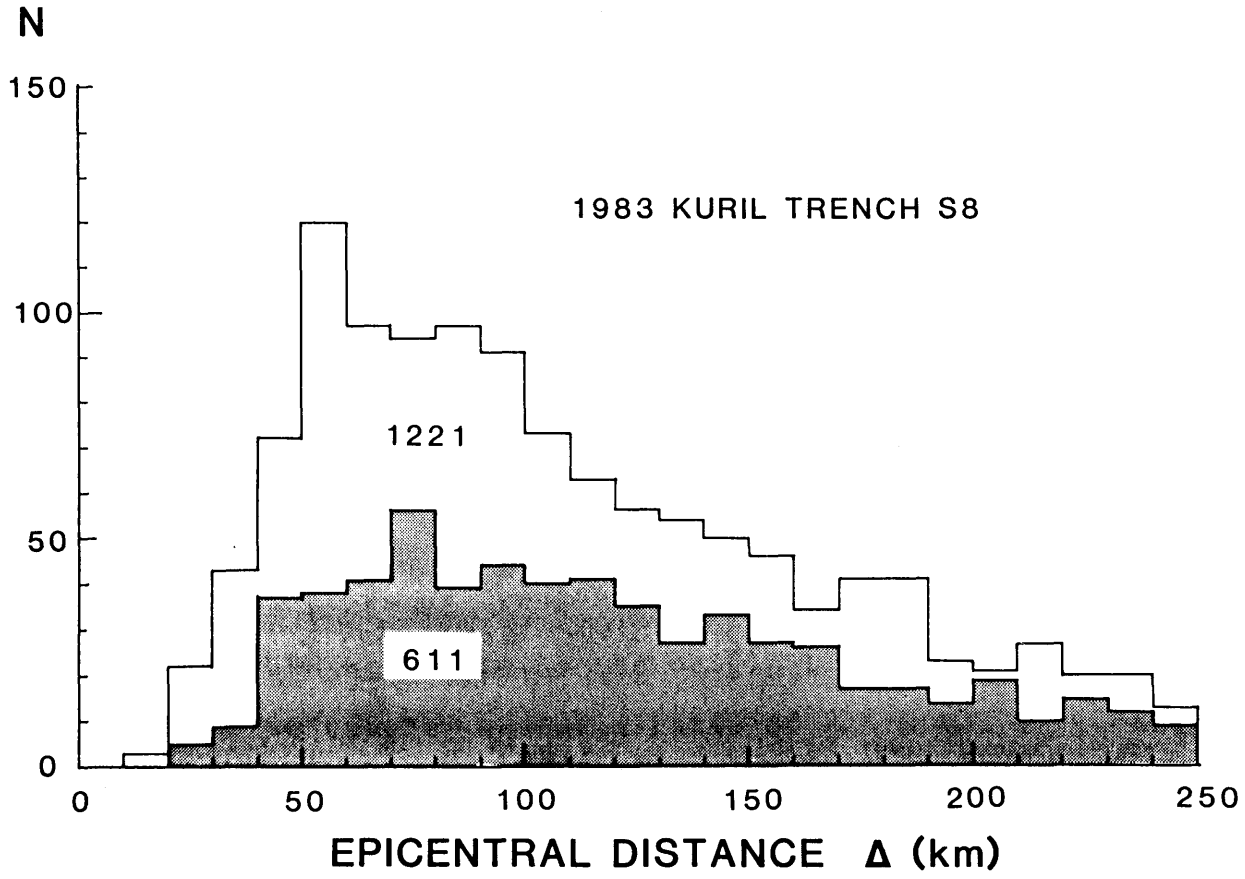

Fig. 5-16 Number of events with respect to epicental distance of evry 10 km. There are 1221 events which is detected by S8 and at least one more OBS within 250 km from S8. A shaded area indicate events detected by S8 and at least other four OBSs.The latter is about a half of the former, which shows taht many small events near S8 are not recorded by distant OBSs. The distances are estimated from the relation shown in Fig. Note that although individual distance has a large error, the whole distribution of the number of events is meaningfull enough to see the entir property of the data.

6 Spatial distribution of microearthquakes in the vicinity of trenches

6-1 Application of the new method of hypocenter determination

A new method for locating local earthquakes from arrival time data has been accomplished by applying the quasi-linear inverse theory developed in chapter 4. Input data for the inversion are arrival times of P-phases, initial guess of the hypocenter and probable errors in the data and the initial guess.

The arrival times of first P-phases are used for hypocenter determination. When we determine the origin time of an event from S-P time data, we usually assume a ratio of V_P to V_S. It is well known that the choice of V_P/V_S ratio affects not only estimations of origin times but also those of focal depths. In the numerical examples in 4-4, we demonstrated that the origin time and the focal depth strongly correlates to each other especially in under-determined case (Fig. 4-13). In the analysis of OBS data, the S-wave velocity structure is not well defined because of a thick unconsolidated sedimentary layer. To avoid the systematic errors due to ambiguity in the S-wave velocity structure, we often use only P-wave arrival time data for the location of earthquakkes. This method may cause more numerical instability than the method using both P- and S-wave data. The generalized least-squares solution defined in chapter 4 successfully removes the numerical instability existing in the conventional least-squares method by using a priori information about unknown

parameters.

In our method, the initial value of origin time is estimated from S-P times. The initial hypocenter is calculated by the conventional least-squares method for the estimated origin time. Therefore, if the data set of P arrival times has not enough resolving power, the final solution depends on the initial guess which are estimated from P arrival times and S-P times. We can evaluate how much the final solution depends on the initial guess by the analysis of a total covariance matrix of estimate. It should be noted that the S arrival time data affect the solution only through initial guess of origin time. In this sense the solution depends weakly on the S arrival time data.

Probable errors in the arrival time data are assumed as follows; residuals between observed and calculated arrival times are regarded as the sum of errors due to ambiguous onset of arrivals, those due to fluctuations in TCG and those due to discrepancies between a theoretical model and a real velocity structure. The TCG may fluctuate within 0.05 s. Standard eorros of 0.02 s, 0.1 s and 0.5 s were assigned to the reading errors of onsets depending on quality of records. About 1 % of travel time for each seismic ray was assigned to the errors due to the discrepancy in the velocity structure. Errors in locations of OBS stations are estimated about 0.2 km; the location of the ship from which the OBS was launched was determined by the Navy Navigation Satellite System with an accuracy of 0.1 n.m. Since P-wave velocity is 4-8 km/s, these errors may contribute the residuals by 0.05-0.02 s. As a whole, we usually assibned the standard errror of 0.1-1.0 s to the arrival time data and

constructed the covariance matrices $C[N]$s in 4-2-3.

6-2 Velocity structure model for earthquake location

Usually oceanic crust is covered by a low velocity sedimentary layer; the thickness of this layer may vary among OBS sites. The velocity structure near the OBS arrays were investigated by refraction and/or reflection surveys as was mentioned in 2-3. Air-gun refraction surveys were conducted in our experiment over most of OBS stations to obtain the local structure beneath each OBS.

Combining these results with the results of former surveys, we have chosen the velocity structure of profile 8 along 144°E in Ludwig et al. (1966) as a standard velocity model for the 1980 array (Fig. 6-1). The deviation of actual velocity structure from this standard model at each OBS site is calculated and added to observed arrival times as station correction. The correction for the sedimentary layer was done by using P-S converted phases recorded on a horizontal component and seismic profiler records by Murauchi et al. (1973). For the 1981 array, profile 7 along 143.5°E in Ludwig et al. (1966) was chosen (Fig. 6-2). The standard velocity model for the 1982 array is based on profile 4 in Asano et al. (1979) (Fig. 6-3). For the 1983 array the standard model is constructed from results by Nishizawa et al. (1984b) (Fig. 6-4). These models have no discontinuity in velocity and consist of flat layers with constant velocity gradient with depth as discussed in chapter 4.

In the trench area, the velocity structure of S-wave is not

as well understood as that of P wave. We suppose a ratio V_P/V_S to be 2.76 in the sedimentary layer; this was obtained by the analysis of the aftershocks of the 1978 Miyagi-oki earthquake (Yamada, 1980). A V_P/V_S ratio of 1.73 is assumed for the deeper part below the sedimentary layer. The assumption about S-wave velocity structure is used only to estimate the initial guesss of the origin time.

6-3 Analyses of errors in hypocenters by a total variance

The number of OBSs that can record the onsets of P-wave with enough SNR changes event by event; sometimes the effective number of arrival time data is less than the number of unknown parameters. The sparse distribution of stations may introduce errors due too poor resolution into the estimates of hypocenter parameters.The generalized least-squares solution can evaluate a proper confidence region forf the solution, even in the under-determined case, by defining a total covariance matrix of estimates. We examine the uncertainty of each estimated hypocenter in terms of the total covariance matrix.

To determine how much estimates are resolved by the OBS P-arrival time data, we calculate an error ellipse for each event by Eq. (4-81) with $\gamma = 1$ as was described in 4-4. The error ellipses for events in the 1980 through 1983 experiments are illustrated in Figs. 6-5 through 6-8. The large error ellipses show poorly resolved solutions which depend strongly on the initial guesses based on P- and S-wave data. Those events whose estimated probable errors do not fall below those of the initial

hypocenters may have as much error in the estimations of uncertainties as in the initial hypocenters. Such solutions are not used in detailed discussion, particularly on depths, because the prior constraint on focal depth is extremely poor.

Figure 6-5 shows the error ellipses for hypocenters determined by the 1980 array. Probable errors in the initial guesses are assumed to be 5 s for origin times and 25 km for epicenters. Depths are assumed to have errors of 50 % of their own depths for events deeper than 40 km or errors of 20 km for those shallower than 40 km. Errors in arrival time data are assigned as described in 6-1. Figure 6-5 shows that, in general, nearly uniform detectability can be expected within the latitude range of 39.5°-41.5°N and the longitude range of 143°-146.5°E.

The error ellipses for hypocenters determined by the 1981 array are shown Fig. 6-6; probable errors in the initial guesses are assumed to be 5 s for origin times, 25 km for epicenters and 50 km for focal depths. The 1981 array has nearly uniform detectability for events with magnitude greater than 2 in the latitude range of 39°-41°N and the longitud range of 142°-145.5°E. The error ellipses for hypocenters determined by the 1982 array are shown in Fig. 6-7; errors in the initial guesses are assumed to be the same as for the 1981 array. We can expect that the 1982 array has nearly uniform detectability within the latitude range of 40°-42.5°N and the longitude range of 141.5°-145°E. Figure 6-8 shows the error ellipses for hypocenters determined by the 1983 array. The 1983 array is expected to have nearly uniform detectability within the range of 40.5°-43°N and 143.5°-147°E. Errors in the initial guesses are assumed to be 0.3

s for origin times, 25 km for epicenters and 50 km for focal depth.

6-4 Epicentral distributions

Epicentral distributions determined from OBS data in the series of experiments from 1980 through 1983 are shown in Figs. 6-9 through 6-12 with bathymetric features. Within the area where the uniform detectability of events is expected, we can point out the following features in the epicentral distribution; there are seismic activities beneath the seaward trench wall and the continental slope. The seaward activity is concentrated within 100 km of the trench axis and beneath the oceanic basin the seismic activity is low. Although the landward activity widely exists beneath the continental slope, there is a gap in seismicity beneath the inner trench wall; the seaward and landward activities are separated by the gap.

6-4-1 Seismicity beneath the seaward trench wall

The 1980 OBS array located 65 earthquakes, which are shown in Fig. 6-9. About a half of these events are located just beneath or searward side of the trench axis. The seaward seismic activity has an eastern boundary along the edge of the seaward wall of the trench. The eastern edge of activity coincides with the isobath of 5500 m, where the western edge of the outer rise of the trench lies. The 1980 array has almost uniform detectability up to 146.5°E, as mentioned in 6-3. Hence we can

conclude that the microearthquake activity seaward of the trench axis is restrained beneath the seaward wall of the trench. In this region, the seismic activity beneath the oceanic basin low. The distribution of number of events with respect to number of stations which detect the events as shown in Fig. 5-4 is consistent with the epicentral distribution in Fig. 6-9; P9 and P12, which were located on the Northwest Pacific Basin, detected a small number of events near these OBSs. Data obtained by the 1981 array also show the high seismicity beneath the seaward wall of the Japan Trench (Fig. 6-10).

The 1983 array located microearthquakes on the both sides of the axis of the Kuril Trench. The seaward activity in the Kuril trench is also restrained beneath the outer trench wall and low beneath the oceanic basin (Fig. 6-12).

6-4-2 Seismicity beneath the continental slope and low seismic activity beneath the landward trench wall

Many earthquakes are located beneath the continental slope by the 1980, 1981, 1982 and 1983 arrays. But no event is located by the 1980 array beneath the area west of the trench axis between isobaths of 6000 and 4000 m (Fig. 6-9); the area is situated within the OBS array. This feature does not change even if the errors in location are taken into consideration, as shown in Fig. 6-5. The 1980 array observed high seismicity beneath the western part of the continental slope at a water depth of less than 4000 m and a gap in seismicity beneath the landward wall of the Japan Trench at least during our observational period.

The 1981 array located events beneath the continental slope at a water depth of less than 3000 m (Fig. 6-10). OBS P10 of the 1981 array was located just on the landward wall of the Japan Trench. S-P time distribution obtained at each OBS shows that OBS P10 and P12 have observed relatively distant events as compared with all the others (Fig. 6-13). Furthermore, records at P10 have larger S-P times on average than those at P12. The smallest S-P time clearly recorded by P10 was 5.8 s. Although S-wave arrivals are delayed by the sedimentary layer, it is clear that the level of the seismicity is very low near P10 of the 1981 array.

The area off Urakawa, Hokkaido, is the most active area in seismicity beneath the continental slope at the junction of the Japan Trench and the Kuril Trench. The 1982 array located many microearthquakes around OBS P1 and P2. Most of them are aftershocs of the 1982 Urakawa-oki earthquake on the coast line of the Urakawa. The seismicity is high beneath the western part of the continental slope and low beneath the eastern part of the slope. S-P time distributions also show that the level of seismicity is low around P3 and P6. The S-P time distribution at P1 shows prominent double peaks; the peak of 10 s corresponds to the steady state activity off Urakawa and the peak of 18 s to the aftershocks of the 1982 Urakawa-oki earthquake.

Figure 6-12 shows the epicentral distribution determined by the 1983 array. Generally speaking, beneath the deeper part of the continental slope at water depth of 3000 to 6000 m, the seismicity is low. In particular, no event was located in the area with the water depth of 4000 - 6000 m; the seismicity gap beneath the inner trench wall exists also in the Kuril Trench

area. On the contrary, beneath the shallower part of the continetal slope, some concentrated seismic activities are detected near OBS SG, S8 and S9, which seems to be correlated with oceanic canions; the most prominent one near the OBS array occured along the Erimo Canion located west of OBS SG.

It seems to exist seaward seismic activity and seismicity gap beneath the inner trench wall also in the northeast of the 1983 array. Directions of wave approaching and apparent velocities show that one group of seismic signals with S-P time of less than 30 s came from the direction of 40-60° clockwise from the north and another group came from the direction of 70-80° (Fig. 6-15). The latter group corresponds to the seaward seismic activity in the northeast region. Further, a gap (60-70°) between these two group corresponds to the seismicity gap beneath the inner wall of the Kuril Trench.

6-5 Focal depths

In order to confirm the depth distribution of microearthquakes, it is necessary to select events which have good accuracy in depth. Events having large error ellipses depend strongly on the initial guess. Vertical cross-sections of hypocenter distribution obtained by the 1980 array are shown in Fig. 6-16; these are viewed from S10W parallel to the trench axis and from E10S perpendicular to the axis. There are 32 events on this cross-section. These hypocenters satisfy the condition that the total standard error of the solution is less than 30 km for epicenter and 20 km for depth, and residuals are within 0.5 s for

P-wave arrival times and 5 s for S-P times. Most of the selected events have residuals within 0.2 s for P arrival times and 2.0 s for S-P times. Figure 6-16 shows clearly that earthquakes beneath the seaward wall of the trench occur within the depth of a few tens kilometers and that foci start to deepen westward exactly at the trench axis, with a very low dip angle; microseismicity beneath the trench area is concentrated only in the shallower part of the oceanic lithosphere.

Figure 6-17 shows the depth distribution of microearthquakes determined by the 1981 OBS array. OBS data show that earthquakes occur in the uppermost oceanic lithosphere. It is seen from this cross-section that there are two separate zones of seismicity. The first one is seismic activity beneath the seaward and/or the trench axis, which extends from 30 to 60 km in depth. The second zone is a shallower extension of the double structured seismic zone. The hypocenters are concentrated in that part shallower than 50 km, which forms a seismic zone dipping landward with a very low angle. This can be regarded as the shallower extension of the upper plane of the double structured seismic zone. The 1981 OBS array located no event which was situated in a shallower extension of the lower plane beneath the array.

There is a little difference in depth distribution between the two results obtained from the 1980 data and the 1981 data (Figs. 6-17 and 6-18); for events located westward of the trench axis, the location determined by the 1980 array is systematically deeper than that by the 1981 array by about 10km. This discrepancy arises from the geometry of each array relative to events considered. Beneath the continental slope, the focal depth

distribution obtained from the 1981 data gives more reliable result than that from the 1980 data, because most part of the area is covered by not the 1980 but the 1981 array. Comparing these results, the focal depths determined by the 1980 array should be shifted shallower by about 10 km in the landward area. On the contrary, the depth distributions just beneath the trench axis agree with each other because the area is covered by both the 1980 and the 1981 array. In the area seaward of the trench, the focal depth obtained from the 1980 data gives more reliable results than that from the 1981 data.

Figure 6-18 shows a depth distribution beneath the Kuril Trench from data obtained by the 1983 observation. Selected hypocenters with good accuracy are projected on a plane approximately perpendicular to the strike of the Kuril Trench. The distribution is similar to that beneath the Japan Trench; the activity searward of the trench occurs from 0 to 30 km in depth and the activity westward of the trench forms a distribution dipping landward with a low angle. However, it is to be noted that the foci of the landward activity are slightly deeper as compared with those beneath the Japan Trench.

The apparent velocities for the events detected by the 1983 array are consistent with the results by the hypocenter determination (Fig. 6-15); the P-wave incoming from the direction of between 120° and 170° to the tripartite OBSs of SE, S11 and S12 have an apparent velocity of about 6.5 km/s. The apparent velocity and the directions of waves approaching mean that the seaward seismic activity occurs in an oceanic crust or a very shallow portion of the oceanic lithospher.

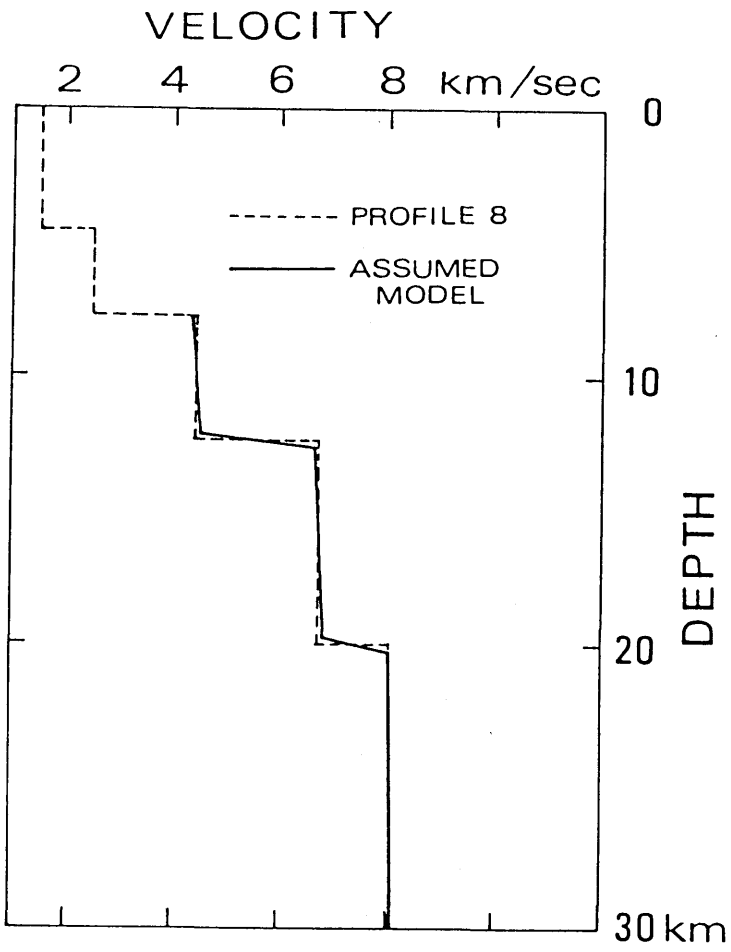

Fig. 6-1 An adopted *P*-wave velocity model for hypocentre locations based on a velocity structure derived from refraction profile 8 in Ludwig *et al.* (1966). The original model for profile 8 is indicated by a broken line. The position of the profile is indicated in Fig. The assumed model consists of five flat layers having a constant velocity gradient without velocity discontinuity. The difference in thickness of the sedimentary layer among OBS sites is taken into account by applying appropriate station corrections to arrival time data.

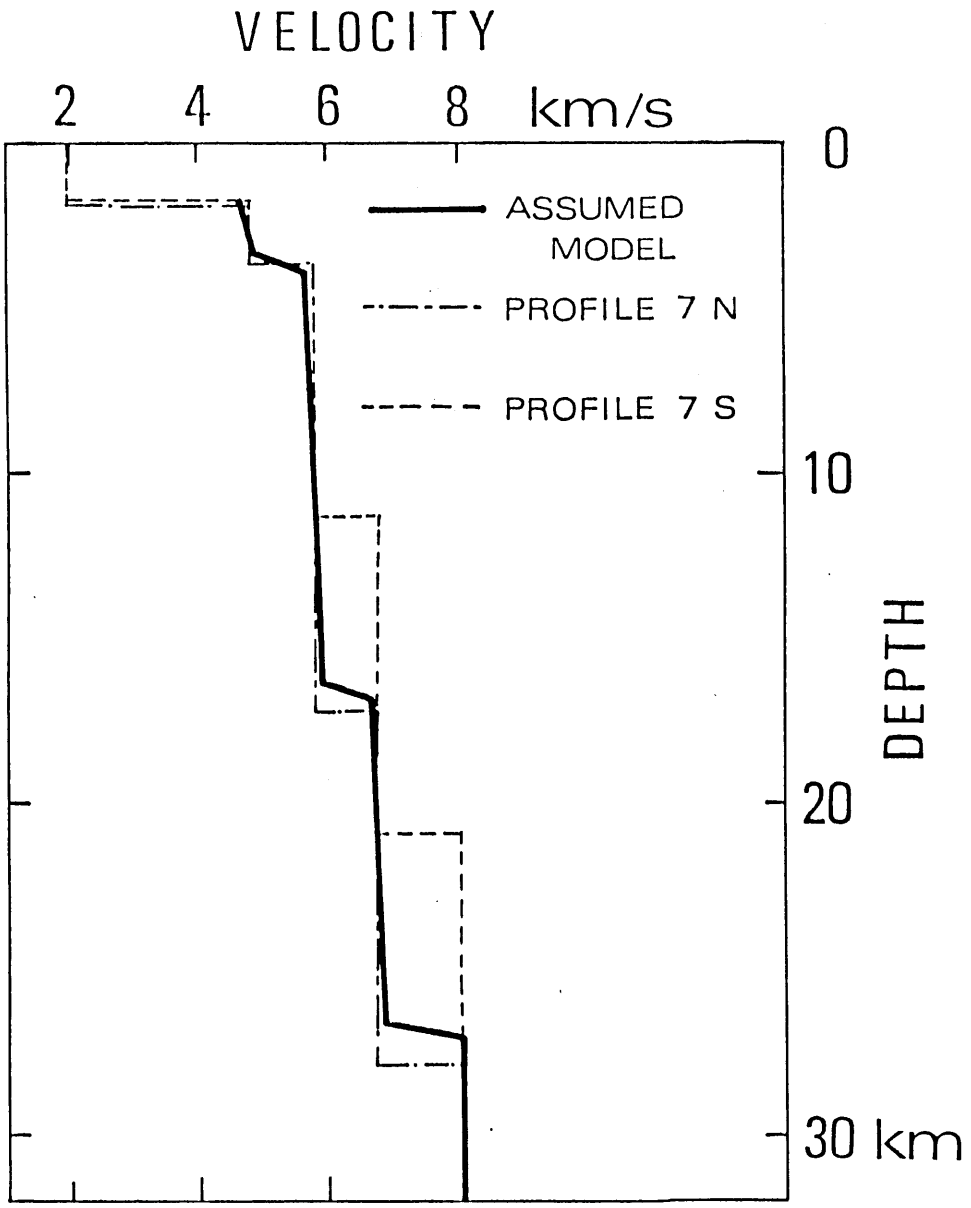

Fig 6-2 An adopted P-wave velocity model for hypocenter location, which is based on a velocity structure derived from refraction profile 7 in Ludwig et al. (1966). The original model for the north end of profile 7 and the south end are displayed. The position of the profile is shown in Fig. The assumed model consists of seven flat layers having a constant velocity gradient without velocity discontinuity. The difference in thickness of the sedimentary layer among OBS sites is taken into account by applying appropriate station corrections to arrival time data.

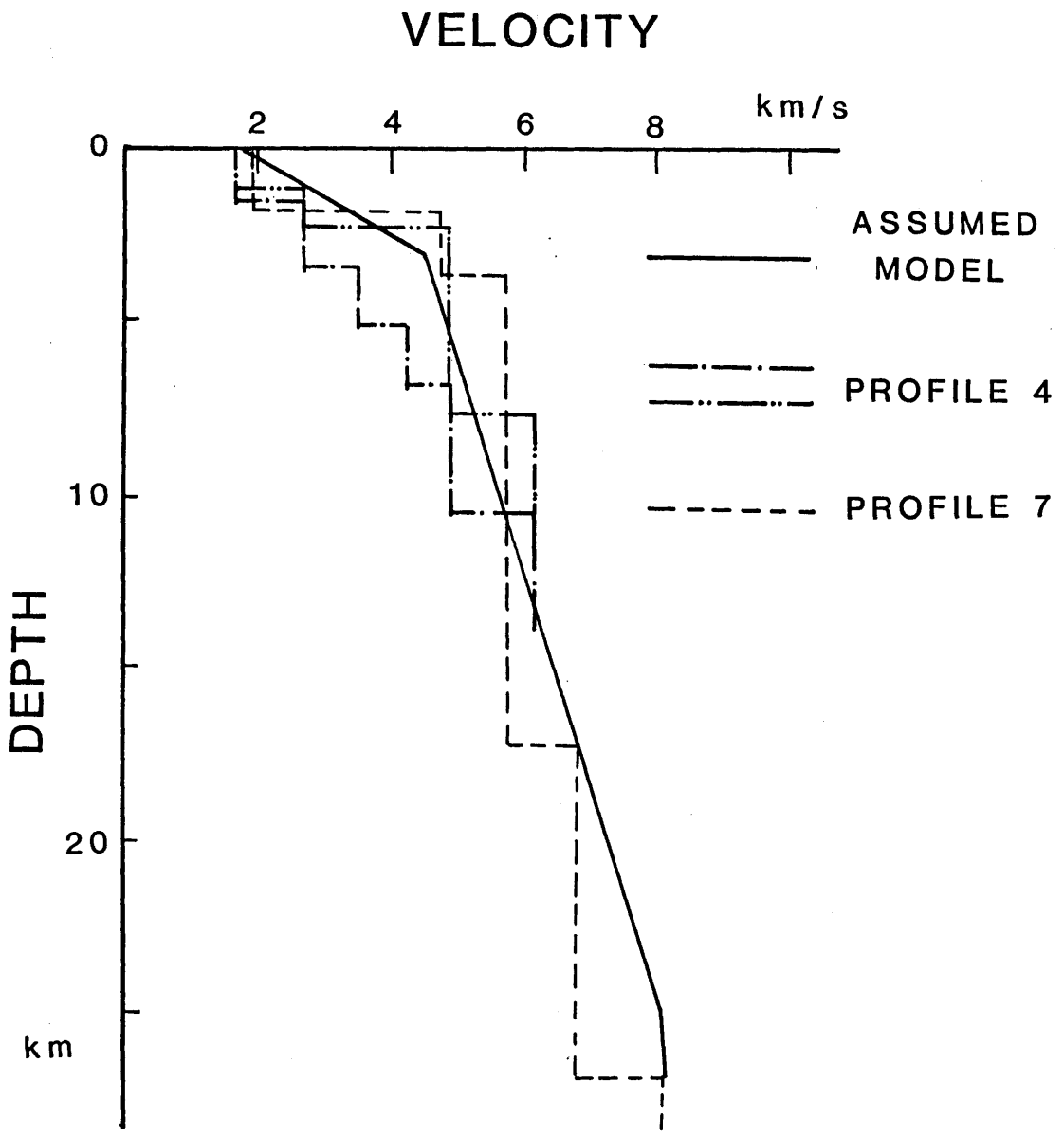

Fig.6-3 An adopted P-wave velocity structure model for hypocenter location. The model is derived from refraction profile 4 in Asano et al. (1979) and profile 7 in Ludwig et al. (1966).

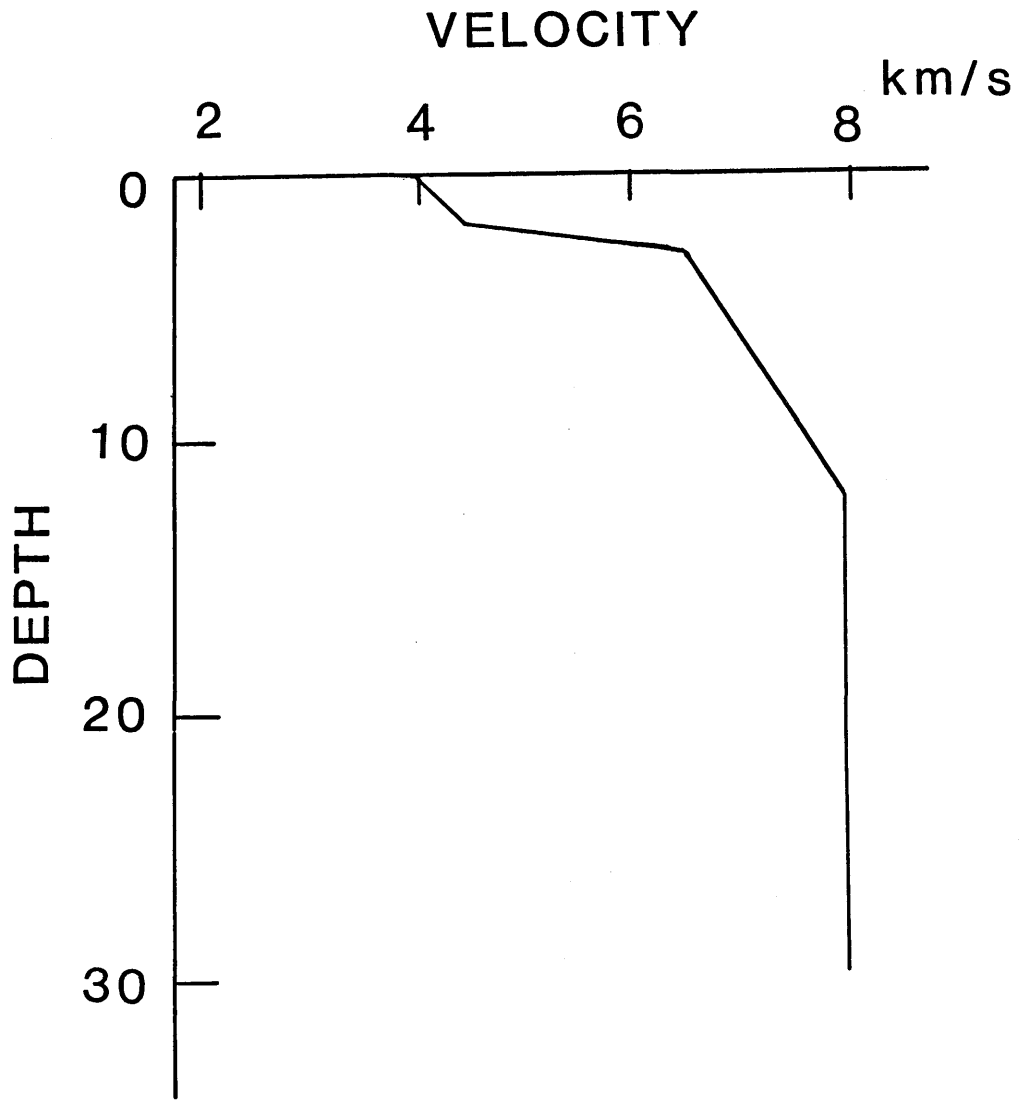

Fig.6-4 An adopted P-wave velocity structure model for hypocenter location. The model is derived from Nishizawa et al. (1984b).

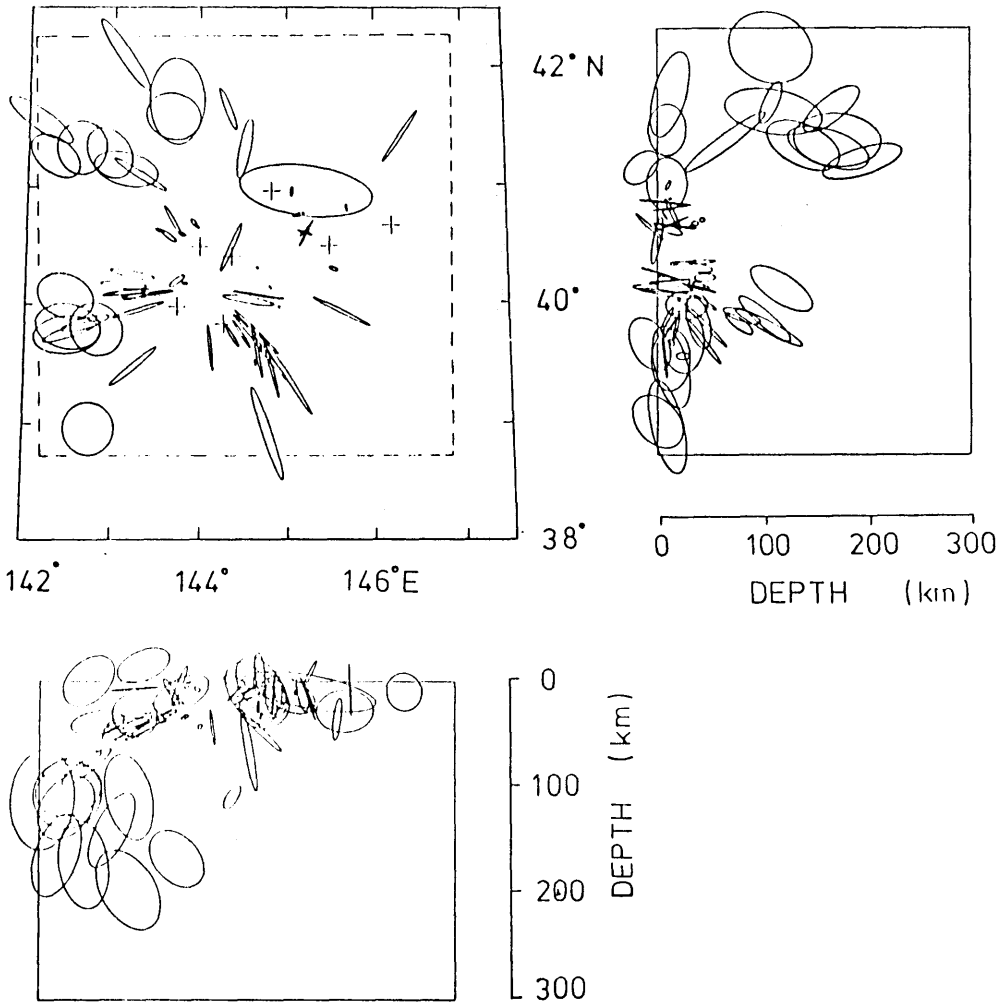

Fig. 6-5 A horizontal section and vertical sections indicating errors in estimated hypocentres. Dimensions of ellipses represent standard deviations of solutions. The resolution of the OBS array to locate events is taken into account in the procedure for evaluating errors in estimation. Within or nearby the OBS array, errors in solutions are small compared with those far away from the OBS array. Events with a large ellipse near the array are located by a small number of OBS stations. The OBS array has a spatially uniform capability of earthquake location within the latitude range of 39.5°–41.5°N and the longitude range of 143°–146.5°E, a total of over 300 km covering both sides of the trench axis. Within this area the locations of events are accurate enough to show patterns of seismicity.

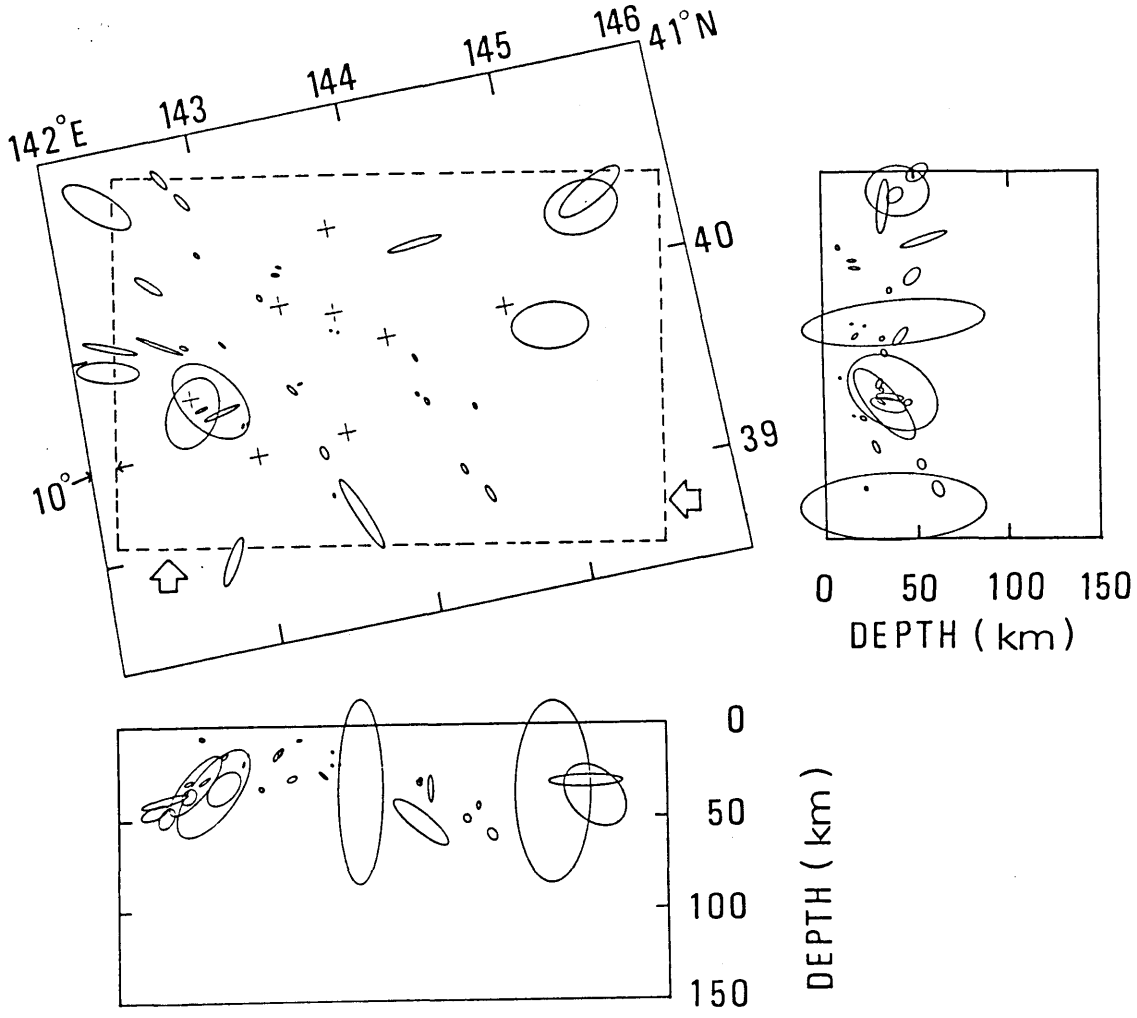

Fig.6-6 A horizontal section and vertical sections indicating errors in hypocenters determined by the 1981 OBS array. Dimensions of ellipses represent one standard errors of solutions.

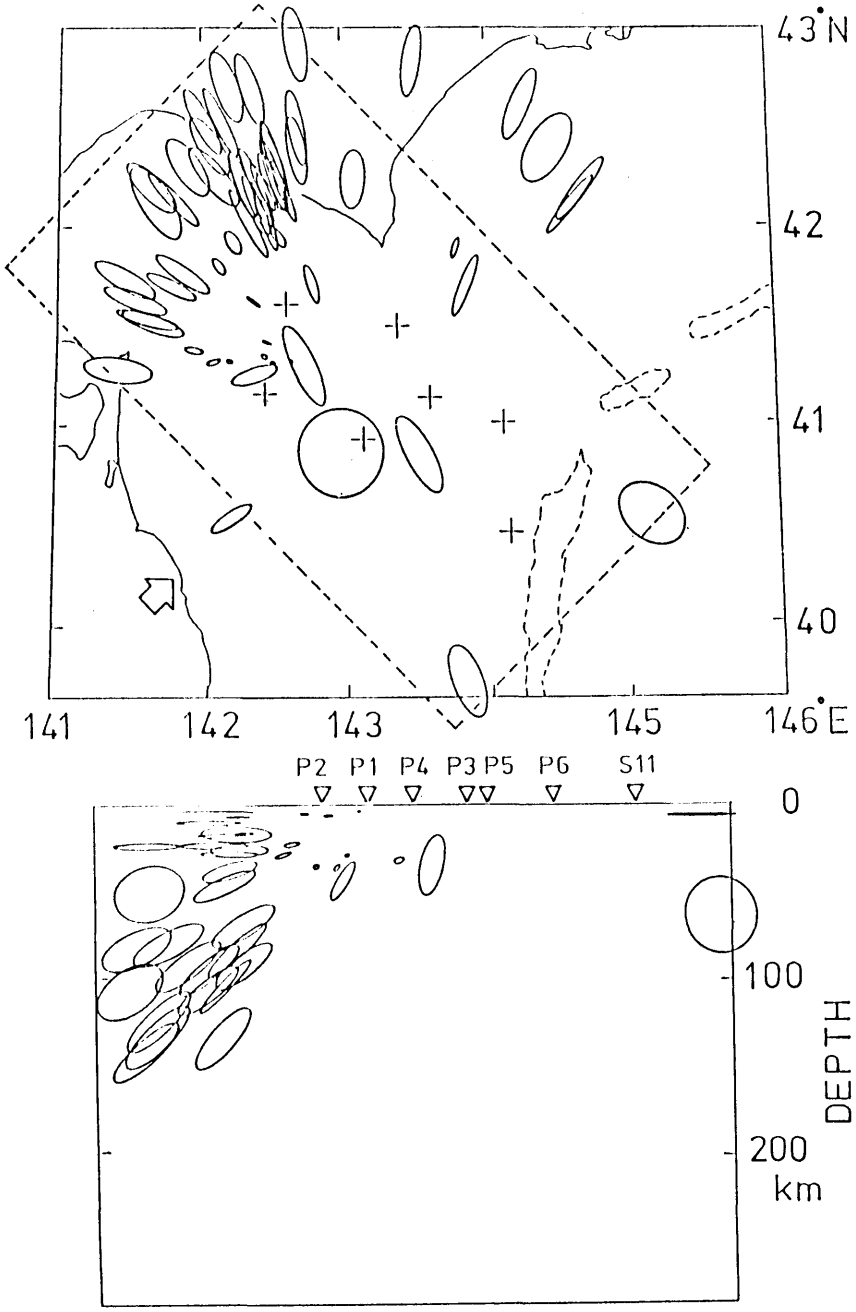

Fig.6-7 A horizontal section and a vertical section indicating errors in hypocenters determined by the 1982 OBS array. Dimensions of ellipses represent one standard errors of solutions.

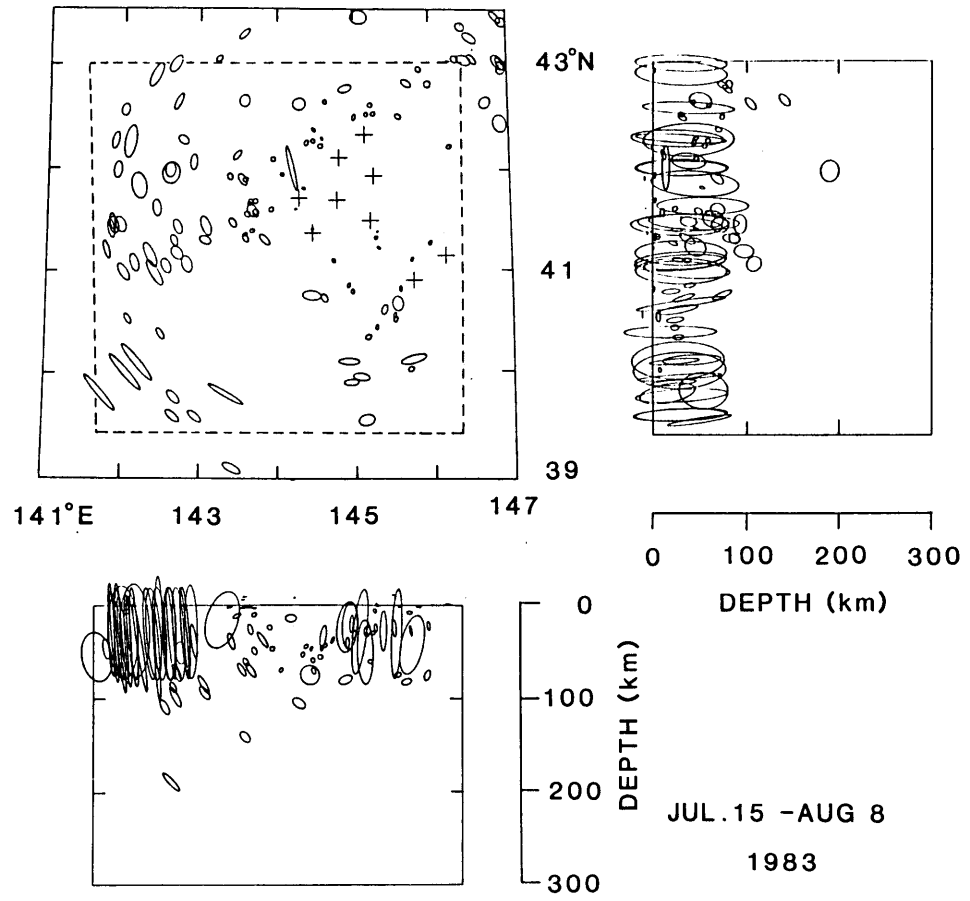

Fig. 6-8 Hypocentral distribution determined from first arival time data. Dimension of each ellipsis represents a standard deviation of the solution of hypocenter. Note that events with a large error strongly depends on an initial guess of the solution. Within the OBS array solutions have enough accuracy to resolve some concentrated activities.

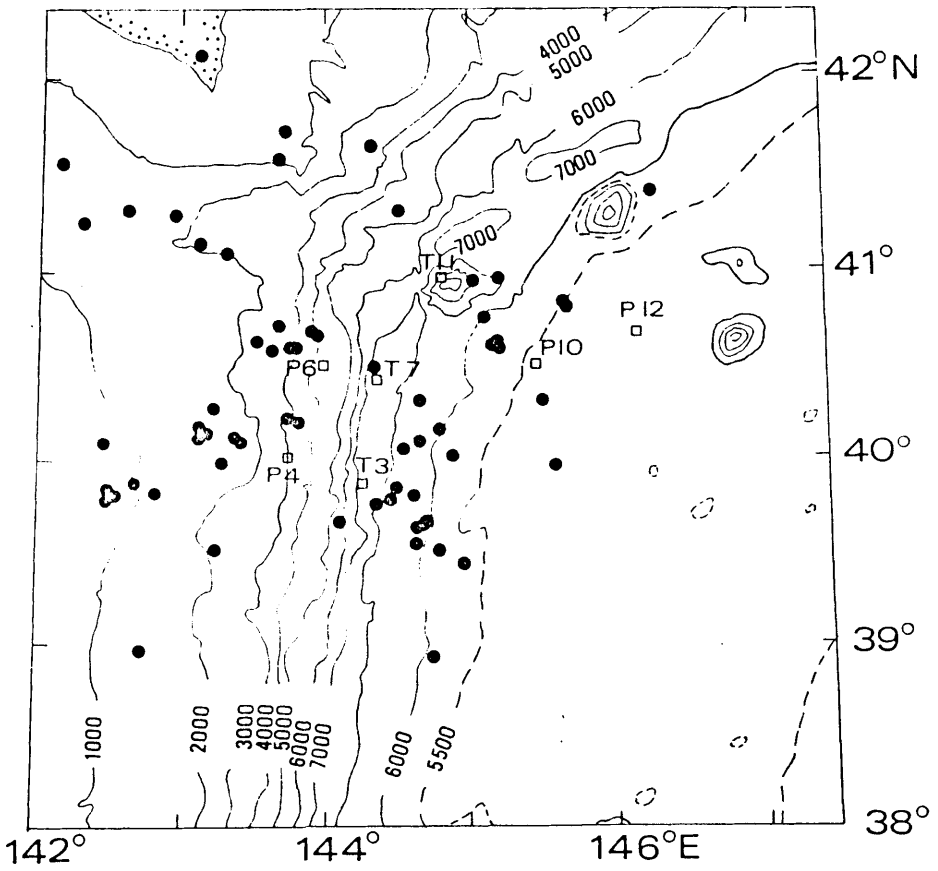

Fig. 6-9 Hypocentres located by the OBS array. Open squares represent the positions of OBSs. A bathymetric feature is indicated by isobaths in metres. Active seismicity beneath the seaward trench wall is shown. The seaward activity is concentrated within the area deeper than 5500 m. No event is located within the area surrounded by the four western OBSs with sea depth between 4000 and 6000 m. (1980)

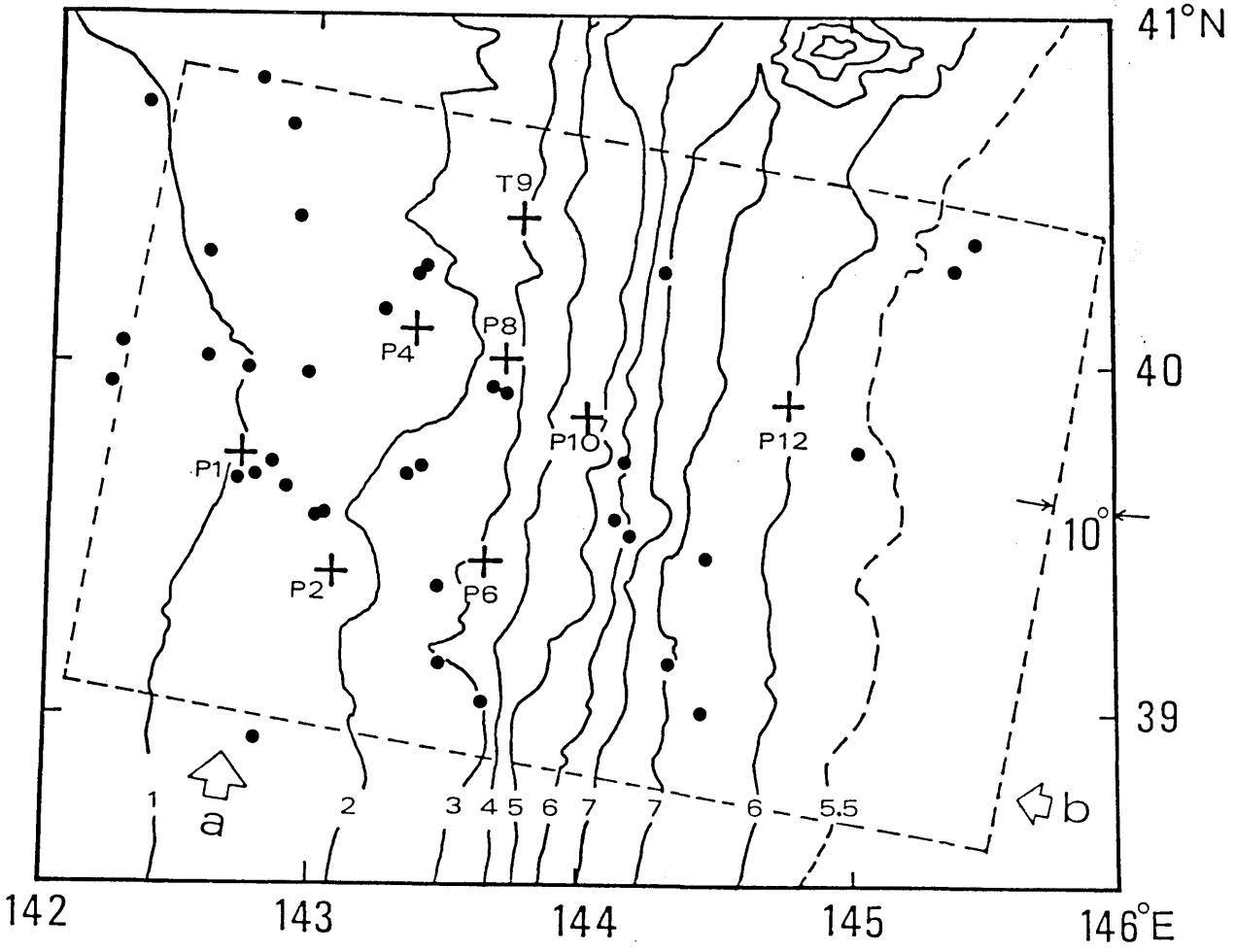

Fig. 6-10 Epicenters located by the 1981 OBS array (solid circles). Positions of OBSs are shown by crosses. A bathymetric feature is indicated by isobaths in kilometers. Seismic activities exist on the both sides of the trench axis. No event is located beneath the inner trench wall with water depth of between 3 and 6 km.

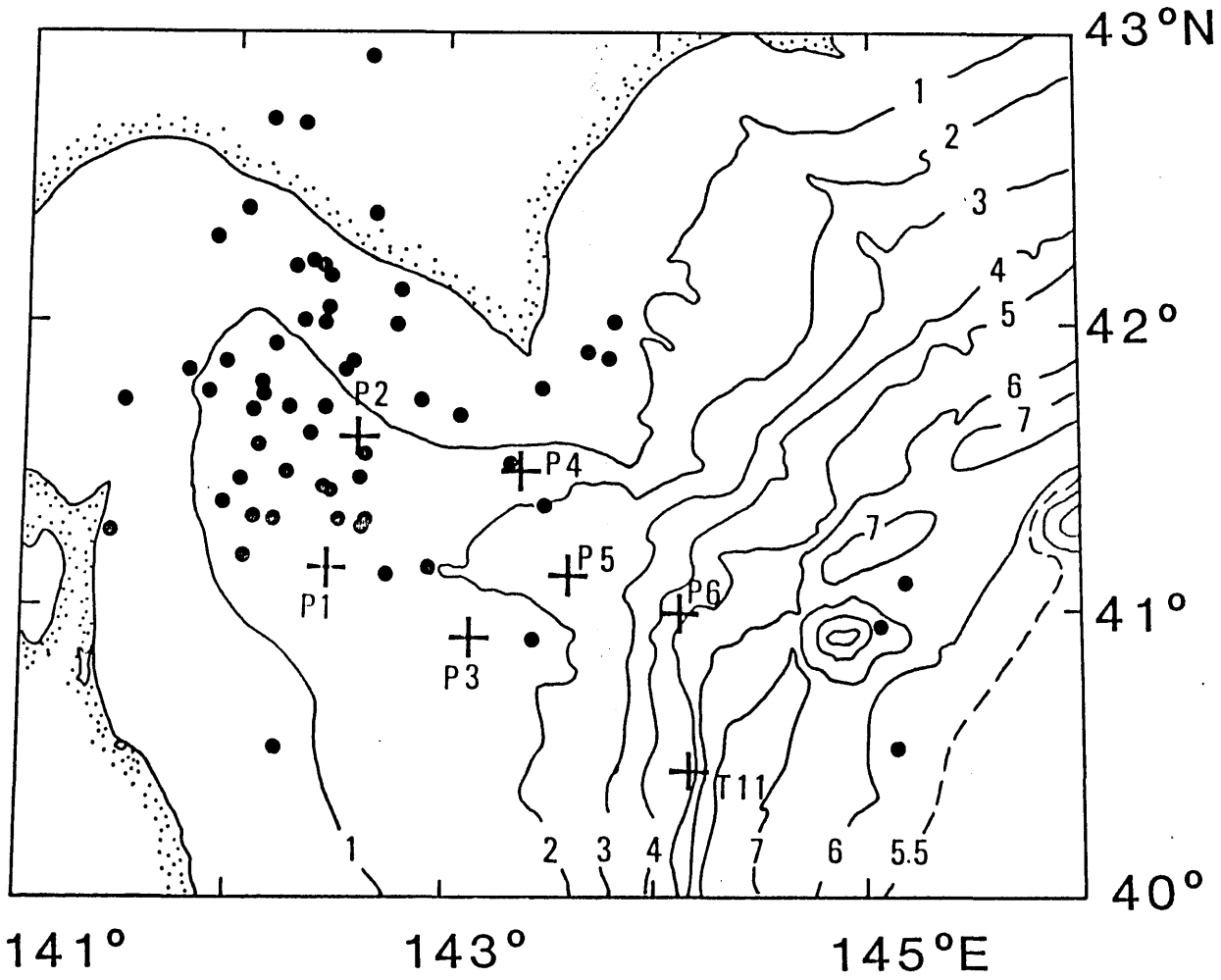

Fig.6-11 Epicenters located by the 1982 OBS array (solid circles). Positions of OBSs are shown by crosses.

Fig. 6-11

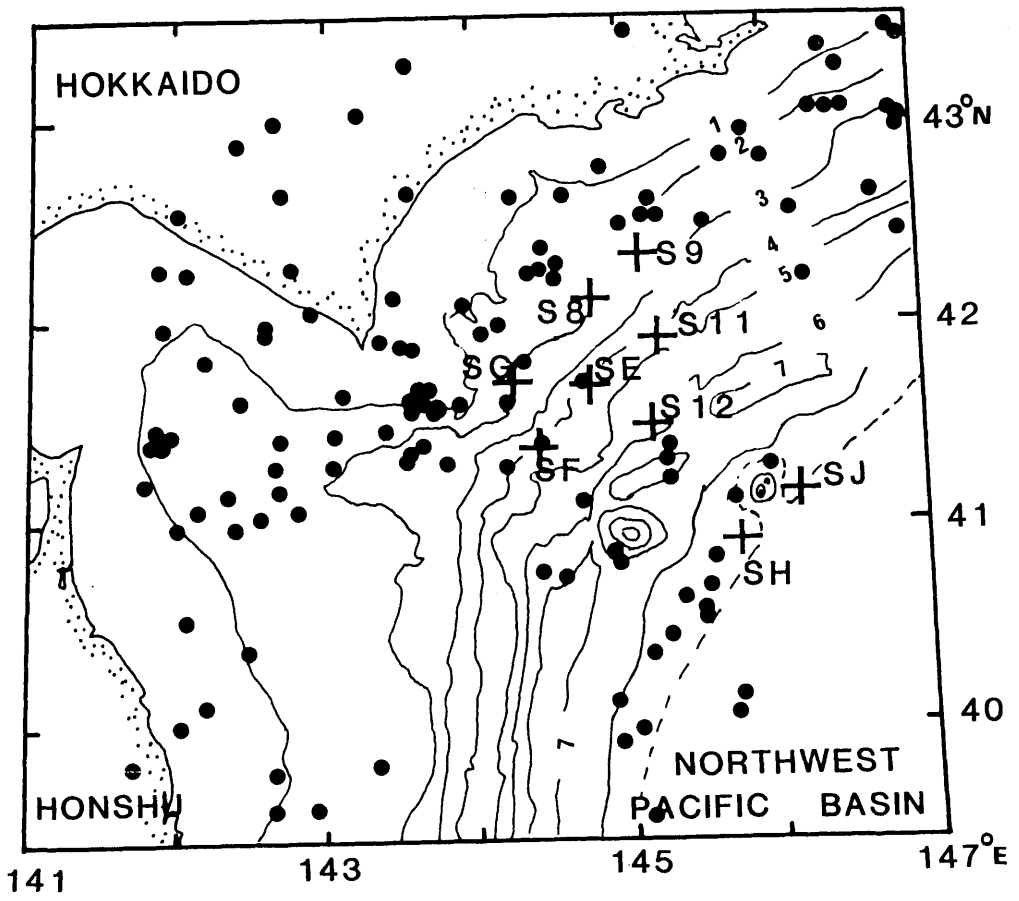

Fig. 6-12 Correlation between epicentral distribution and bathymetry. Beneath the outer trench wall with water depth of greater than 5500m, there is a prominent shallow activity, while seismic activity beneath the northwest pacific basin is very low. The seismicity gap exists beneath the inner trench wall with a water depth of between 4000 m and 6000 m, which has been found in the Japan Trench area off the Sanriku Coast. Some concentrated activities are seen near OBSs(SG, S8 and S9), which seems to be correlated with oceanic canions.

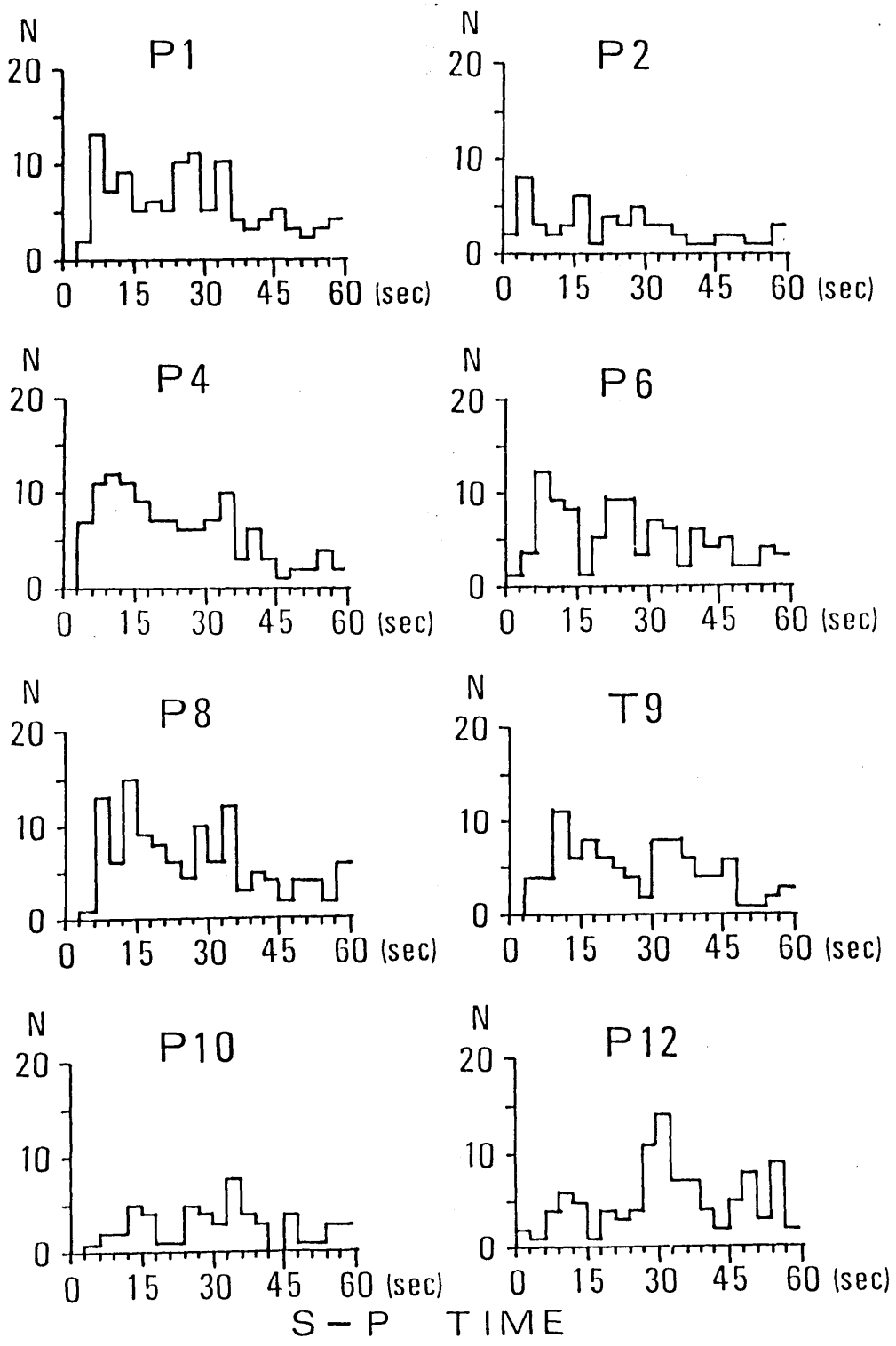

Fig. 6－13 Histograms of S-P times recorded by OBSs operated in 1981, positions of which are shown in Fig.2-6. A S-P time distribution at OBS P10 shows relatively low seismicity near this station which is located on the inner wall of the Japan Trench. The smallest S-P time recorded by P10 was 5.8 s. Recording period of each OBS is listed in Table 2-3.

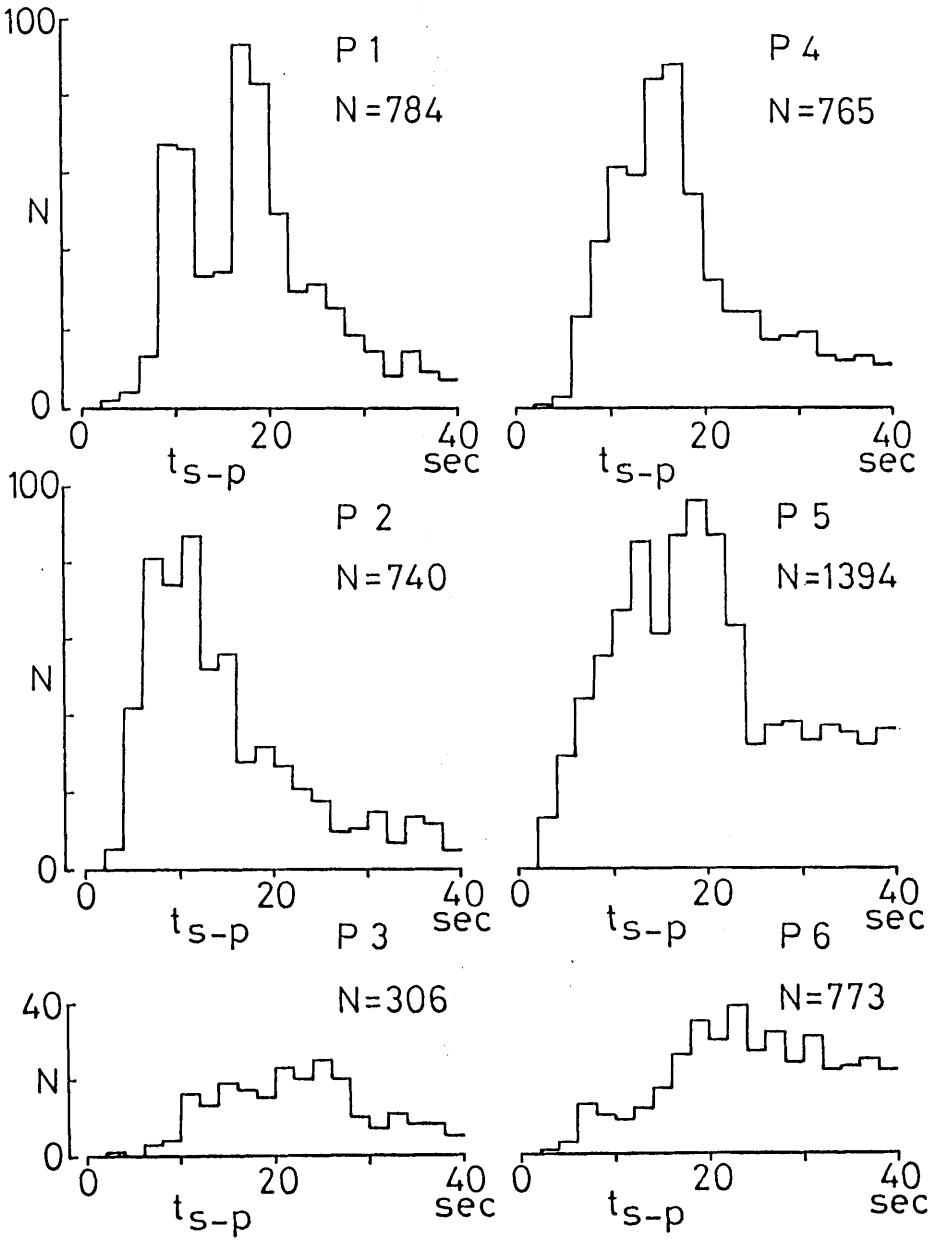

Fig.6-14 Histgrams of S-P times recorded by OBSs operated in 1982, positions of which are shown in Fig. 2-7. S-P time distributions at OBSs P3 and P6 show relatively low seismicity near these stations.

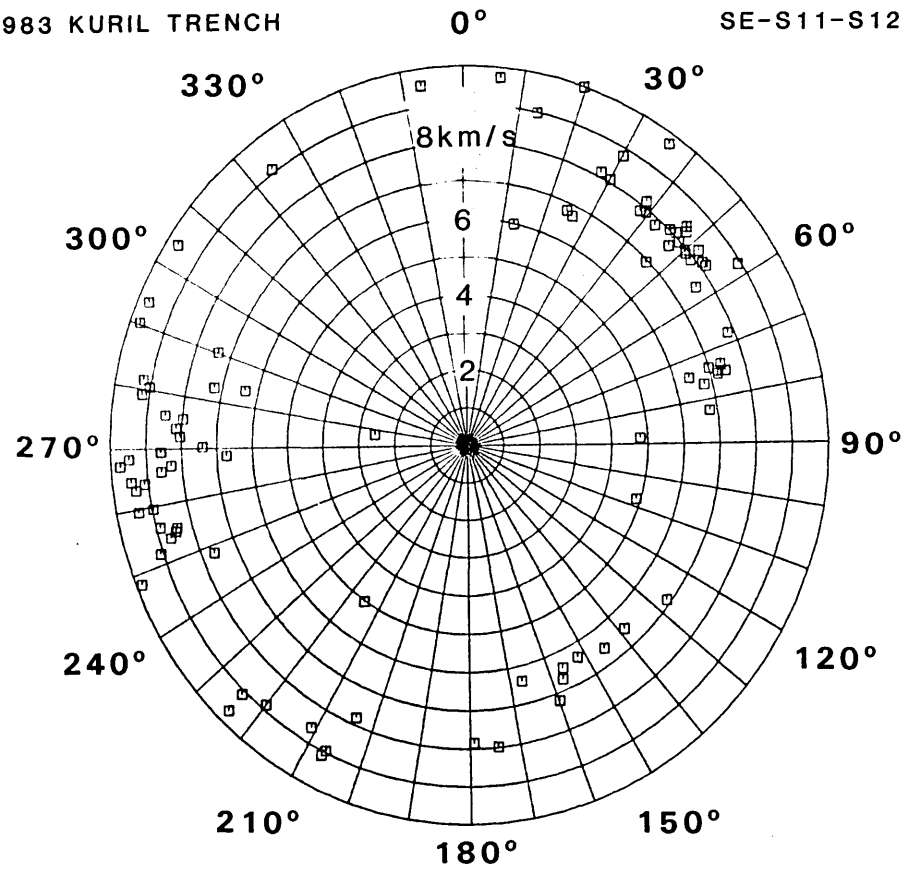

Fig. 6-15

Distribution of direction of wave approaching and apparent velocity measured by the three OBSs (SE,S11 and S12). Directions are measured clockwise from the north. Note that a gap between 60° and 70° corresponds to the inner trench gap beneath the Kuril Trench. Seaward activity plotted between 120° and 170° shows apparent velocity of about 6.5 km/s, which means these events exist in a very shallow portion of the oceanic lithospher or the oceanic crust.

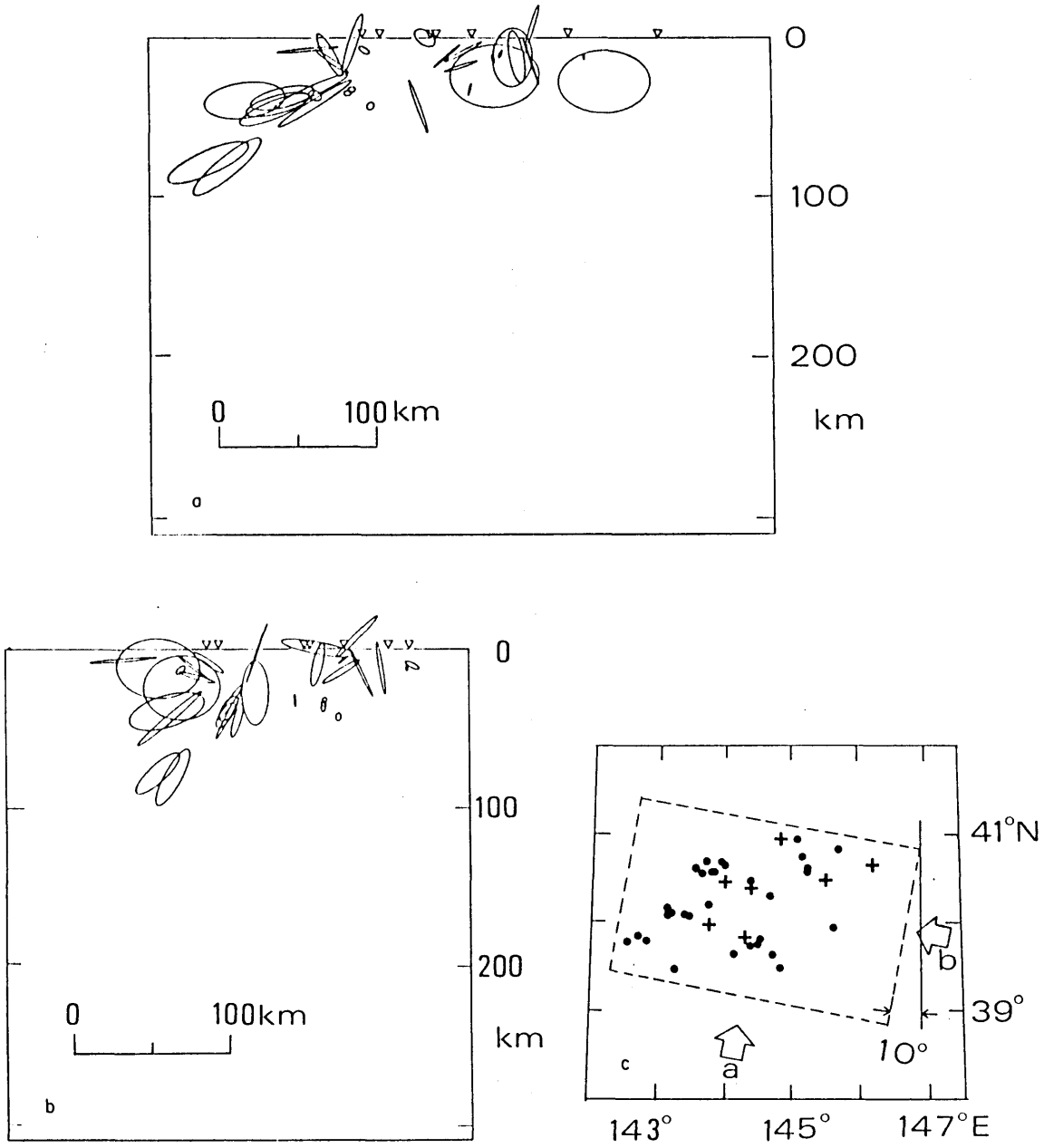

Fig. 6-16 Vertical cross-sections composed of events with good accuracies in depth. The criteria for selecting events are described in the text. (a) Cross-section viewed from 10° clockwise from the south. Sizes of ellipses represent the standard deviations of hypocentre solutions. (b) Viewed from 10° clockwise from the east. (c) Epicentres of selected events. Arrows indicate the projection directions of (a) and (b). (1980)

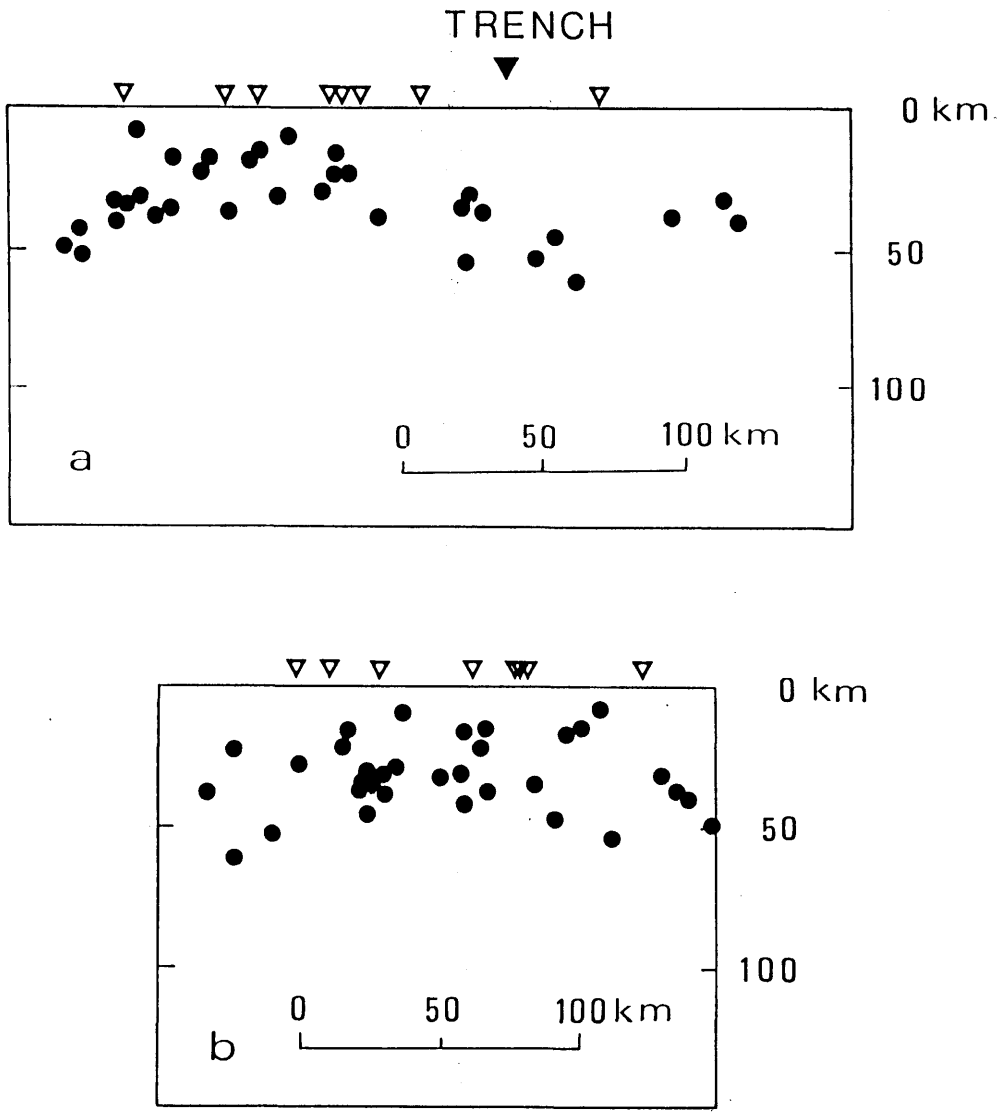

Fig. 6-17 Vertical cross-sections of events plotted in Fig. 6-10 where projection directions of (a) and (b) are indicated. Open triangles show locations of OBSs. A solid triangle indicates the position of the trench axis. (a) Cross-section perpendicular to the trench axis, which is viewed from 10° clockwise from the south. Activity landward of the trench axis is concentrated in the uppermost part of the lithosphere. Focal depth increase landward with a very low dip angle. (b) Viewed from 10° clockwise from the east.

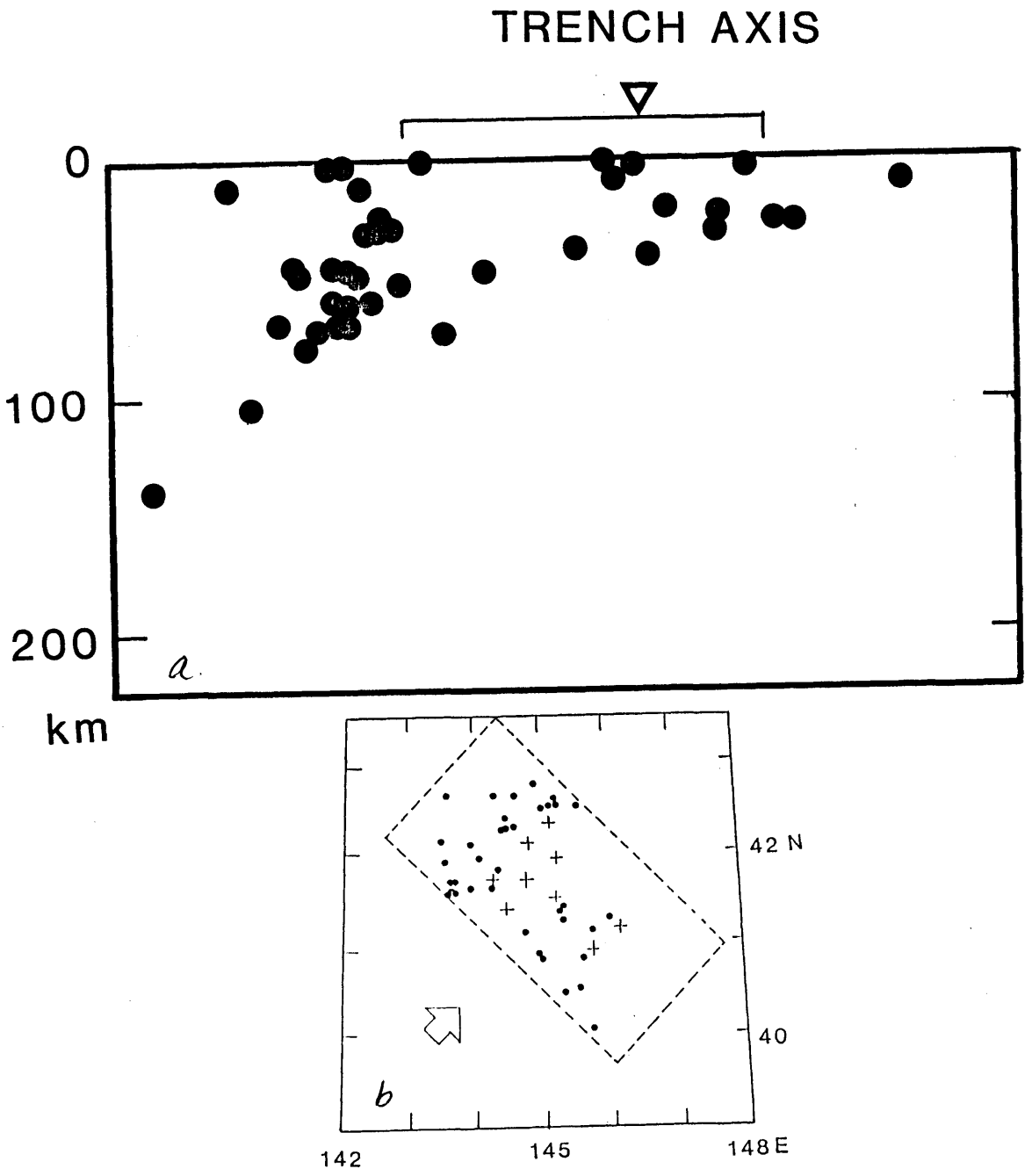

Fig.6-18 Vertical cross-section of earthquakes beneath the Kuril Trench and their epicenters. (a) Events with good accuracies in depth are selected and projected onto a plane striking NW to SE, which is perpendicular to the trench axis. The projection direction is shown in (b).

7 Discussion

7-1 High seismicity beneath the seaward trench wall and low seismicity beneath the oceanic basin

Observations by the 1980 and the 1981 OBS arrays have revealed high seismic activity beneath the outer wall of the Japan Trench and low seismic activity beneath the oceanic basin (Fig. 7-1). Seismicity detected by the land network over the past several years also indicates high seismicity beneath the seaward wall and low seismicity beneath the Northwest Pacific Basin (OCEP, Tohoku University, personal communication). However, the observations by the land network are not sufficiently sensitive to determine a definite boundary between the area with high seismicity and that with low seismicity. Past OBS observations in the Japan Trench area (Nagmo et al., 1970a, 1970b, 1976) are also in agreement with our results.

The epicentral distribution obtained from the 1982 and the 1983 OBS data is illustrated in Fig. 7-2; it clearly shows high seismicity seaward of the trench axis in the southernmost part of the Kuril Trench. In the area northeast of the 1983 array near (42.4°N, 148°E), seismic activity seaward of the trench axis seems to be high. This is also indicated from the analysis of the direction of wave approaching (Fig. 6-15). In the southernmost part of the Kuril Trench, the seaward seismicity is concentrated in the area beneath the seaward trench wall and just beneath the axis; the seismicity is low beneath the oceanic basin. Nishizawa et al. (1984b) pointed out that S-P time distributions at an OBS

array, which was deployed in the same area as in our 1983 OBS array just before the 1983 experiment, clearly show the low seismicity beneath the oceanic basin. One of their OBSs was located more than 150 km seaward from the trench axis and it detected no event with S-P time of less than 10 s, while OBSs located on the seaward trench wall detected many microearthquake near these OBSs. Kasahara and Harvey (1976) reported low seismicity beneath the outer wall of the Kuril Trench. They deployed a single OBS at a point of (41.415°N, 146.417°E); our result (Fig. 7-2) shows the low seismicity in this area. The area of low seismicity is corresponds with the area which was referred to as Ic by Suzuki et al. (1981); they pointed out that the offshore part of Ic is low in seismicity as compared with adjacent areas. These results suggest variation in seismicity along the trench.

In the Central Alutians, similarly, a high seismic activity on the outer trench slope has been reported from OBS measurements by Frolich et al. (1980,1982).

Asada and Shimamura (1971b, 1974, 1976) reported low seismicity seaward of the Kuril Trench, the Bonin Trench (the Western Pacific) and the Mariana Basin. They used S-P times of earthquakes recorded by OBSs on the oceanic basins. Although their instruments were sensitive enough to detect events with magnitudes less than -1 at distances of up to 100 km, no earthquake was detected in the area seaward of the trenches. Nagumo et al. (1976) also reported low seismicity in the Mariana Basin area. All of these studies suggest low seismicity in the areas at least 200 km seaward of the trench axis. However, the

OBSs used in these studies were too widely separated from trench axes to resolve the definite boundary between the seismically active region and the quiet region. Therefore we cannot conclude from their results that the high sismicity beneath the seaward trench wall does not exist in the Kuril Trench area, the Bonin Trench area and the Mariana area.

7-2 Focal depth distribution beneath the trench area

Figure 7-3 shows a vertical section of seismicity across the Japan Trench determined by the OCEP land network (Tohoku University). For this network, Ishii and Takagi (1978) has pointed out that the detectability and the accuracy of hypocenter, especially focal depths, are poor beneath the trench area. Within this limitation, Haswgawa et al. (1978a, 1978c) predicted that the actual seismicity would extend down to at least 70 km, from the analysis of apparent velocities and of waves incoming at the Kitakami seismic array of Tohoku University.

Our results demonstrate that the earthquakes are distributed dwon to 30 km depth beneath the seaward trench wall and down to 50 km depth just beneath the trench axis. Therefore, the scattered activity beneath the trench area determined by the land network must be an artificial feature due to its limited power of resolution.

From long-range refraction experiments and apparent velocity measurements by OBSs, a two-layered structure of the oceanic lithosphere with a total thickness of about 80 km is derived for

the West Pacific (Asada and Shimamura, 1976; Shimamura and Asada, 1976). Although the existence of velocity anisotropy makes it difficult to estimate the thickness of the lithosphere, recent results indicate that the total thickness may be greater than 80 km (Shimamura et al., 1983). The subducting plate beneath the Japan Trench region is estimated by a study of travel-time residuals for deep earthquakes and found to be a two-layered structure about 120 km thick (Suyehiro and Sacks, 1979). The concentration of microearthquakes in the upper part of the oceanic lithosphere is consistent with the idea that earthquakes occurring beneath the trench are due to the bending of the oceanic plate, which consists of a brittle upper layer and a ductile lower layer (Chapple and Forsyth, 1979).

Focal depths of microerthquakes under the continental slope start to deepen westward, with a very low dip angle of less than 10°. A vertical cross-sectoion of hypocenter distribution obtained by the 1980 and the 1981 experiment is shown in Fig. 7-6, where the shallower extension of the double seismic zone determined from OCEP land network data (Hasegawa et al., 1983) is also illustrated. It can be seen that the landward seismic activity beneath the 1981 OBS array is a shallower extension of the upper plane of the double seismic zone. On the other hand, the seismic activity corresponding to the lower plane has not observed beneath the 1981 array. From the land observation the lower plane exists up to 75 km in depth and 142.5°E in longitude at a latitude of about 40°N (Hasegawa et al., 1983). This is concordant with our results obtained from OBS data.

In the Kuril Trench area, the landward seismicity observed

by the OBS array seems to be a shallower extension of the lower plane as shown in Fig. 7-5, where both hypocenters determined by the OBS array and those by the land seismic network (Suzuki et al.,1983) are illustrated. The difference in depth of landward seismicity between the Japan Trench area and the Kuril Trench area may correspond to the difference in activity between the upper and the lower seismic plane in these areas; it has been pointed out that the upper plane is more active in the Tohoku District and the lower in the Hokkaido District (Suzuki et al., 1983).

Teleseismic hypocenter determinations using pP-P times indicate very shallow seismicity near the trench axis (Yoshi, 1979; Seno and Pongsawat, 1981; Kawakatsu and Seno, 1983). To get reliable results in focal depth, they omitted many events with magnitude less than 4 from the original seismic section based on ISC parameters. The microseismicity investigated in the present study indicates that small events with magnitude range of 1-4 are also concentrated within the shallower part of the oceanic lithosphere.

7-3 Seismicity gap beneath the inner trench walls

Both results obtained from the 1980 and the 1981 OBS data show a low seismicity beneath the inner wall of the Japan Trench. Although each observational period of these experiments was about two weeks, the general agreement of the two observational results strongly suggests the existence of a seismicity gap beneath the inner wall of the Japan Trench. The 1983 observation also shows

the existence of a seismicity gap in the Kuril Trench.

The seismicity gap has not been clearly seen from the local network of seismic stations on land. The detectability of the local land network is low in the vicinity of the trench axis (Hasegawa et al., 1978b; Ishii and Takagi, 1978) and also a lateral heterogeneity of the uppermost mantle beneath the sea and the land area causes a systematic bias in hypocenter determination (Utsu, 1967; Suzuki, 1975; Yoshii et al., 1981; Yamamoto and Kono, 1982).

From teleseismic observations, the seismicity gap has not been identified in the trench areas of the present study. There are small number of events whose hypocenters are determined with enough accuracy to discuss the seismicity in detail, although the seismici activity seems low beneath the inner trench wall (Yoshii, 1979). Past OBS observation in the Japan Trench area (Nagumo et al., 1976; Kasahara et al., 1982) also suggest high seismicity near the trench and low seismicity below the inner trench wall.

A seismicity gap beneath the inner trench wall has been found by OBS observations in the Central Aleutians (Frohlich et al., 1982). In the Northern Ryukyu Trench (Suyehiro et al., 1982), the Eastern Aleutians (Lawton et al., 1982) and the New Hebrides (Coudet et al., 1981; Chen et al., 1982), the existence of a seismically quiet area beneath the inner trench wall was suggested. These observational results suggest the possibility that the seismicity gap beneath the inner trench wall is a general feature in an island-arc trench system. Its origin may be related to the bending and unbending of the oceanic plate; the

bending stress is low beneath the inner trench wall (Chapple and Forsyth, 1979; Bodine et al., 1981; Frohlich et al., 1982). Chen et al. (1982) have tried to explane the seismicity beneath the inner trench walls in terms of the accreated wedge made of sediments. As far as in a shallow part of the lithospher, the seismicity gap may be explained by the high water content and low strength of unconsolidated sediments. Furthere investigations by OBS observations are needed to confirm the seismicity gap in various trenches and to clarify the relation between the gap and the tectonic circumstances such as stress state.

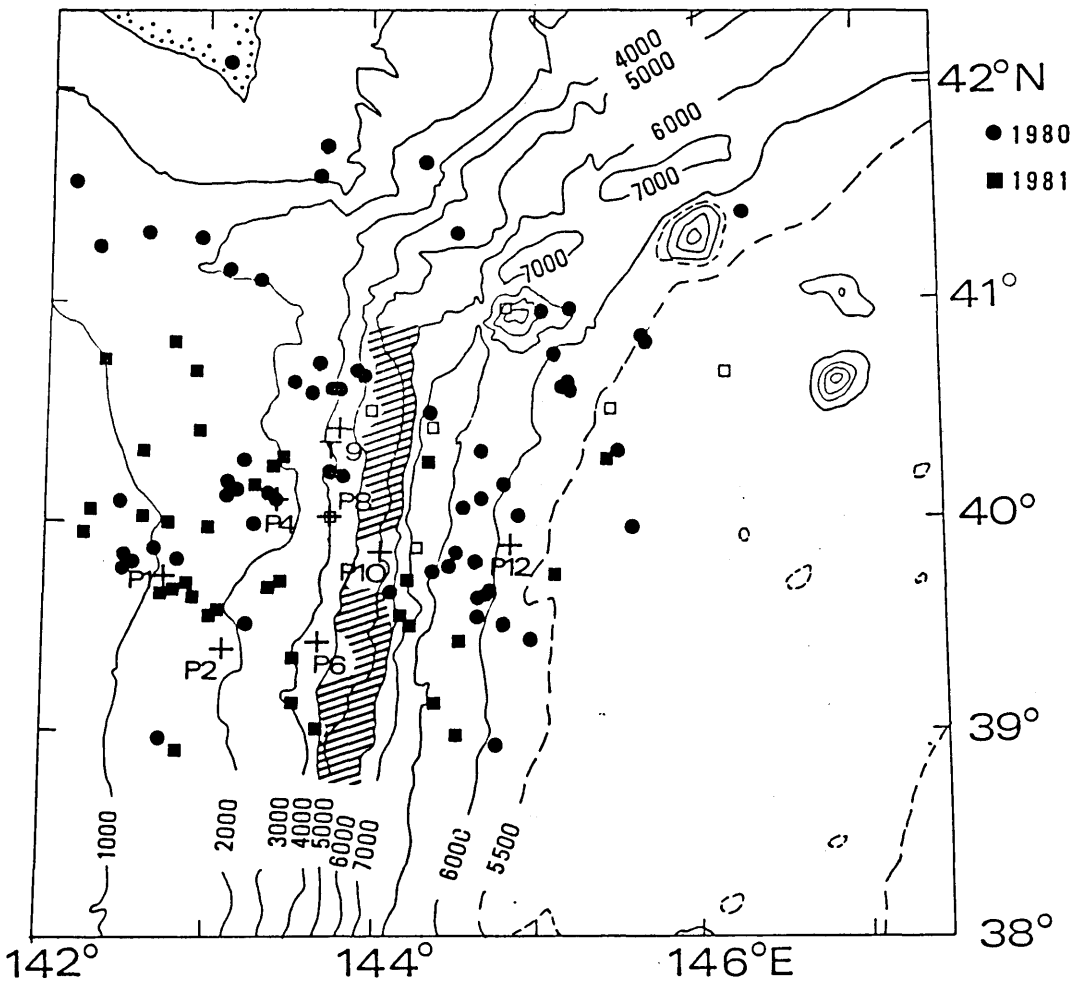

Fig. 7-1 Epicentral distribution constructed by combining data obtained in 1980 and those in 1981. Solid circles show events located by the 1980 data and solid squares show those by the 1981 data. Positions of OBSs are represented by open squares (1980) and crosses with a numeral (1981). Beneath the inner trench wall, which was indicated by a shaded area with a water depth of between 4000 and 6000 m, no events were located also in the Japan Trench area.

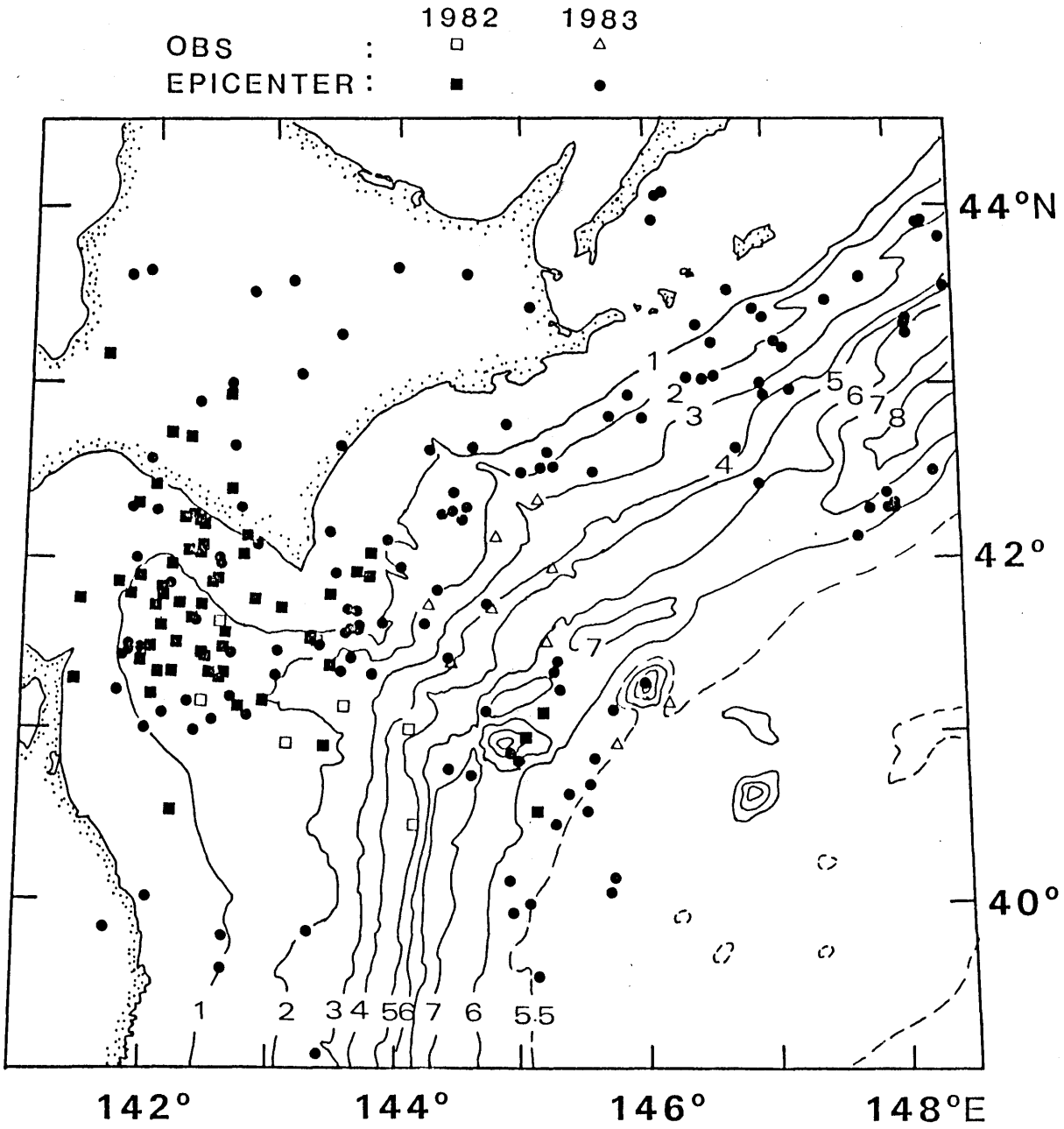

Fig.7-2 Epicentral distribution constructed by combining data obtained in 1982 and those in 1983. Solid squares show earthquakes located by the 1982 array and solid circles show those by the 1983 array. Positions of OBSs are shown by open squares (the 1982 array) and open triangles (the 1983 array). Isobaths are in kilometers.

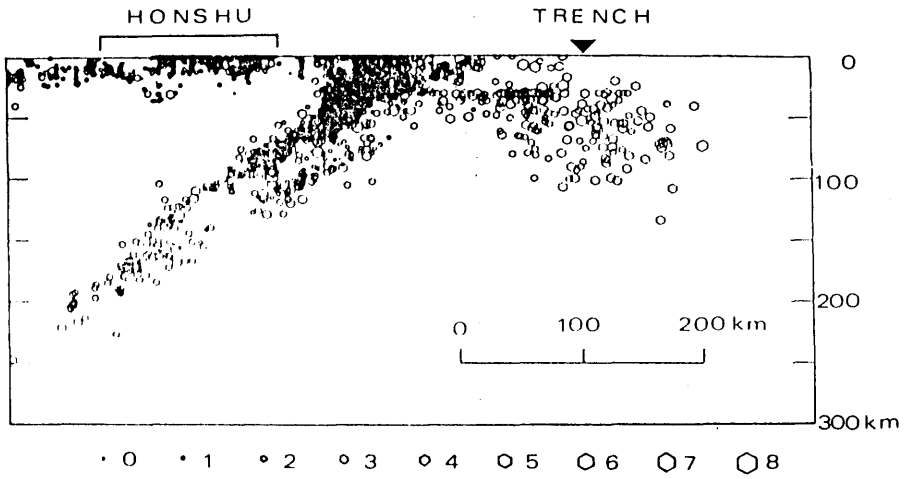

Fig. 7-3 Seismic cross-section viewed from the land network operated by OCEP. Events within 200 km width during 1980 are projected on the vertical plane from 40.8°N, 139.0°E to 40.0°N, 146.5°E, which is perpendicular to the trench axis. Sizes of events indicate their magnitudes. Largely scattered activity beneath the trench down to 100 km depth has been doubted because of limited resolution in hypocentre determination by the land network.

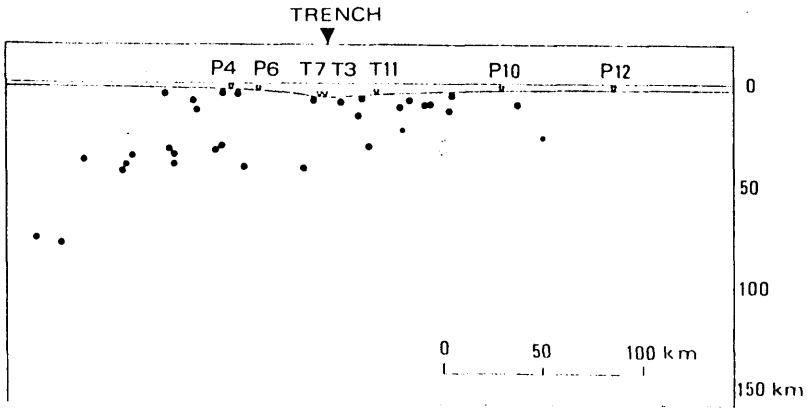

Fig. 7-4 Vertical seismicity section striking 10° clockwise from E to W at 40°N, determined by OBS observation for about two weeks. Thirty-two well-determined events are plotted. OBS locations are shown by triangles. There is no event deeper than 50 km beneath the trench axis. The seaward activity of the trench axis extends only as far as 100 km from the axis and is within 30 km depth. A seismicity gap is indicated beneath the landward trench wall between P6 and T7.

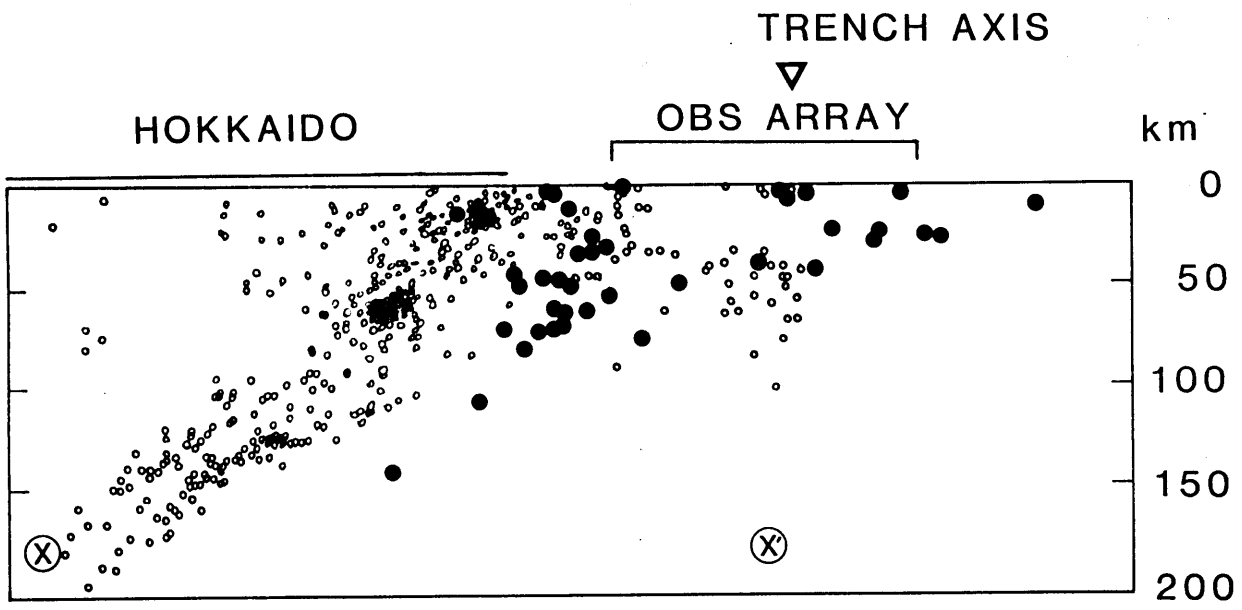

Fig. 7-5 Cross section of the microseismicity near the Kuril Trench, projected on the vertical plane perpendicular to the strike of the trench. Solid circles indicate hypocenters constructed from OBS data. Small open circles show hypocenters determined by the land networks(Suzuki et al.,1983). Just beneath the trench axis, determination by the land observtion is largely scattered with depth down to 100 km. OBS data indicates the seaward activity exists in the shallower portion of the oceanic lithospher at less than 50 km in depth.

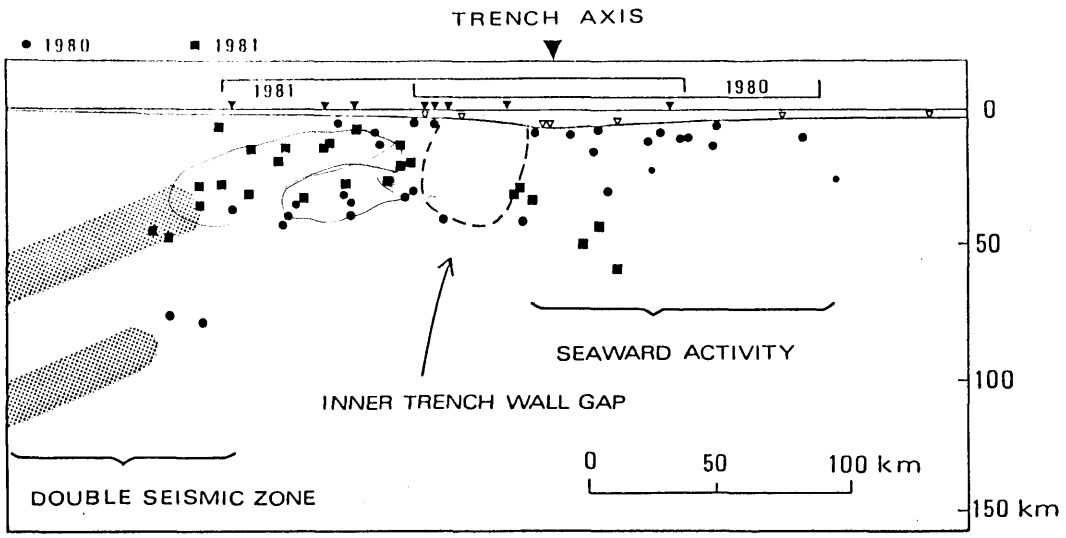

Fig.7-6 Combined vertical seismicity section constructed from events located by 1980 data and those by 1981 data. The cross-section is striking 10° clockwise from E to W at about 40° N and is perpendicular to the trench axis, position of which is indicated by a solid triangle. Circles indicate events located by the 1980 array. Solid squares show well-determined events by the 1981 data. Events with a standard deviation of the solution of less than 10 km for a epicenter and 15 km for a depth are plotted. Shadows indicate the position of a double seismic zone which is estimated from studies by land observations. An inner trench wall gap of seismicity separates the seaward activity from the shallower extension of the double seismic zone.

8 Conclusions

To investigate seismicity in trench areas, a series of OBS experiments was caried out near the Japan Trench and the Kuril Trench in 1980, 1981, 1982 and 1983. The observational period in each experiment is 10-30 days. Continuous records of about 15,000 hours in total were obtained. To process the large amount of data, a play-back system for OBS records was developed; the system utilizes a mini-computer equiped with a high speed analogue to digital convertor. This system enables us to obtain digital waveform data in a well organized format, from which we produce arrival time data for locating earthquakes. A new method of arrival time inversion for locationg earthquakes was developed on the basis of the quasi-linear inverse theory. In this theory, a new solution to the least-squares problem is defined by using a priori information about unknown parameters.

About 50 microearthquakes were detected by each OBS per day. Out of these events 5-10 earthquakes per day were located in and around the OBS array by using the newly developed method of hypocenter determination. Common features in hypocenter distribution were found in the Japan Trench area and the Kuril Trench area. The first of them is high seismic activity beneath the seaward trench wall. The activity has an eastern boundary along the edge of the seaward trench wall. The eastern edge of activity coincides with an isobath of 5,500 m, where the western edge of the outer rise of the trench lies. Second, beneath the oceanic basin seaward of the edge, the seismicity is low; no detectable event with magnitude greater than 2 was observed.

Third, there is a seismicity gap beneath the inner trench wall, while the seismiciy is high beneath the continental slope. Fourth, the microearthquakes beneath the seaward trench wall are distributed from 0 to 30 km in depth and just beneath the trench axis they are from 0 to 50 km. Fifth, the microearthquakes beneath the continental slope form a seismic zone dipping landward with a low dip angle of less than 10°; the landward seismicity obtained from OBS data seems to be a shallower extension of the upper plane of the double structured seismic zone in the Japan Trench area and that of the lower plane in the Kuril Trench area.

Thus we conclude that the seismicity widely scattered in the entire lithosphere is an apparent feature due to the limited resolution capability of the land network; microearthquakes are concentrated only in the upper part of the oceanic lithosphere. The spatial distribution of microearthquakes found in the Japan Trench area and the Kuril Trench area is similar to that found in the Central Alutians. Since the high seismic activity beneath the seaward trench wall and the seismicity gap beneath the inner trench wall are suggested in other trenches, the hypocenter distribution obtained in the present study may be related to the physical properties and the stress state of the subducting oceanic lithosphere in the vicinity of the trench.

Acknowledgments

I would like to express sincerely thanks to Dr.M.Matsu'ura for giving me valuable suggestions and support, and critically reviewing the manuscript.

I am grateful to Prof.R.Sato and Dr.T.Kanazawa for their encouragement and support in accompiling this study.

I thank Dr.H.Shimamura, Dr.T.Kanazawa, Dr.K.Suyehiro, Mr.H.Inatani, Dr.T.Iwasaki and Mr.T.Urabe for their help and useful suggestion in the OBS opperations.

I tank Mr.T.Urabe for his help in data processing of OBS record by a computer system. Discussions with Miss.A.Nishizawa were helpful.

I thank my colleagues in Geophysical Institute, Faculty of Science, the University of Tokyo for helpful comments and suggestions.

References

Aki,K., 1965. A computer program for precise determimation of focal mechanism of local earthquakes by revising focal depths and crust- mantle structure, Bull. Earthq. Res. Inst., 43, 15-22.

Asada,T. and Shimamura,H.,1971a. Sur l'observation seismique au fond oceanique (in Japanese), La Mer,Bull.Soc.Franco-Japonaise Oceanogr.,9,35-45.

Asada,T. and Shimamura,H.,1971b. Observation of earthquakes with ocean bottom seismomerters at ocean basin, Preliminary Report of 'the Hakuho Maru Cruise KH-71-3, Ocean Research Inst., Tokyo Univ.,68-69.

Asada,T. and Shimamura,H.,1974. Ocean bottom seismographs and new geophysics (in Japanese), Kagaku,44,278-285.

Asada,T. and Shimamura,H.,1975. An ocean bottom seismograph - A small and simple instrument for obtaining many obsevations in any circumstances, unpublished manuscript, Geophys. Inst., University of Tokyo, Tokyo.

Asada,T. and Shimamura,H.,1976. Observation of earthquakes and explosions at the bottom of the westeren Pacific: structure of oceanic lithosphere revealed by longshot experiment,In Sutton,G.H.,Manghnani,M.H. and Moberly,R.(editors), The geophysics of the Pacific Ocean Basin and its mergin, Geophys. Monogr., 19,135-154, A.G.U., Wash.,D.C.

Asada, T. and Shimamura,H., 1979. Long-range refraction experiments in deep ocean. Tectonophysics, 56:67-82.

Asada,T., Suzuki,Z. and Tomoda,Y., 1951. Note on energy and frequency of earthquakes, Bull. Earthq. Res. Inst., 29, 289.

Asada,T., Yamada,T. and Shimamura,H.,1979. Pop-up OBS (in Japanese), Program. Abstr., Seismol. Soc. Japan, 2, 114.

Asano,S., Den,N., Hotta,H., Yoshii,T., Ichinose,Y., Sakajiri,N. and Sasatani,T., 1979. Seismic refraction and reflection measurements around Hokkaido Part 2. Crustal structure of the continental slope off Hidaka, J. Phys. Earth, 27, 497-509.

Asano,S., Yamada,T., Suyehiro,K., Yoshii,T., Misawa,Y. and Iizuka,S., 1981. Crustal structure in a profile off the Pacific Coast of northeastern Japan by the refraction method with ocean bottom seismometers. J. Phys. Earth, 29:267-281.

Backus,G. and Gilbert,G., 1970. Uniqueness in the inversion of inaccurate gross earth data, Philos. Trans. R. Soc. London., Ser.A, 266, 123-192.

Benioff,H., 1949. Seismic eidence for the fault origin of oceanic deeps, Bull. Geol. Soc. Amer., 60, 1837-1866.

Benioff,H., 1954. Orogenesis and deep crustal structure - additional evidence of seismology, Bull. Geol. Soc. Amer., 65, 385-400.

Benioff,H., 1955. Seismic evidence for crustal structure and tectonic activity, Bull. Geol. Soc. Amer., Spec. Paper 62, 61-74.

Bodine,J.H., Steckler,M.S., and Watts,A.B., 1981. Observations of flexure and rheology of the oceanic

lithosphere, J. geophys. Res., 86, 3695-3707.

Bolt,B.A., 1970. Earthquake location for small network using the generalized inverse matrix, Bull. Seismol. Soc. Am., 60, 1823-1828.

Bradner,H. and Dodds,J.G., 1964. Comparative seismic noise on the ocean bottom and land., J. Geophys. Res., 69, 4339-4348.

Buland,R., 1976.Mechanics of location earthquakes, Bull. Seismol. Soc. Am., 66, 173-187.

Chapple,W.M., and Forsyth,D.W.,1979. Earthquakes and bending of plates at trenches,J.geophys.Res.,84,6729-6749.

Chen, A.T., Frohlich, C. and Latham, V., 1982. Seismicity of the forearc marginal wedge (accretionary prism). J. Geophys. Res., 87:3679-3690.

Coudert,E., Isacks,B.L., Barazangi,M., Louat,R., Cardwell,R., Chen,A., Dubois,J, Latham,G. and Pontoise,B.,1981. Spatial distribution and mechanisms of earthquakes in the Southern New Hebrides Arc from a temporary land and ocean bottom seismic network and from worldwide observations,J.geophys.Res., 86,5905-5925.

Den,N., Hotta,H., Asano,S., Sakajiri,N., Ichinose,Y.,Motoyama,M., Kakiichi,K., Beresnev,A.F. and Sagalevitch,A.A., 1971. Seismic refraction and reflection measurement around Hokkaido, Part 1, Crustal structure of the continental slope off Tokachi, J. Phys. Earth, 19, 329-345.

Duschenes,J., Lilwall,R.C. and Francis,T.J.G, 1983. The hypocentral resolution of mocroearthquake survey carried

out at sea, Geophys. J. R. astr. Soc., 72, 435-451.

Eckart,C and Young,G., 1939. A principal axis transformation for non-Hermitian matrices, Am. Math. Soc. Bull., 45, 118-121.

Ewing,J. and Ewing,M., 1961. A telemetering ocean-bottom seismograph, J. Geophys. Res., 66, 3863-3878.

Flinn,E.A., 1965. Confidence regions and error determinations or seismic event location, Rev. Geophys., 3, 157-185.

Francis,T.J.G. and Porter,I.T,1972. Microearthquake survey of the Mid-Atlantic ridge,Nature,240,547-549.

Franklin,J.N, 1970. Well-posed stochastic extension of ill-posed linear problems, J. Math. Anal., Appl., 31, 682-716.

Frohlich, C., Billington, S., Engdahl, E.R. and Malahoff, A., 1982. Detection and location of earthquakes in the Central Aleutian subducting zone using island and ocean bottom seismograph staions. J. Geophys. Res., 87:6853-6864.

Frohlich, C., Caldwell, J.G., Malahoff A., Latham, G.V. and Lawton J., 1980. Ocean bottom seismograph measurements in the Central Aleutians. Nature, 286:144-145.

Fujii,S., 1983. Seismic data processing system using 8/16 bit MPU, Geophys. Bull. Hokkaido Univ., 42, 389-294.

Fujita, K., Engdahl, E.R. and Sleep, N.H., 1981. Subduction zone calibration and teleseismic relocation of thrust zone events in the Central Aleutian islands. Bull. Seismol. Soc. Am., 71:1805-1828.

Geiger,L., 1910. Herdbestimmung bei Erdbeben aus den

Ankunftszeiten, K. Geseu. Wiss. Gott., 4, 331-349.

Hamada,N., 1983. Observation of ocean bottom seismogaph (TKOBS) off the coat of Tokai area, Zisin 2, 36, 449-462.

Hasegawa,A., Umino,N. and Takagi,A., 1978a. Double-planed structure of the deep seismic zone in the northeastern Japan Arc, Tectonophysics 47, 43-58.

Hasegawa,A., Umino,N., Takagi,A. and Suzuki,Z.,1979. Double-planed deep seismic zone and anomalous structure in the upper mantle beneath northern Honshu (Japan), Tectonophysics, 57,1-6.

Hasegawa,A., Umino,N., Takagi,A., Suzuki,S., Motoya,Y., Kameya,S., Tanaka,K. and Sawada,Y., 1983. Spatial distribution of earthquakes beneath Hokkaido and Northern Honshu, Japan. Zisin (J. Seismol. Soc. Jpn.) 2, 36:129-150 (in Japanese, with English abstract).

Hasegawa, A., Yamamoto, A. and Umino, N., 1978b. Micro-seismicity off Cape Erimo. In:H.Miki(Editor), Research of Seismicity in two Areas of Specified Observation: Special studies on natural disaster No.A-53-5,pp.26-43 (in Japanese).

Hasegawa,A., Yamamoto,A. and Umino,N., 1978c. Micro-seismicity off Cape Erimo (in Japanese), in Miki,H. (editor), Research of seismicity in two area of specified observation, Special studies on natural disaster No.A-53-5, 26-43.

Herrin,E., Taggart,J. and Brown,Jr.C.F., 1962. Machine computation of earthquake hypocenters, J. Grad. Res. Center, Southern Methodist Univ., 30, 79-106.

Hirata,N., Kanazawa,T., Urabe,T., Iwasaki,T., Suyehiro,K.

and Shimamura,H., 1984. Seismicity off Fukushima Prefecture and seismic activity associated with the 1982 Ibaraki-oki earthquake determined from observation by ocean bottom seismometers, Prog. Abstr., Seismol. Soc. Jpn., 1, 51.

Hyndman,R.D. and Rogers,G.C.,1981. Seismicity survey with ocean bottom seismographs off Western Canada, J.geophys.Res.,86, 3867-3880,1981.

Ichikawa,M.,1978. Lateral heterogeneity under the Southern Kuril Trench and its vicinity and systematic discrepancy in epicenter locations, Geophys.Mag.,38,1-19.

Ichikawa,M.,1979. Distribution of hypocenters of earthquakes occuring off the east coast of northern Honshu (in Japanese), Quart.J.Seismol.,43,59-65.

Inatani,H. and Furuya,I.,1980. A microprocessor controlled time code generatoer for an OBS system, J.Phys.Earth, 28, 281-292.

Ishii,H. and Takagi,A., 1978. On the detectability of earthquakes and crustal movements in and around the Tohoku District (North-eastern Honshu) (I) Microearthquakes. Zisin (J. Seismol. Soc. Jpn.) 2,31:287-298 (in Japanese, with English abstract).

Ishimoto,M. and Iida,K., 1939. Observations sur les seismes enregistres par le Microseismographe construit dernierement (1), Bull. Earthq. Res. Inst., 17, 443-478.

Iwasaki,T., Hirata,N., Suyehiro,K., Kanazawa,T., Urabe,T., Moriya,T., and Shimamura,H., 1983. Aftershock Distribution of the 1982 Urakawa-oki Earthquake

determined by ocean bottom seismographic and land observations. Submitted to J. Phys. Earth.

Jackson,D.D., 1972. Interpretation of inaccurate, insufficient and inconsistent data, Geophys. J. R. astr. Soc., 28, 97-109.

Jackson,D.D., 1979. The use of a priori data to resolve non-uniquness in linear inversion, Geophys. J. R. astr. Soc., 57, 137-157.

James,D.E., Sacks,I.S., Lazo L,E., and Aparicio G,P., 1969. On locating local earthquakes using small networks, Bull. Seismol. Soc. Am., 59, 1201-1212.

Jeffreys,H., 1959. The Earth, 4th ed., Cambridgde Univ. Press, 420pp.

Jordan, T.H. and Sverdrup,K.A., 1981. Teleseismic location techniques and their application to earthquake clusturs in the south-central Pacific, Bull. Seismol. Soc. Am., 71, 1105-1130.

Kasahara,J. and Harvey,R., 1976. Ocean bottom seismometer study of the Kuril Trench area, Joint technical repot with Joint Tsumani Reserach Effort, Pacific Marine Environmental Lab., Hawaii Inst. Geophys., Univ. Hawaii, Hawaii.

Kasahara,J., Nagumo,S., Koresawa,S., Nishi,Y. and Sugimoto,H., 1982. A linear trend of hypocenter distribution in the outer slope region of the Japan trench revealed by OBS array - Preliminary report -. Bull. Earthq. Res. Inst., 57:83-104.

Kasahara,Z., 1981. Time code reader for ocean botto,m seismometer using microprocessor and its application for

new data processing., Bull. Earthq. Res,. Inst., 56, 195-205.

Katsumata,M., 1955. Vertical distribution of earthquakes near Japan, Quart. J. Seismol., 20, 59-63.

Katsumata,M., 1956. Vertical distribution of earthquake foci in and around Japan, Geophys. Mag., 27, 483-486.

Katsumata,M., 1967. Seismic activities in and near Japan (II) - vertical distribution of foci of earthquakes in and near the Japanese islands, Zisin (J. Seismol. Soc. Jpn), 2, 20, 1-11.

Katsuyama,Y., Hamada,K., Fukui,T. and watanabe,I., 1975. Digital rpocess of long time analog tape recording for earthquakes - A use of TOSBAC-3400, TOSBAC-40 systems and their A/D, D/A converters -, Zisin 2, 28, 379-386.

Kaula,W.M., 1966. Theory of Satellite Geodesy, Chap.5, Blaisdell, Waltham, Massachusetts.

Kawakatsu,H. and Seno,T., 1983. Triple seismic zone and the regional variation of seismicity along the Northern Honshu Arc. J. Geophys. Res., 88:4215 -4230.

Kishinouye,F., Yamazaki,H., Kobayashi,H. and Koresawa,S., 1963. A submarine seismograph; the first paper, Bull. Earth. Res. Inst., 41, 819-824.

Kishinouye,F., 1966. The submarine seismograph; the second paper, Bull. Earthq. Res. Inst., 44, 1443-1447.

Lanczos,C., 1Linear Differential Operators, Chap.3, Van Nostrand, London.

Lawton,J., Frohlich,C., Pulpan,H and Latham G.V., 1982. Earthquake activity at the Kodiak Continental Shelf, Alaska, determined by land and ocean bottom seismograph

networks. Bull. Seismol. Soc. Am., 72:207-220.

Levenberg,K., 1944. A method for the solution of certain non-linear problems in least-squares, Q. Appl. Math., 2, 164-168.

Lilwall,R.C. and Francis,T.J.G., 1978. Hypocentral resolution of small ocean bottom seismic networks, Geophys. J.R. astr. Soc., 54, 721-728.

Lilwall,R.C., Francis,T.J.G. and Poter,I.T.,1981. A microearthquake survey at the junction of the East Pacific Rise and the Wilkes (9 S) fracture zone,Geophys.J.R.astr.Soc.,66,407-416.

Ludwig,W.J., Ewing,J.I., Ewing,M., Murauchi,S., Den,N., Asano,S. Hotta,H., Hayakawa,M., Asanuma,T., Ichiwawa,K. and Noguchi,I., 1966. Sediments and structure of the Japan Trench, J.geophys.Res.,71, 2121-2137.

Marquardt, D.W.., 1963. An algorithm for least-squares estimation of nonlinear parameters, J. Soc. Ind. Appl. Math., 11, 431-441.

Matsu'ura,M. and Hirata,N., 1982. Generalized least-squares solutions to quasi-linear inverse problems with a priori information. J. Phys. Earth, 30:451-468.

Matsu'ura,M., Yamada,T., Shibuya,K., Inatani,H., Tanimoto,T., Hirata,N. and Ito,J., 1978. Observations of aftershocks of the Miyagi-oki earthquake of 1978 by ocean bottom seismographs II. Progr. Abstr. Seismol. Soc. Jpn., 2: 4 (in Jpanese).

Matsuzawa,A., Tamano,T., Aoki,Y. and Ikawa,T.,1980. Structure of the Japan trench subduction zone, from multi-channel seismic reflection records, Marine

Geology,35,171-182.

Meteorological Research Instite, Seismolgy and Volcanology Research Division, 1980. Parmanent ocean-bottom seismograph observation system , Tecncal Rep. Met. Res. Inst., 4.

Miyamura,S., 1962. Seismicity and geotectonics, Zisin (J. Seismol. Soc. Jpn.), 2, 15, 23-52.

Moriya,T. and Takeda,K., 1979. Coded crystal clock and code reader for DAR earthquake observation system, Zisin 2, 32, 98-201.

Murauchi,S. and Ludwig,W.J.,1980. Crustal structure of the Japan trench: The effect of subduction of ocean crust, Initial Reports of the Deep Sea Drilling Project, Vol.LVI,LVII,463-469.

Murauchi,S., Asanuma,T. and Ishii,H., 1973. Geophysical studies on the sea around Hokkaido. Mem. Nat. Sci. Mus., Tokyo, 6:163-182 (in Japanese, with English abstract).

Nagumo,S. and Kasahara,J.,1976. Ocean bottom seismographic study of the western margin of the Pcific, in Sutton,G.H., Manghnani,M.H. and Morbely,R. (editors), The geophysics of the Pacific Ocean Basin and ist margin, Geophys.Monogr., 19, 155-168, A.G.U., Wash.,D.C.

Nagumo,S., Hasegawa,S., Koresawa,S. and Kobayashi,H.,1970a. Ocean-bott seismographic observation at the offside of Japan Trench near the Erimo Seamount - Seismic activity of the ocean lithosphere and velocit structure around the geophysical "Ocean-continet boundary", Bull. Earthq.Res.Inst.,48,769-792.

Nagumo,S., Hasegawa,S., Koresawa,S. and Kobayashi,H.,1970b. Ocean-bott seismographic observation off Sanriku - Aftershock activity of the 1968 Tokachi-oki earthquake and its relation to the Ocean-continent boundary fault, Bull.Earthq.Res.Inst.,48,793-809.

Nagumo,S., Kasahara,J. and Koresawa,S., 1976. Structure of micro-earthquake activity around Japan Trench, off Sanriku, obtained by ocean-bottom seismographic network observation. J. Phys. Earth, 24:215-225.

Nagumo,S., Kasahara,J. and Koresawa,S.,1980. OBS airgun seismic refrac survey near sites 441 and 434 (J-1A),438 and 439 (J-12), and proposed site J-2B: Legs 56 and 57, Deep sea drilling project, Initial Reports of the Deep Sea Drilling Project,Vol.LVI,LVII,459-462.

Nishizawa,A., Suyehiro,K., Kanazawa,T. and Shimamura,H., 1984a. Crustal structure southeast off Hokkaido near the Kuril Trench, Prog. Abst., Seismol. Soc. Jpn., 1, 171.

Nishizawa,A., Suyehiro,K., Kanazawa,T. and Shimamura,H., 1984b. Crustal structure southeast off HOkkaido near the Kuril Trench, Prog. Abst., Seismol. Soc. Jpn., 2, 236.

Officer,C.C., 1958. Introduction to the theory of sound transmission, McGraw-Hill, New York.

Ouchi,T., Brahim,A.K.I., and Latham,G.V., 1982. Seismicity and cructal structure in the Orozco Fracture Zone: Project Rose Phase II, J. geophys. Res., 87, 8501-8507.

Ouchi,T., 1978. Seismicity and the spectral structure of seismic body wave in the Mariana region derived by using ocean bottom seismographs, PhD Thesis, The University of Tokyo, Tokyo (in Japanese with English abstract).

Penrose,R., 1955. A generalized inverse for matrices, Proc. Cambridge Philos. Soc., 51, 406-413.

Peters,D.C. and Crosson,R.S., 1972. Application of prediction analysis to hypocenter determination using a local array, Bull. Seism. Soc. Am., 62, 775-788.

Project Rose Scientists, 1981. Microearthquake activity on the Orozco Fracture Zone; Preliminary results from Project Rose, J. geophys. Res., 86, 3783-3790.

Rykunov,L.N. and Sedov,V.V., 1956. Seismic noise in the 2-15 cps frequency range on the bottom of the Black sea, Izv. Phys. Solid Earth, 7, 443-448.

Rykunov,L.N. and Sedov,V.V., 1976. An ocean-bottom seismograph., Izv. Phys. Solid Earth, 8, 537-541.

Seno,T. and Pongsawat,B., 1981. A triple-planed structure of seismicity and earthquake mechanisms at the subduction zone off Miyagi Prefecture, northern Honshu, Japan. Earth Plnet. Sci. Lett., 55:25-36.

Shimamura,H. and Asada,T., 1974. A cassette recorder for an ocean bottom seismometer. Geophys. Bull. Hokkaido Univ., 32:17-24.

Shimamura,H. and Asada,T.,1976. Apparent velocity measurements on oceanic lithosphere,Phys.Earth planet.Int.,13,15-22.

Shimamura,H., Asada,T., Suyehiro,K., Yamada,T. and Inatani,H., 1983. Longshot experiments to study velocity anisotropy in the oceanic lithosphere of the northwestern Pacific. Phys. Earth Planet. Inter., 31:348-362.

Shimamura,H., 1977. A new version of precision calibrator for crystal clocks. Zisin (J. Seismol. Soc. Jpn.) 2,

30: 230-233 (in Japanese).

Sugawara,M., Katsuyama,Y., Ohmura,K. and Fukui,T., 1974. Automatic detecting methos for micro-eathquakes, Rep. Nat. Res. Cent. Disaster Prev., 9, 1-9.

Suyehiro,K. and Sacks,I.S.,1979. P- and S-wave velocity anomalies associated with the subducting lithosphere determined from travel-time residuals in the Japan region,Bull.seism.Soc.Am.,69,97-114.

Suyehiro,K., Nishizawa,A. and Shimizu,H., 1982. Microearthquake activity in the West Philippine Basin and Northern Ryukyu Trench region as observed by ocean bottom seismometers at the Amami Plateau. J. Phys. Earth, 30: 509-516.

Suzuki,S. and Motoya,Y., 1981. Microearthquake activity in Hokkaido observed by the telemetering system, Zisin (J. Seismol. Soc. Jpn.), 2, 34, 251-267.

Suzuki,S., Motoya,Y., Umino,N., Hasegawa,A., Kameya,S. and Tanaka,K., 1983. Hypocentral distribution and composite focal mechanisms of shallow earthuakes near the junctions between the Kuril and the Northern Japan Arcs, Zisin (J. Seismol. Soc. Jpn.), 2, 36, 407-421.

Suzuki,S., 1975. Determination of earthquake hypocenters in consideration of the lateral variation of velocity in the upper mantle beneath the island-arcs of Japan - on the Nemuro-Hanto-oki earthquake of 1973 -. Zisin (J. Seismol. Soc. Jpn.) 2, 28:181-199 (in Japanese, with English abstract).

Tamano,T., Toba,T. and Aoki,Y.,1981. Multichannel reflection seismic profiles across the Japan Trench and

the Nankai Trough (in Japanese), Butsuri-tanko (Geophysical exploration),34,204-221.

Tomoda, Y., 1973. Maps of Free Air and Bouguer Gravity Anomalies in and around Japan, University of Tokyo Press, Tokyo.

Tsumura,K., 1967. Determination of earthquake magnitude from duration of oscillation, Zisin 2, 20, 30-40.

Tsumura,K., 1973. Microearthquake activity in the Kanto district. In: Spatial Publication for the 50th Annive. of the Great Kanto Earthquake, Earthquake Research Institute, Tokyo, pp. 67-87 (in Japanese).

Uhrhammer,R.A., 1980. Analysis of small seismographic station network, Bull. Sesimol. Soc. Am., 70, 1369-1379.

Umino,N. and Hasegawa,A., 1975. On the two-layered structure of deep seismic plane in Northeastern Japan Arc. Zisin (J. Seismol. Soc. Jpn.) 2, 27:125-139 (in Jpanese, with English abstract).

Urabe,T. and Kanazawa,T., 1984. A high reliability timer for an OBS system. submitted to Zisin.

Urabe,T., 1984. A microcomputer-aided playback system for a direct analog tape recording of seismic data, Zisin 2, 37, 119-122 (in Japanese).

Utsu,T.,1967. Anomalies in seismic wave velocity and attenuation associated with a deep earthquake zone (1),J.Fac.sci.,Hokkaido Univ., Ser.7(Geophysics),3,1-25.

Wadati,K. and Iwai,Y. 1954. The minute investigation of seismicity in Japan (I), Geophys. Mag., 25, 167-173.

Wadati,K. and Iwai,Y. 1956. The minute investigation of

seismicity in Japan (II), Geophys. Mag., 27, 11-15.

Wadati,K., 1927. Study of deep earthquakes, Kishou-shushi, 2, 5, 119-145.

Wadati,K., 1928. Shallow and deep earthquakes,, Geophys. Mag., 1, 161-202.

Wadati,K., 1929. Shallow and deep earthquakes: 2nd paper, Geophys. Mag., 2, 1-36.

Wadati,K., 1931. Shallow and deep earthquakes: 3rd paper, Geophys. Mag., 4, 231-283.

Wadati,K., 1935. On the activity of deep-focus earthquakes in the Japan Island and neighbourhoods. Geophys. Mag., 8, 305-325.

Watanabe,H., 1971. Determination of earthquake magnitude at regional distance in and near Japan, Zisin 2, 24, 189-200.

Wiggins,R.A., 1972. The general linear inverse problem: Implication of surface wave and free oscillations for earth structure, Rev. Geophys. Space Phys.,10, 251-285.

Wolberg,J.R., 1967. Prediction Analysis, D. Van Nostrand Co. Inc., Proinceton, N.J. Bolt,B.A., 1960. Earthquake epicenters, focal depths, and origin times using a high-speed computer, Geophys. J., 3, 433-440.

Yamada,T., Inatani,H., Matsu'ura,M., Shibuya,K., Tanimoto,T., Hirata,N., Asada,T., Murakami,H. and Takagi,A.,1978. Observations of aftershocks of the Miyagi-oki earthquake of 1978 by ocean bottom seismographs I (in Japanese), Program. Abstr., Seismol. Soc. Japan, 2, 31.

Yamada,T., Shimamura,H. and Asada,T., 1976. Resolving

power of OBS recording system using compact cassette magnetic tape in determining time difference between signals in separate channels. Zisin (J. Seismol. Soc. Jpn.) 2, 29: 287-297 (in Japanese, with English abstract).

Yamada,T., 1980. Spatial distribution of microearthquakes and crustal structure in the subduction area revealed by ocean bottom seismographic observations, PhD thesis, The University of Tokyo, Tokyo (in Japanese).

Yamada,T. Asada,T. and Shimamura,H.,1981. A pop-up type system for an ocean bottom seismograph (in Japanese), Program.Abstr., Seismol.Soc.Japan, 2, 126.

Yamamoto,A. and Kono,T., 1982. Crust and upper mantle structure in the Northeastern Japan derived from the velocity and azimuth anomalies observed at the Kitakami seismic array. Tohoku Geophys. J. (Sci. Rep. Tohoku Univ., Ser. 5), 29:1-40.

Yoshii,T., Okada,H., Asano,S., Ito,K., Hasegawa,T., Ikami,A., Moriya,T., Suzuki,S. and Hamada,K., 1981. Regionality of the upper mantle around Northeastern Japan as revealed by big explosions at sea. II. Seiha-2 and Seiha-3 experiment. J. Phys. Earth, 29:201-220.

Yoshii,T., 1979. A detailed cross-section of the deep seismic zone beneath northeastern Honshu, Japan. Tectonophysics, 55:349-360.